ABSTRACT

Title of Document: MEASURING INTERACTIONS OF DNA WITH CATIONIC CARRIERS AT THE SINGLE MOLECULE LEVEL: A STEP TOWARD A RATIONAL DESIGN OF CATIONIC CARRIERS TO REACH MAXIMUM TRANSFECTION EFFICIENCY

Amy Lee, Doctor of Philosophy, 2015

Directed By: Assistant Professor Joonil Seog, Department of Materials Science and Engineering

Gene delivery has seen limited clinical success due to poor transfection efficiency or risk of carrier toxicity. Little understanding exists about the dynamic mechanical properties of DNA:carrier complexes, which we hypothesize are critical for protection and release of DNA. Using optical tweezers, we investigated the DNA condensation behaviors of 19-mer poly-L-lysine (PLL), a histidine-lysine peptide, 25 kDa branched polyethylenimine (PEI), G2-triethylenetetramine conjugated gold nanoparticles (G2-TETA), and two triblock copolymers to identify the optimal force signature for efficient transfection.

Force-extension profiles indicate that PLL and HK peptides condense DNA, showing force plateaus. When free peptide is removed, the force plateau of HK complexes decreased, but hysteresis persisted, indicating that some HK remains bound. Upon changing the pH from 7.4 to 5, HK complexes recovered plateau forces, due to

protonation of bound HK. This charge-regulated mechanical behavior is enhanced when the DNA:HK complex is exposed to Zn^{2+}, resulting in the formation of a mechanically stiff complex.

DNA:PEI complexes showed transient force plateaus with a maximum of 35 pN. Shortening of contour length was observed for condensation with 5 nM PEI. 1 M NaCl destabilized DNA:PEI complexes suggesting electrostatic interactions as the major force driving complexation. When 50 nM G2-TETA binds DNA, ~10 pN force plateaus appeared, disappeared, and contour length decreased despite pulling forces up to 50 pN. Neither 1 M NaCl nor 5 mg/mL heparin disrupted the complex. Contour length increased in 5% sodium dodecyl sulfate solution indicating that hydrophobic interactions play a major role in forming mechanically rigid condensates.

Both guanidinylated and base copolymers show maximal plateau behavior followed by reduction in contour length. Recovery of the extension for the DNA:base copolymer complex is achieved by a combination of glutathione and either high salt or heparin. Conversely, high salt or heparin conditions alone are sufficient for destabilization of DNA:guanidinylated copolymer. Thus, guanidinylation of the copolymer enhanced sensitivity to ionic environments.

Condensed DNA force profiles using different agents were unique regarding their condensation behaviors and responses to environmental changes. Regulation of these interaction forces between DNA and carriers during complex preparation and under physiological conditions will improve transfection efficiencies *in vivo*.

Measuring Interactions Of DNA With Cationic Carriers At The Single Molecule Level: A Step Toward A Rational Design Of Cationic Carriers To Reach Maximum Transfection Efficiency

Amy Lee

Dissertation submitted to the Faculty of the Graduate School of the
University of Maryland, College Park, in partial fulfillment
of the requirements for the degree of
Doctor of Philosophy
2015

Advisory Committee:

Assistant Professor Joonil Seog, Committee Chair
Associate Professor Jason D. Kahn
Professor and Associate Dean Peter Kofinas
Assistant Professor Silvina Matysiak
Professor Archibald J. Mixson

Dedication

This dissertation is dedicated to my family who has helped me culture an enthusiasm for science, research, and learning while always maintaining unconditional love and support.

Acknowledgements

I would first like to express my thanks to my advisor and mentor, Dr. Joonil Seog, for his patience, guidance, and support during my graduate career at the University of Maryland. He has provided me with many opportunities, and has inspired me to become a better critical and independent researcher.

My colleagues, past and present, have been instrumental in helping me through my studies. Particular thanks go to Adam Karcz for his patience in teaching me to operate the optical tweezers. The HK peptide group including Dr. Kahn, Dr. Mixson, Dr. Seog, Dr. Justin Chou, Dr. Lucas Tricoli, Jason Hustedt, and Adam Karcz provided stimulating discussions and data which were key in understanding the molecular interactions between the HK peptide and DNA. I owe many thanks to my undergraduate researchers Steven Ramiro, Tai Zheng, Ryan Akman, and Maria Oei who have helped immensely in the collection, interpretation, and analysis of data. I also with to thank my committee for their support and constructive feedback which has helped to direct my work. I also thank all past and present members of the Molecular Mechanics and Self-Assembly Lab for their comments, critiques, and friendship.

Finally, I would love to thank my parents, Yea-shun Cheng and Day-chyuan Lee, my brother, David Lee, my boyfriend Sirin Bulakul, and all my friends for their love, encouragement and support through this incredible journey!

Table of Contents

List of Figures

1 Introduction

Gene therapy has been widely regarded as a promising approach for the treatment of disorders such as cancers and hereditary conditions [1-3]. In its present state of development, a major roadblock in gene therapy is the lack of a safe and efficient delivery vehicle. Thus, the focal point of gene delivery carrier design is non-viral vectors such as cationic polymers and peptide carriers, which tackle the issue of biocompatibility; however they display limited transfection capabilities as compared to viral vectors [4]. The potential reasons for limited efficiency lie in the set of physiological obstacles that the complexes must navigate: these include the stable transport of packaged DNA in the bloodstream, targeting to specific cells, endocytosis, endosomal escape, unpackaging of DNA, and nuclear transport [5].

Surmounting some of these barriers requires delicate regulation of the forces between nucleic acid and carrier. For example, carrier and nucleic acid complexes must remain stable in the bloodstream, but upon cellular internalization, the complex must respond to changes in the environment by releasing nucleic acids from the complex. However, there is a lack of understanding of the optimal interaction forces between DNA and carrier required to protect or release DNA and how these forces are regulated under various physiological environments. Such understanding may be required for rational design of more efficient carriers for gene delivery.

The specific objective of this dissertation is to utilize optical tweezers and single molecule mechanics to correlate the structure of the carrier to mechanical properties with the aim to elucidate the delivery mechanism as well as identify the optimal force signature for efficient transfection. The central hypothesis is that the mechanical

properties of a highly efficient carrier will demonstrate changes in mechanical response to both temporal and spatial factors, in order to circumvent biological barriers and provide adequate protection from degradation, yet allow for release of nucleic acid at the target location.

Using custom built optical tweezers, force vs. extension profiles were collected for DNA condensed with polylysine and histidine-lysine peptides (Chapter 2), polyethylenimine (PEI) and PEI-mimicking ligand coated gold nanoparticles (Chapter 3), and bi-functional triblock polymers (Chapter 4). Each condensing agent produces a characteristic force profile which is determined by the chemical interactions between the cationic carrier and the DNA. Furthermore, dynamic mechanical responses to environmental stimuli such as pH, high salt, and reducing environments are revealed. We then correlate these mechanical behaviors to their transfection efficiencies to identify key mechanical criteria for the design of transfection agents (Chapter 5). Finally, we offer future directions for single molecule studies and gene carrier development based on this body of work (Chapter 6).

1.1 Biological barriers and current approaches to gene delivery

There are many biological barriers that limit the efficacy of a DNA-based gene delivery system. In order to successfully transfect a single cell, approximately 10^6 plasmids must be internalized, and out of those, only 10^2-10^4 will successfully be localized to the nucleus [6, 7]. The first criteria that must be met is the carrier's ability to provide stability in extracellular spaces. The extracellular compartment is comprised of intercellular and intravascular spaces. Here chemical and physical stability is important because nucleases are present in these locations and will degrade unprotected nucleic acids regardless if they are administered via intravenous or intramuscular injections [8,

9]. Condensation by using polycations has been shown to minimize exposure to nuclease activity [10]. Colloidal stability within the vasculature network can also present a challenge for efficient delivery. If the complex has a near net neutral charge, aggregation can occur via van der Walls forces. The variety and high concentration of biological molecules in the extracellular space can also disrupt charged complexes. Such interactions may lead to screening of ionic interactions between polycations and DNA, or screen electrostatic repulsion between complexes leading to aggregation despite the complex having a net charge. Specifically, many species of negatively charged molecules, such as glycosaminoglycans and serum albumin, can be found in the extracellular compartments and their interactions with the complexes may be unfavorable for transfection. In particular, these molecules can induce aggregation or compete with DNA to bind to polycations [11].

DNA must associate with cell surfaces to initiate the endocytotic process; uptake cannot occur without such an interaction, and increased circulation of the polyplex only increases the chances for renal clearance. Without a delivery vehicle, DNA is unlikely to associate to the cell surface, which has a highly negative charge density due to the phospholipid groups. By shifting the net charge of the overall complex towards net positive charge, i.e. through condensation via polycations, a favorable electrostatic association between the complexes and the cell surface is created. It has been hypothesized that these surface interactions are mediated by heparin sulfate proteoglycans, which are present on all cell surfaces, and also have a high negative charge density [12]. Generally, upon association with the cell surface, nonspecific clatherin mediated endocytosis is likely the preferred method of endocytosis. Other

pathways are accessible, but are in general triggered using targeting moieties or specialized cells [12]. There has been some evidence that cationic agents themselves may induce endocytosis by charged-based modulation of the endocytotic pathway [13].

Upon internalization, the vesicles fuse into an endosome, and escape from this compartment has been generally regarded as the major rate limiting barrier for efficient transfection. In the early endosomal stage two types of early endosomes with different fates have been identified. The sorting endosome redistributes material from the cell surface within the cell, while the recycling endosome returns internalized material to the cell surface and expels it. Currently, there is little knowledge about the factors which determine these endosomal fates, how the two populations are regulated, and if gene delivery systems have a propensity to end up in one or the other. However, if the nanoplex fails to escape at the early endosome stage, it will find itself in either a late endosome or a lysosomal compartment. At this stage DNA is degraded enzymatically.

Several mechanisms of escape have been proposed, and vary by the properties of the particular delivery vehicle. For example, cationic lipids mix with the endosomal lipid bilayer, which leads to membrane destabilization and disruption. The release of DNA is hypothesized to be based on the anionic lipids competing with DNA for binding of the cationic lipids [14]. As cationic and anionic lipids mix and fuse, the charge density of the lipids interacting with the DNA decreases, thus allowing for release of the nucleic acid. This mixing process also destabilizes the endosomal membrane and leads to disruption. Fluorescence experiments demonstrate that this mixing and release occurs early after endocytosis and can be observed as a gradual process [15]. It is interesting to note that disruption only occurs at endosomal membranes and not at cell membranes. Researchers

attribute this difference to different lipid composition at the two interfaces. In an analogous mechanism, cationic polymers such as polyaminoamide (PAMAM) dendrimers and poly-L-lysine (PLL) have been shown to directly disrupt lipid bilayers [16]. PEI has also been shown to disrupt specific membranes, again suggesting that targeting endosome lipid bilayer destabilization can be mediated by lipid composition [17].

Perhaps the most well-known mechanism for endosomal escape is the proton sponge hypothesis. In this process, acidification of the endosome caused by proton pumps in the endosomal membrane, leads to protonation of carriers with a pKa in the slightly acidic range. Simultaneously, as protons are pumped in, counter ions also enter the endosome to maintain electrostatic balance. The increased ion concentration leads to swelling and osmotic lysis [18].

After endosomal escape, DNA must localize to the nucleus for transcription. Free diffusion of plasmid DNA is limited due to the crowded environment, and little evidence has been published for active transport of the plasmid to the nucleus. Unprotected DNA is again subject to nucleases in the cytosol, and it has been reported that the half-life of DNA in the cytosolic compartment is on the order of 50-90 minutes [19]. In the case of polycationic condensing species, there is evidence that DNA may be still partially complexed to cations after endosomal escape [14, 20-22].

In one study injection of PEI or PLL complexed DNA into the cytoplasm led to transfection, whereas injection of the unprotected gene directly did not, suggesting that at this stage protection is still needed [20]. One hypothesis exists that positively charged complexes are passively transported by a gradient of cell localized polyanions. The

complex would traverse from proteoglycans to microtubules, microfilaments, and finally to the nucleic acid rich nuclear region. If this is the case, it would necessitate that the polycationic species remain bound.

The final barrier for transfection is for the nucleic acid to penetrate the nuclear envelope. Delivery of plasmid to the nucleus is essential for transcription, and three possible routes of penetration have been suggested. The first is that the DNA enters through the nuclear pores.

These pores have two conformational states, open and closed. In the smaller closed states, only molecules with a diameter of <9 nm are permitted to diffuse in. In the open state, molecules up to 26 nm may diffuse through the nuclear envelope. Some groups are employing certain techniques to enhance the probability of transport through these pores such as incorporating nuclear localization sequences (NLS), or including binding sites along the DNA sequence for transport proteins such as karyophilic proteins [23]. It has also been hypothesized that cationic regions of the complex may themselves serve as a NLS, but experimental data demonstrates that nuclear localization is still limited. DNA complexed with PLL and PEI directly injected into the nucleus were able to be transcribed, which proves that complexes bound by PLL and PEI are still accessible to genetic machinery [20]. The other hypothesis for localization within the nuclear envelop is that the gene incorporates with chromatin during mitosis, when the cell initiates disassociation of the nuclear envelope [24]. This hypothesis has been supported by examining transfection ability with respect to the cell cycle. Based on the aforementioned biological barriers to gene delivery, it is apparent that there is a need for

a biocompatible delivery vehicle which can provide a mechanism for internalization, endosomal escape, and localization to the nucleus.

1.2 Non-viral vectors for single molecule investigation

While viruses have been nature's method of choice for gene delivery, risk of immunogenic response has led to the development of many non-viral vectors. Previous studies have shown that cationic peptides strongly bind and condense the DNA into nanoscale complexes (polyplexes) [25]. Poly-L-lysine, one of the first polymers to be studied for non-viral gene therapy, is a poor carrier due to limited ability to escape endocytotic pathways [26, 27]. PEI, whose transfection levels have been considered the gold standard in non-viral delivery, has been found to accumulate in cells and induce significant levels of apoptosis, with one PEI study reporting a cell death rate of 98% [28-30]. The overall ability of PEI to act as an effective delivery vehicle is often attributed to its buffering capacity. At physiological pH, approximately 15-20% of the amines are protonated [31]. However, a high buffering capacity may not be the essential parameter controlling gene delivery. It has been shown that acetylation of a 25 kDa branched PEI in amounts up to 43% demonstrated improved *in vitro* transfection [32]. Titrations confirmed that acetylation decreased buffering capacity, yet enhanced transgene delivery was observed in two cell lines.

1.2.1 Histidine-lysine peptides

Histidine-lysine based peptides have been developed as a gene delivery carrier based on a design that combines lysine residues for DNA compaction, and histidine residues to mimic the proton sponge capacity for which PEI is often credited for its transfection ability [33]. For this dissertation the particular HK peptides used have four

branches around a three-lysine core (Figure 1.1). Each branch has a repeating sequence of three histidines and a lysine. For the HK peptides used in this work, each of the four branches has the sequence: GKHHHKHHHGKHHHKHHHK. Earlier research has shown that polymers consisting of lysine and histidine or imidazole containing groups are able to efficiently transfect an array of cell lines, up to four orders of magnitude higher than with PLL, without cytotoxic effects [34, 35].

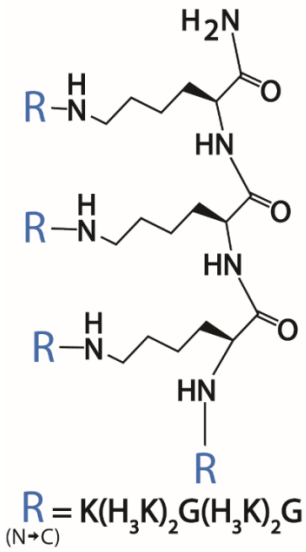

Figure 1.1 Structure of HK peptide, showing a three lysine core and the amino acid sequence of each branch.

1.2.2 Surface-modified gold nanoparticles

AuNPs are good candidates for gene delivery applications for several reasons including ease of functionalization and synthesis [36]. Their small size leads to a high surface area-to-volume ratio which maximizes the payload/carrier ratio. Additionally, they can be synthesized with good control of charge and hydrophobic properties by controlling ligand attachment. The gold nanoparticle cores are also regarded as being non-toxic [37].

The particular nanoparticles of interest have been developed by the Rotello group at the University of Massachusetts, Amherst, and are functionalized using polyethyleneimine-like triethylenetetramine (TETA) ligands (Figure 1.2) [38]. The particles have a 2 nm gold core and approximately 80 ligands per particle; this leads to a maximum charge of +240, +480, and +960 for G0, G1, and G2 particles respectively. The particles combined with the ligand shell leads to a hydrodynamic diameter of $d_{G0} = 11.7 \pm 4.1\,nm$, $d_{G1} = 15.7 \pm 3.8\,nm$, and $d_{G2} = 15.7 \pm 4.5\,nm$. These sizes make them comparable to histone octamers which have been reported to be 6.5 nm in diameter [39]. G2 nanoparticles have been proven to be efficient in delivering siRNA *in vitro*; DNA transfection results have not been reported. Lysine coated nanoparticles, however, have demonstrated the ability to deliver plasmid DNA, with branched lysine moieties enhancing the transfection. The improvement as compared to poly-L-lysine was 5-fold for the lysine AuNPs and 28-fold for the AuNPs functionalized with a branched lysine moiety [38].

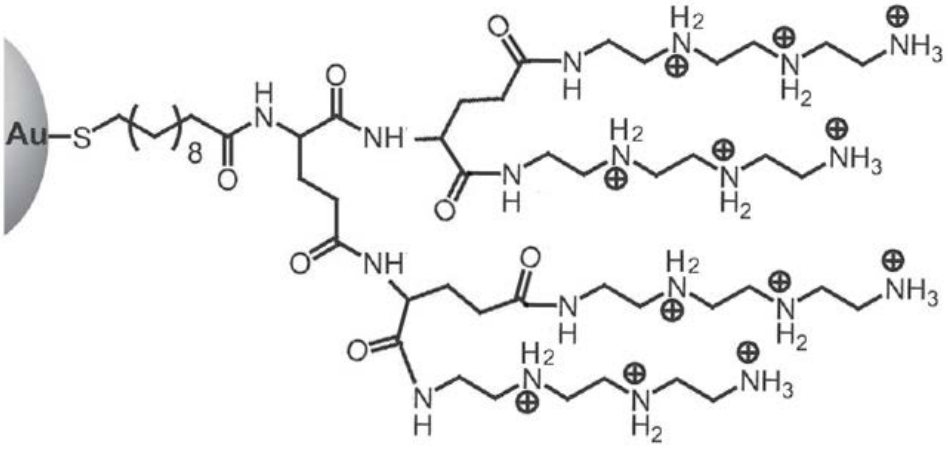

Figure 1.2 Structure of G2-TETA. Modified from [40].

1.2.3 Dual responsive polymers

This work will also seek to compare the aforementioned delivery systems with dual responsive polymers. Specifically, we aim to characterize the mechanical properties and dynamic environmental response of a block copolymer developed for *in vivo* gene transfer developed by the Pun Lab at the University of Washington. The particular polymer we intend to test is composed of a poly(ε-caprolactone) (PCL) block, a oligoamine tetraethylenepentamine (TEPA)-poly(glycidyl methacrylate) (PGMA) block, and an oligo (ethylene glycol) block; the blocks are hydrophobic, pH-responsive, and hydrophilic, respectively. The rationale behind the design of this particular polymer is that the PCL block provides improved blood circulation time, as well as low toxicity due to biodegradability, and the pH responsive block is suggested to aid in endosomal escape [41]. After the complex enters the cytoplasm, the reductive environment may be able to remove the PCL block via reduction of a di-sulfide bond and thus initiate release of DNA from the polymer similar to the predicted mechanism for release from gold nanoparticle systems. *In vitro* studies have shown this ternary copolymer to be capable of transfection with both plasmid DNA as well as siRNA.

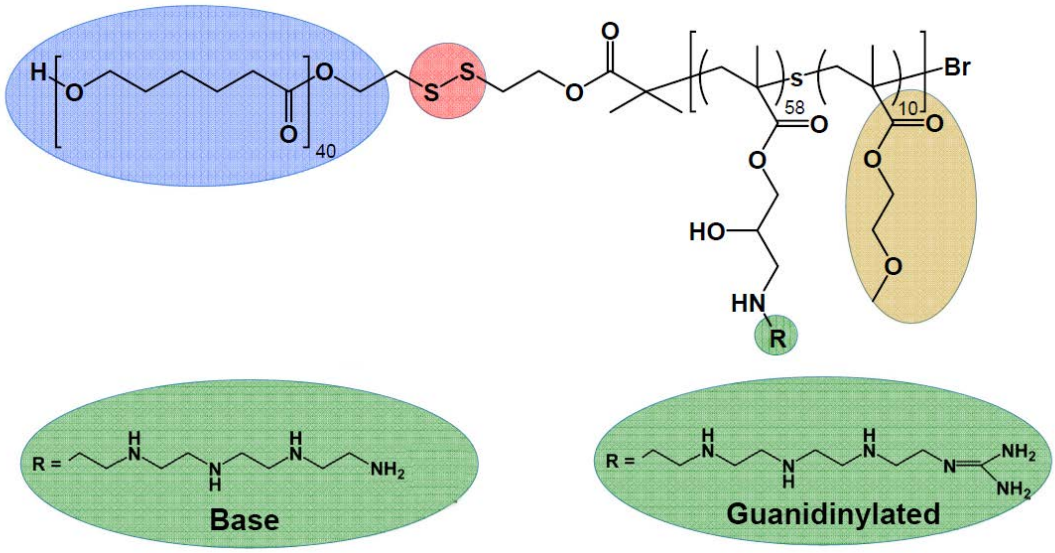

Figure 1.3 Structure of base and guanidinylated copolymers. PCL block is indicated in blue, ethylene glycol in yellow, and the TEPA-PGMA block is in green with both the base and guanidinylated structures shown. Modified from [42].

1.3 Optical tweezers

Custom built optical tweezers will be used to directly probe the DNA compaction and release process, similar to methods used to probe the structure of chromatin, multivalent cation interactions with DNA, and PAMAM:DNA complexes (Figure 1.2) [43-46]. The optical tweezers uses a focused laser beam to trap a dielectric bead near the focal point [47-49]. Figure 1.2a shows a schematic of the optical path. Infrared light from twin diode lasers (845 nm) is carried through optical fibers into piezo-electric wigglers. The piezo-electric optical fiber wigglers move the end of the optical fiber and thus move the trap. A small fraction of the light is picked up by a pellicle beam splitter and sent to a position sensitive detector (PSD) to infer the trap positions. Light leaving each trap is collected by the opposite objective and directed, by virtue of its polarization, into force-detector optics: two momentum-flux detectors measure force on the trapped object by changes in the momentum of the trapping light, without laborious calibration [50, 51].

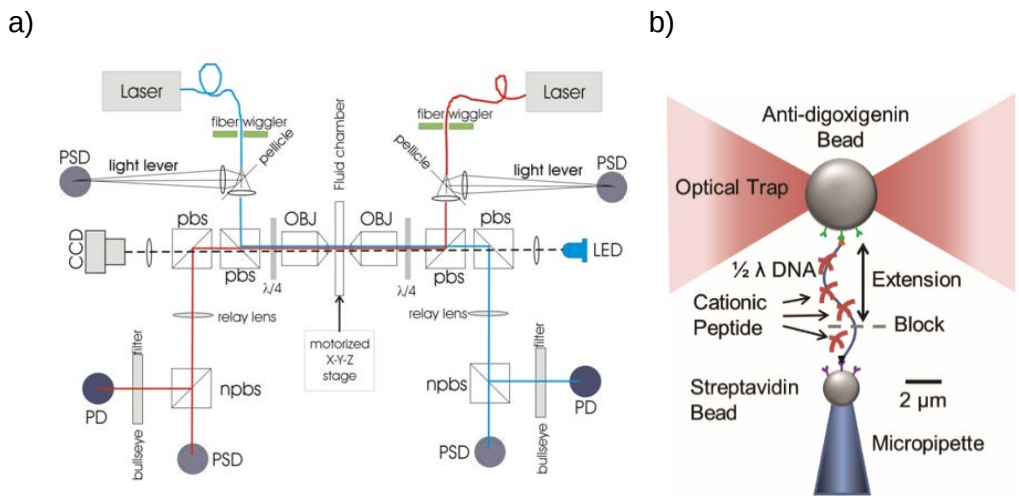

Figure 1.4 a) Schematics of optical paths. Components: OBJ=water immersing objective lens, pbs=polarizing beam-splitter, PSD=position-sensitive photo detector, PD=photodiode, npbs=non-polarizing beam-splitter, CCD=charge coupled device camera, LED=light emitting diode. b) Schematic showing optical tweezer setup.

The fluid sample chamber is fixed on a motorized x-y-z stage. The instrument is equipped with force clamping capability that enables us to monitor the extension variation at constant force level with millisecond time resolution. The force resolution is less than 1 pN and the spatial resolution is ~1 nm [50, 51].

1.3.1 Single molecule studies of DNA

The mechanics of single molecule dsDNA has been well characterized using optical and magnetic tweezers. The force vs. extension behavior of DNA has reliably fits worm-like-chain dynamics [52]. At a physiological salt concentration (150 mM NaCl), dsDNA will exhibit a persistence length of ~47 nm, and thus, based on a known contour length of the molecule, the force extension curve can be predicted. Because DNA has well defined properties, it is an ideal system to study the changes as other molecules are incorporated to the system. The force profile of DNA has been studied bound to

intercalating agents, and major/minor groove binders [53]. Intercalation drastically changes the elastic response of DNA to force, and can readily be observed [54, 55].

Mechanics of DNA condensation have also been studied in various systems using optical tweezer setups. Chromatin fibers have been examined to determine the nature and strength of the molecular level interactions between histone proteins (and their aceytlated tails) and DNA [43, 56, 57].

More recently, these approaches have also been applied to DNA:cationic condensing systems such as multivalent cations, PAMAM dendrimer, and self-aggregating cationic and hydrophobic peptides [44-46, 58]. These studies not only act as proof of concept that mechanical changes in DNA are easily identifiable, it also suggests that regulation of DNA condensation and unraveling is a biological task that the cell already performs on a regular basis.

1.4 Significance and innovation

Despite all the steps taken to circumvent biological barriers, **the efficiency of delivering genes via non-viral carriers has not yet improved to the point where they are clinically useful.** Surmounting these barriers requires delicate regulation of the forces for efficient protection and release of the nucleic acids. In recent work, single molecule techniques have provided direct evidence about how mechanical force may influence gene regulation in biological systems [59]. For instance, individual nucleosomes have been disrupted by the application of forces between 20-40 pN [43]. The procession of RNA polymerase is shown to be halted around 20 pN [60]. Viruses compact DNA inside their capsules exerting ~70 pN forces [61]. Additionally, DNA polymerases can exert 15 pN to separate DNA [62]. These single molecule measurements indicate that the

interaction forces of DNA complexes are highly regulated. These results suggest that interactions between DNA and cationic carriers need to be carefully regulated within a narrow force range in order for transfection to proceed without any mechanical barriers. In particular, it has been demonstrated that binding inhibits transcription, which suggests modulation of the release of DNA may be of utmost importance [63].

This body of work aimed to measure interaction forces between DNA and cationic carriers under relevant environmental stimuli in order to establish a quantitative measure of the complex mechanical response. Force-based criteria can subsequently be applied for the intelligent design of novel cationic carriers with improved transfection efficiencies.

This work is innovative because it capitalizes on the ability of the optical tweezers to directly measure the mechanical properties of the complex formed from a single DNA molecule in real time, including response to sequential changes of environment. The advantages of single molecule data include the ability to track a single "complex" through various changes. This is accomplished by the use of microfluidics which allows for a well-controlled and well-defined environment. Whereas biological assays have variation due to cell line, culturing conditions, etc., the environmental parameters such as solute species, solute concentrations, pH, and solvent quality are all precisely and accurately tuned in the microfluidics setup. This becomes useful when extreme conditions, such as high salt (as compared to physiological conditions), are necessary to perturb responses that would not otherwise show up *in vitro* or *in vivo.*

Another benefit of the single molecule setup is the ability to observe various responses and see the whole ensemble of possible behaviors. In bulk, typically the result from the average ensemble behavior is the only one observed. Optical tweezers allow for the exploration of the temporal aspect of the response and observe the time evolution of a particular single molecule response. Additionally, by approaching characterization from a mechanical standpoint, these assays may show differences between carriers that have similar physical properties or chemical compositions. Being equipped with a resolution of 0.1 pN and 1 nm makes the optical tweezers very sensitive to changes that may otherwise be missed in other force spectroscopic tools such as AFM or magnetic tweezers. Another limitation of AFM is the necessity of the sample to be surface bound, and the optical tweezers allows for molecular level interactions to occur in all three dimensions in a relatively unconstrained manner.

Bulk experiments cannot track the process, just correlate the start point with the result and the coupling of single molecule to bulk studies will provide a mechanistic understanding of transfection outcomes due to different carriers.

2 Direct Observation of Dynamic Mechanical Regulation of DNA Condensation by Environmental Stimuli[1]

2.1 Introduction

Gene therapy, the delivery of genetic materials to targeted cells, has great potential for the treatment of hereditary diseases and cancers [26]. Significant efforts have been made to develop effective carriers in viral and non-viral platform [26]. Non-viral carriers have been extensively investigated because of their lower toxicity and more facile manufacture in comparison to viral vectors. Among non-viral carriers, synthetic cationic peptides have been shown to strongly bind and condense DNA into nanoscale complexes that are an effective platform for delivery [25]. However, the efficiency of delivering genes via synthetic carriers has not yet improved to the point where they are clinically useful. The potential reasons for limited efficiency lie in the set of physiological obstacles that the complexes must navigate: these include the stable transport of packaged DNA in the bloodstream, targeting to specific cells, endocytosis, endosomal escape, unpackaging of DNA, and nuclear transport. Surmounting some of these barriers requires delicate regulation of the forces between nucleic acid and carrier. For example, stable and uniform interaction between carrier and nucleic acid is required to protect DNA in the bloodstream, but later or in response to changes in the environment the interaction needs to weaken to release nucleic acids from the complex. However, there is a lack of understanding of the optimal interaction forces required to protect or

[1] This chapter has been adapted (with permission of the publisher) from: Lee, A., et al. (2014). "Direct observation of dynamic mechanical regulation of DNA condensation by environmental stimuli." Angewandte Chemie, International Edition in English **53**(40): 10631-10635.

release DNA and how these forces are regulated under various physiological environments, which prevents rational design of more efficient carriers for gene delivery.

Single molecule force spectroscopy can provide mechanistic insights into biological processes at a level of detail inaccessible in bulk studies [60, 64, 65]. Previously, interaction forces between DNA and a cationic polyaminoamide (PAMAM) dendrimer were measured at the single molecule level [46]. The interactions are electrostatic, and dendrimers remained bound to DNA after a washing step, exerting ~10 pN forces during stretching. Recently, the mechanical properties of the complex between DNA and the self-aggregating peptide Kahalalide F were measured using optical tweezers, revealing a two-step kinetic process that forms highly rigid aggregates via electrostatic interaction and hydrophobic collapse [58].

Here, we use optical tweezers to directly observe dynamic changes in the interaction forces between DNA and carrier in response to concentration, pH and metal ions. Custom-built tweezers with high force and spatial resolution are utilized to probe mechanical behaviours of DNA complexes [66]. Two different cationic peptide agents, 19-mer poly-L- lysine (PLL), and histidine-lysine (HK) based peptides, are examined to compare dynamic behaviours as they interact with DNA.

Histidine-lysine based peptides have been developed as a gene delivery carrier that contains lysine residues for DNA binding and compaction, and histidine residues to carry out the proton sponge mechanism for endosomal escape [33]. The ~80-residue HK peptides used here have four branches around a three-lysine core (Figure 1.1). Each branch has a repeating sequence of HHHK. with the exact sequence of each branch being C-term-GKHHHKHHHGKHHHKHHHK-N-term. Compared to PLL, HK based peptides

have been found to be more effective transfection agents in vitro and in vivo (Chapter 5). Linear PLL is known to condense DNA, but its transfection efficiency from previous work was found to be marginal [67].

2.2 Materials and methods

2.2.1 Materials

Streptavidin (SA)-coated beads (2.1-μm nominal size, Spherotech, Lake Forest, IL) and anti-digoxigenin (AD)-coated beads (4.26-μm nominal size, Spherotech, Lake Forest, IL) are used for the optical tweezers experiments. The DNA construct was synthesized using the method developed by Stone and colleagues, with modifications.[68] Briefly, the single-stranded cos sites of lambda phage DNA were exposed and filled in with a dNTP cocktail containing biotin-14-dATP and biotin-14-dCTP (Life Technologies, Grand Island, NY) using Klenow exo- (New England Biolabs, Ipswich, MA). On the other hand, the digoxigenin-labeled linker was prepared by polymerase chain reaction (PCR) using lambda phage DNA as template, oligonucleotides 5'- TGATTTCCAGTTGCTACCGA -3' and 5'-CAGGTATCGTTTGGAGGCAG -3', and a dNTP mixture containing digoxigenin-11-dUTP (Roche Diagnostics, Indianapolis, IN). The labeled DNA linkers were each digested with XbaI (New England Biolabs, Ipswich, MA). The digestion product from the digoxigenin-labeled DNA was dephosphorylated, and subsequently ligated to the digestion product of the biotinylated DNA. The ligated product was called as ½λ DNA. HK polymers and PLL were synthesized with a Rainin Voyager synthesizer (PTI, Tucson, AZ) in ~100 μg/mL concentrations.

2.2.2 Optical tweezer setup and force measurements

Before the pulling experiment, the beads are first blocked for 20 minutes with 5 mg/mL BSA (Sigma, St. Louis, MO) and 0.1% Tween20 (Sigma, St. Louis, MO). After incubation, beads are centrifuged, the supernatant (which contains excess BSA) is removed, and the beads are re-suspended in a buffer containing 0.1 mM Tris, 150 mM NaCl, 1 mM EDTA, and 0.05% sodium azide, pH 7.4 (Buffer A). AD beads are then incubated with ½λ DNA for 10 minutes. The SA beads are trapped on a micropipette tip and remain stationary during the experiments. AD beads are held by the optical trap. A dsDNA tether is created by moving the AD bead into close proximity to the SA bead and allowing the biotin-labeled end to bind to the SA beads. The beads are separated by a ~5.5 µm block distance imposed by the optical trap which prevents the beads from touching or allowing nonspecific adsorption of DNA onto the bead surfaces. The rate of stretching and relaxation was varied from 50 to 500 nm/sec. The data collection rate was 100 Hz and no data smoothing was performed. The presence of a single DNA molecule between the beads was confirmed by observing the overstretching transition at ~65 pN. Injection of 1 µM peptide solution into the chamber is carried out at a rate of 5 µL/min. To change buffer conditions within the chamber, the complex is washed with 100 µL of a buffer, at a rate of 10 µL/min. Because the channel volume is ~30 µL and the flow is laminar, washing with ~3 times the channel volume is sufficient for a complete exchange of a buffer.

2.2.3 Force profile analysis

Worm-like-chain (WLC) model fitting

Relaxation curves were fit using the Marko-Siggia model [52].

$$F = \left(\frac{k_B T}{L_p}\right)\left[\frac{1}{4\left(1 - {}^{x}/_{L_o}\right)^2} - \frac{1}{4} + \frac{x}{L_o}\right]$$

Where F is force, k_B is Boltzmann's constant, T is temperature, L_p is the persistence length, L_0 is the contour length of the DNA molecule, and x is the extension. The curves were fit from 0-5 pN to avoid a deviation from the model due to elastic modulus contribution. In cases where there was a reduction in contour length, the calculated L_0 was used as a fitting parameter to find the persistence length. (See the following section on contour length calculation)

Contour length calculation

The contour length was obtained by the following method (Figure 2.1). The contour length was calculated by taking a linear fit to the elastic regime of the force profiles near maximum extension (at forces between 30 and 50 pN, where R^2 of linear least squares fitting is greater than 0.95). From each linear fit, the x-intercept was calculated. The difference between the linear fit of the naked DNA and the linear fit for a particular force curve represent a change in contour length. At force ranges above 30 pN we assume that the entropic contribution to the elasticity is negligible, and the force extension relation describing this portion of the line is:

$$F = \left(\frac{K}{L_0}\right)x - K$$

where L_0 is the contour length, K the stretch modulus, x the length and F the force on the biopolymer [43]. Thus the x-intercept ($F = 0$) is where $x = L_0$.

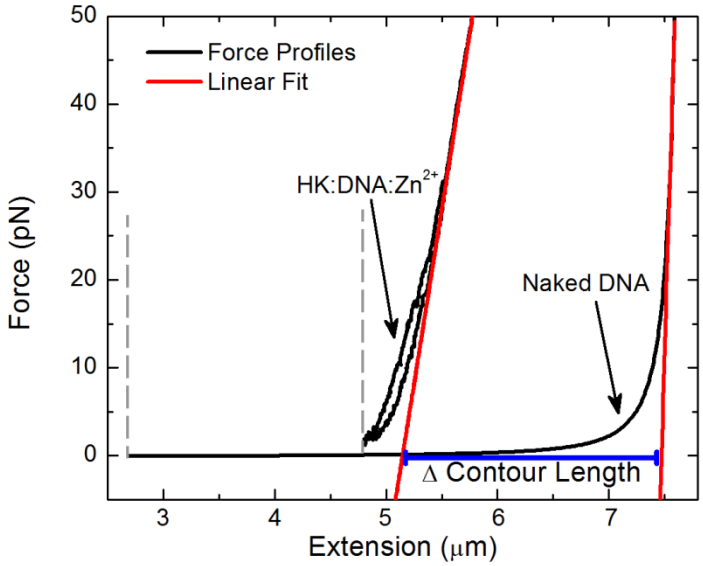

Figure 2.1 Calculation of contour length in the presence of Zn^{2+}. The change in contour length between any force curve and the initial DNA molecule is calculated by linear fitting to the 30-50 pN range of the curves. The x-intercepts ($\boldsymbol{F = 0\ pN}$) are equal to the contour lengths.

Plateau force measurement

For a particular experimental condition, the force values for either the stretch curve or relax curve are graphed as a histogram using Igor Pro 6 (WaveMetrics, Portland, OR). The bin width was autoset and a total bin number was 100. The histogram is then fit with a Gaussian distribution to determine the mean and standard deviation of the plateau force distribution (Figure 2.2).

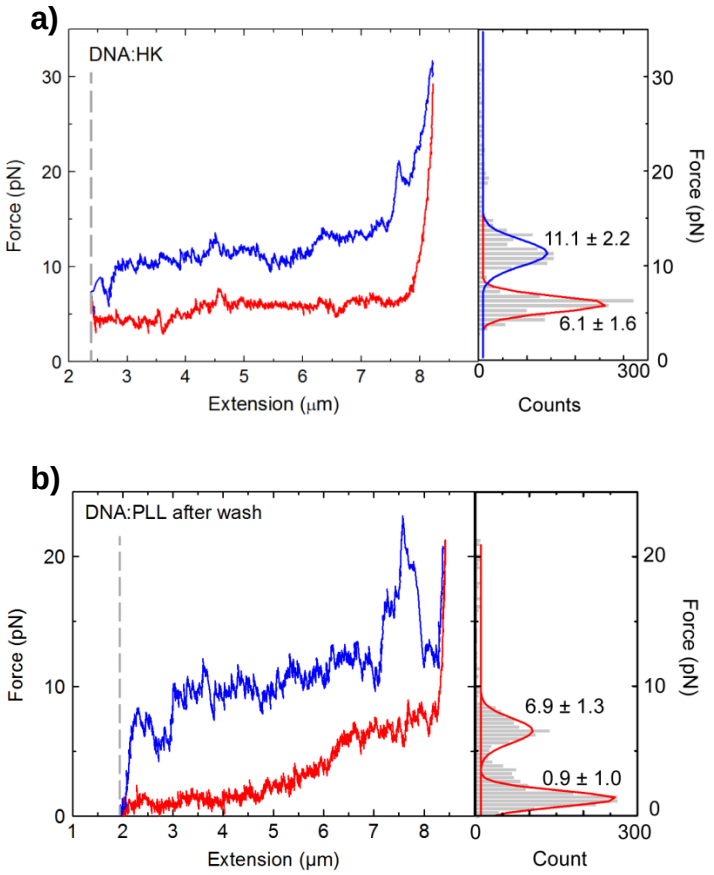

Figure 2.2 Plateau force calculation using a histogram fitting method. (a) From a representative DNA:HK force curve, a histogram is created from the forces recorded for both the stretching (blue) and relaxation (red). The histograms are fit with Gaussian distributions (blue curve to fit data during stretching and red curve to fit data during relaxation) to determine the mean and standard deviation of the plateau forces. (b) A representative DNA:PLL curve after washing exhibits double plateau behavior. Two peaks in the histogram of relaxation curve forces indicates the presence of the double plateau.

2.3 Results and discussion

In our experimental setup, ½ λ double stranded DNA (24 kbp) is functionalized with biotin and digoxigenin and tethered between two beads via specific interactions (Figure 1.1a and Experimental Section) [68]. The upper bead was moved up and down in the optical trap to stretch and relax DNA. The extension distance was controlled by

setting a block that limits the range of motion of the top bead. During injection of agents, the block location was initially set at ~5 µm from the lower, pipette-fixed, bead. In a typical experiment, 1 µM of condensing agent in a buffer (155 mM NaCl, 0.1 mM Tris pH 7.4, 1 mM EDTA, and 0.05% sodium azide) was injected into the chamber at a rate of 5 µL/min while DNA was stretched and relaxed at a rate of 500 nm/s. Injection was stopped after 5 µL, when force profiles that clearly deviated from naked DNA features had developed and stabilized. The condensed DNA is identified by the appearance of stretching and relaxation force plateaus and hysteresis. All the reported force values are the average at least three experiments unless otherwise specified.

2.3.1 Bound PLL displays resistance to washing compared to bound HK peptide

As PLL or HK binds to DNA, the force profile of naked DNA (black trace in Figures 2.3 a and b) is gradually changed to show plateaus during a stretching and relaxation cycle (dark green in Figure 2.3a, dark blue in Figure 2.3b). The appearance of these force plateaus shows that both PLL and HK exert a tension and actively condense DNA. Plateau forces remained at relatively similar levels; no distinctive sawtooth pattern was seen in the profiles, indicating that the binding between DNA and both agents is rather uniform, without apparent large loops or bridged structures. The stretching plateau is at 11.2 ± 0.7 pN for the DNA:HK complex and 12.6 ± 1.6 pN for DNA:PLL (Figure 2.2). Upon slowing the pulling rate down to 50 nm/sec, a decrease in the stretch plateau and an increase in the relaxation force are observed, indicating that the force profile becomes quasi-equilibrium behaviour at the slower rate (Figure 2.4). These force plateau levels are similar to those of PAMAM dendrimers, which showed a stretching plateau at

~10 pN [46], but they are well below the range of rupture forces of nucleosomes, which are observed between 20 and 40 pN [43].

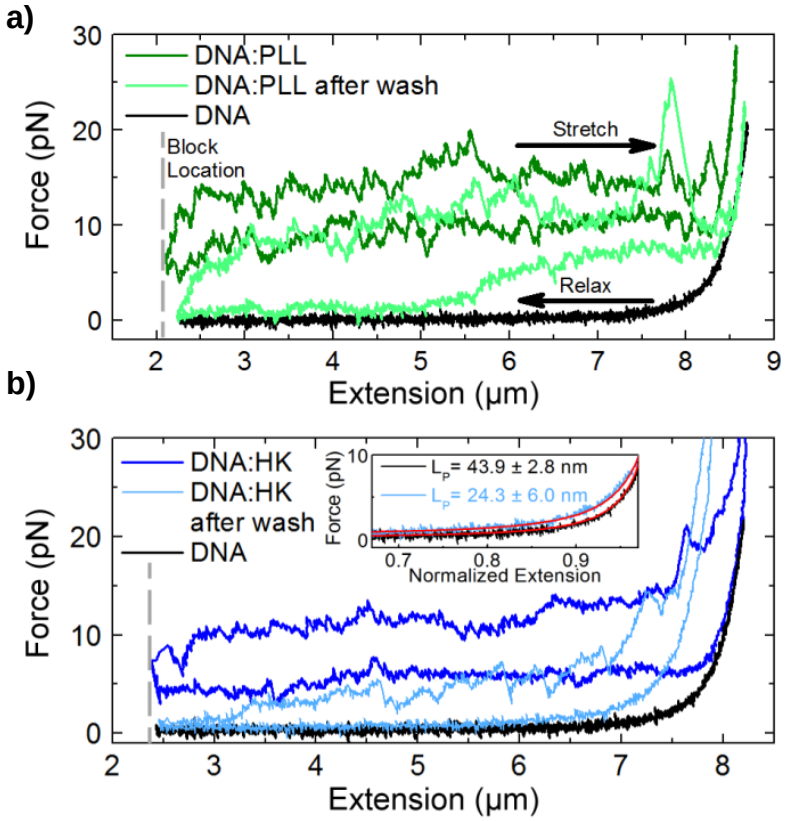

Figure 2.3 Force vs extension profiles of (a) 1 μM PLL and (b) 1 μM HK solution after peptide injection (dark green and dark blue) and after washing (light green and light blue) with Tris buffer. The force vs extension curve of naked DNA is shown in black. The inset in (b) shows the Worm-like-chain model fits for the relaxation curves of naked DNA and the HK:DNA complex after washing.

For HK, the relaxation plateau occurs 6.6 ± 0.4 pN, and similarly PLL is at 8.1 ± 1.4 pN. These relaxation plateau values are similar to the critical condensation force at which an active condensation starts for protamine (~6 pN), and spermidine (~7 pN) [45]. The relaxation plateaus for HK and PLL are higher than that of PAMAM dendrimer (~4 pN) and the critical condensation forces of other multivalent cations such as spermine (~3 pN), cobalt hexamine (1.5 pN), and cobalt sepulchrate (3.5 pN) [45, 46]. The plateau

forces decreased as ionic strength increased, demonstrating that the driving force of this active condensation is largely due to electrostatic interactions between the phosphate backbone and the cationic peptides (Figure 2.5).

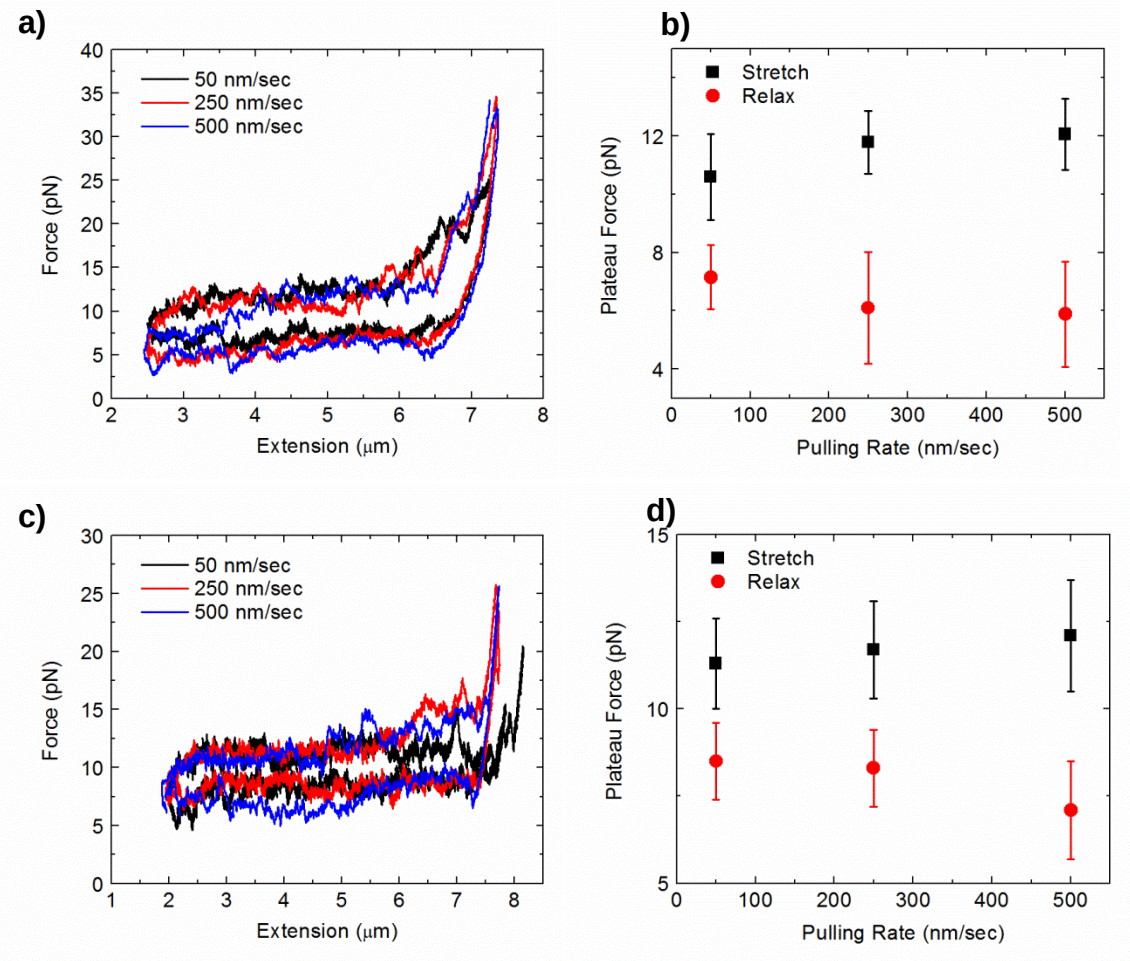

Figure 2.4 The effect of a pulling speed on a plateau force. (a) For DNA:HK complexes, variation of the pulling rate from 50 nm/sec to 500 nm/sec showed a decrease in the relax plateau force and an increase in the stretch plateau force. (b) Stretch plateau forces for 50 nm/sec, 250 nm/sec, and 500 nm/sec are 10.60 ± 1.47 pN, 11.78 ± 1.08 pN, and 12.05 ± 1.22 pN respectively. Relaxation plateau forces for 50 nm/sec, 200 nm/sec, and 500 nm/sec are 7.15 ± 1.11 pN, 6.10 ± 1.91 pN, and 5.88 ± 1.81 pN respectively. (c) For DNA:PLL complexes, variation of the pulling rate from 50 nm/sec to 500 nm/sec showed a decrease in the relax plateau force and an increase in the stretch plateau force. (d) Stretch plateau forces for 50 nm/sec, 250 nm/sec, and 500 nm/sec are 11.29 ± 1.27 pN, 11.66 ± 1.38 pN, and 12.06 ± 1.59 pN respectively. Relaxation plateau forces for 50 nm/sec, 250 nm/sec, and 500 nm/sec are 8.50 ± 1.10 pN, 8.32 ± 1.08 pN, and 7.10 ± 1.41 pN respectively.

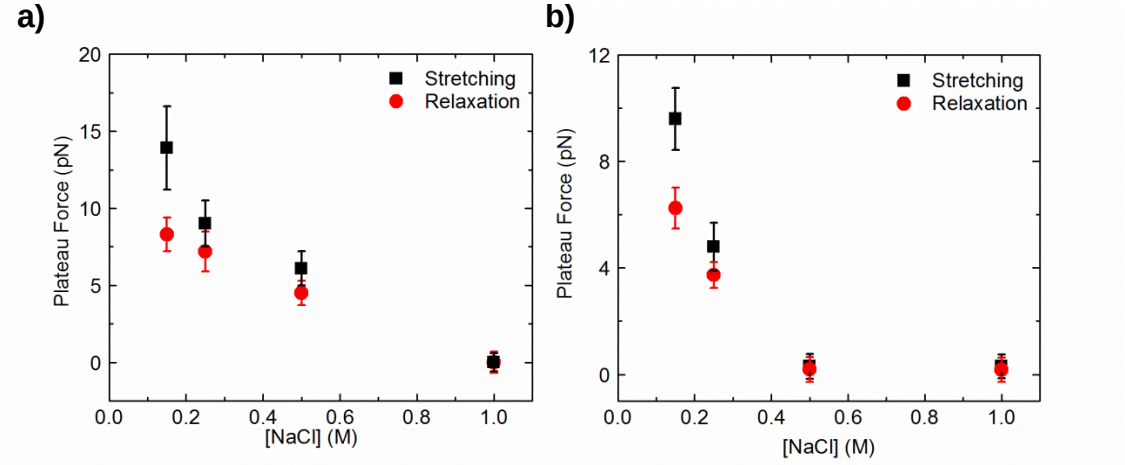

Figure 2.5 The effect of salt on a plateau force. (a) For DNA: HK complexes, titration of NaCl concentration in buffer containing 10 mM acetate, 1 mM EDTA, 0.05% azide at pH 5.0 from 150 mM up to 1 M showed decreasing plateau values until naked-like behavior was obtained at 1 M NaCl. (b) DNA: PLL complexes, as titration of NaCl concentration in 10 mM tris, 1 mM EDTA, 0.05% azide at pH 5.0 increases from 150 mM up to 1 M showed decreasing plateau values until a WLC profile was obtained at 0.5 M NaCl and naked-like behavior is recovered at 1M NaCl. Error bars represent the width of the Gaussian distribution reported by Igor.

To mimic the process of diluting prepared complexes into the bloodstream or a cellular environment lacking free cationic peptides, we washed away free condensing agent by injecting buffer into the chamber. Upon washing the PLL:DNA complex (Figure 2.3a, light green), double relaxation plateaus (at 0.8 ± 1.2 pN and 5.1 ± 3.6 pN) were observed in two out of three experiments, suggesting formation of heterogeneous structure; single plateau behaviour was observed once (Figure 2.6). The stretching plateau decreased slightly (10.5 ± 3.6 pN) indicating that most of PLL molecules still remain bound to DNA after buffer injection.

In sharp contrast, HK showed a significant decrease in both stretching and relaxation plateaus after washing (Figure 2.3b, light blue). The relaxation plateau disappeared, showing a naked DNA -like behaviour, while the stretching plateau value

decreased to 4.8 ± 5.3 pN. The decreases in both plateau forces is attributed to detachment of a significant number of HK molecules from the DNA, thus leading to a net negatively charged complex which exerts lower condensing force after washing. This result is similar to the concentration dependence of condensation force of multivalent ions, for which a decrease in condensation force is observed at lower concentration [45].

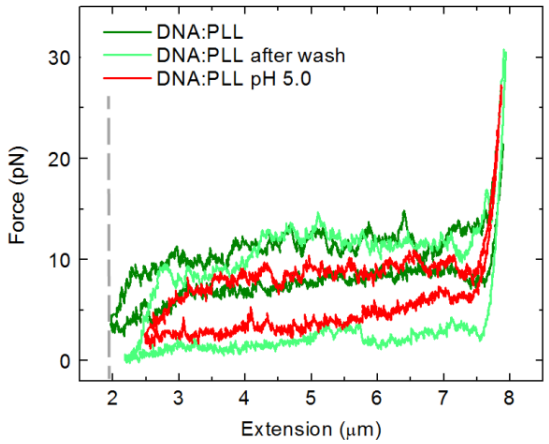

Figure 2.6 The effect of pH on the force profiles of DNA:PLL complex. DNA is condensed with 1 μM PLL (dark green) in tris buffer (pH 7.4). After washing with peptide free buffer (light green), the force profile for this particular experiment exhibits a single plateau in the relax curve. The overall features of the PLL force profile remained similar in the presence of acetate buffer (pH 5) with a decreased hysteresis, showing no significant effect of low pH on their force profiles as observed in HK.

Additionally, the relaxation curve of DNA:HK complex returned to worm-like chain behaviour, with a reduced persistence length (L_p) of 24.3 ± 6.0 nm (n=5) compared to a naked DNA (L_p = 43.9 ± 2.8 nm, n=6). The decrease in L_p is presumably due to charge screening by the HK that still remains bound to DNA after washing [69], as observed for the condensation of DNA by other agents [58, 70]. The observations that the tensile resistance during stretching deceases significantly and the relaxation profile resembles naked DNA behaviour indicate that HK:DNA complex may release HK

readily, allowing more efficient unpackaging when the concentration of cationic agents in the surroundings is low.

2.3.2 DNA:HK complex recovers force plateaus at pH 5

To simulate the low pH environment that the DNA complex would experience upon endocytosis, acetate buffer at pH 5 (10 mM acetate, 155 mM NaCl, 1 mM EDTA, and 0.05% azide) was introduced into the chamber at a rate of 10 µL/min after washing with Tris buffer. The pH drop did not elicit any changes in mechanical behavior of the DNA:PLL complex (Figure 2.6) whereas for the DNA:HK complex, stretching and relaxation plateaus reappeared at 14.0 ± 1.8 pN and 10.0 ± 1.0 pN respectively (Figure 2.7. The return of both plateaus at pH 5 is likely due to the protonation of the 48 histidine residues (pKa ~6) in each HK molecule that remains bound during washing. The increased positive charge density of HK allows stronger electrostatic interactions between HK and DNA. The stretching plateau and relaxation plateau levels decreased as salt concentration increased from 150 mM to 1 M, confirming that electrostatic interactions are the major driving force for active condensation at low pH. (Figure 2.5)

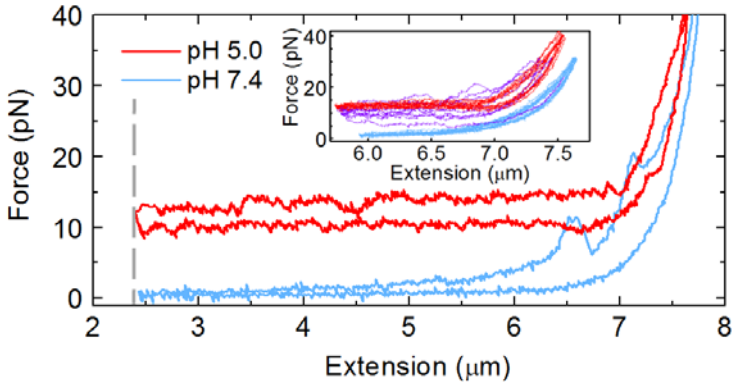

Figure 2.7 The effect of pH on the force vs extension profile of a DNA:HK complex. Force curves at pH 7.4 after washing and at pH 5 are shown in light blue and red respectively. Inset shows dynamic transitional behavior (purple) of force profiles while the pH was changing from 7.4 to 5.

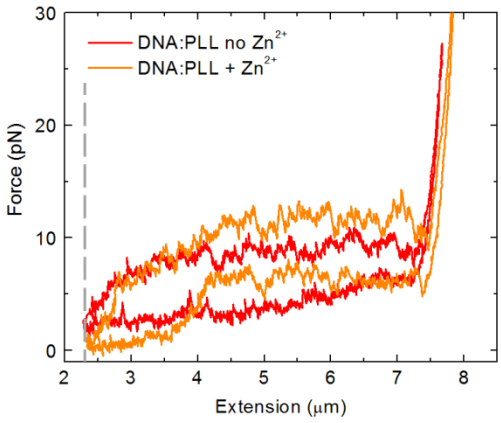

Figure 2.8 The effect of Zn^{2+} on the mechanical properties of DNA:PLL complex. Addition of 1 mM Zn^{2+} did not result in shortening of contour length for a DNA:PLL complex. The stretch plateau in the presence of Zn^{2+} is at 11.1 ± 0.3 pN, and the relax plateau is 6.3 ± 0.5 pN ($n = 3$).

2.3.3 Zn^{2+} chelation reversibly induces a mechanically rigid DNA:HK complex

The dynamic response of the DNA:HK complex was further examined in the presence of divalent cations. When 1 mM Zn^{2+} in acetate buffer (pH 5) was injected into the chamber, the DNA:PLL force profile did not change (Figure 2.8), whereas the DNA:HK complex became mechanically very stiff and its contour length significantly decreased, contracting nearly to the block location at ~5.5 μm (Figure 2.9a and 2.1). The maximum force available in the optical trap (~100 pN) was not large enough to disrupt the complex formed in the presence of Zn^{2+}. Subsequent stepwise movement of the block location in 500 nm increments (dotted grey line) caused corresponding decreases in the contour length of the complex (arrows in Figure 2.9a and b). This indicates that when the complex is allowed to contract, it interacts with zinc ion to form highly mechanically resistant structures (Figure 2.9b). The average final contour length was 2.87 ± 0.26 μm when the final block location was ~2 μm. The compaction does not always continue indefinitely (2 out of 4 experiments), and there is a slack region where the complex

extends at relatively low force (< 2 pN) with no apparent hysteresis (Figure 2.9a). Worm-like chain fitting of the slack region reveals that the persistence length is much longer than that of naked DNA, up to an average of 187.5 ± 23.0 nm (n=3; Figure 2.10). The shape of the force profile along with the increased persistence length indicates that a very stiff complex is formed as DNA:HK complex interacts with Zn^{2+}. A similar behavior is observed when DNA is collapsed by a hydrophobic peptide, although in that case the rigid complex is constrained by hydrophobic forces [58, 71].

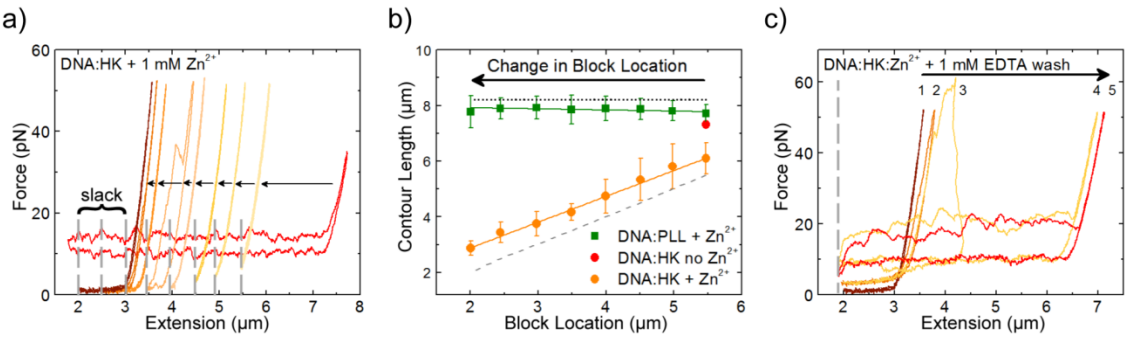

Figure 2.9 The effect of Zn2+ on the mechanical behavior of the DNA:HK complex. **(**a) The red force profile for the DNA:HK complex was obtained after washing at pH 7.4 and then decreasing the pH to 5. As 1 mM Zn^{2+} is added, the maximum extension decreases markedly, indicating the formation of a mechanically rigid complex. Sequential movements of the block location by 500 nm (yellow to brown) resulted in a further decrease of extension as indicated by arrows. (b) A plot of contour length (from fits to the worm-like chain model) vs. block location for the DNA:PLL complex and the DNA:HK complex. The dotted black line represents the original DNA contour length and the dashed grey line shows the 1:1 line between block location and contour length as a guide to the eye. (c) Recovery of extension upon washing with 1 mM EDTA. Numbers indicate sequential stretching and relaxation cycles.

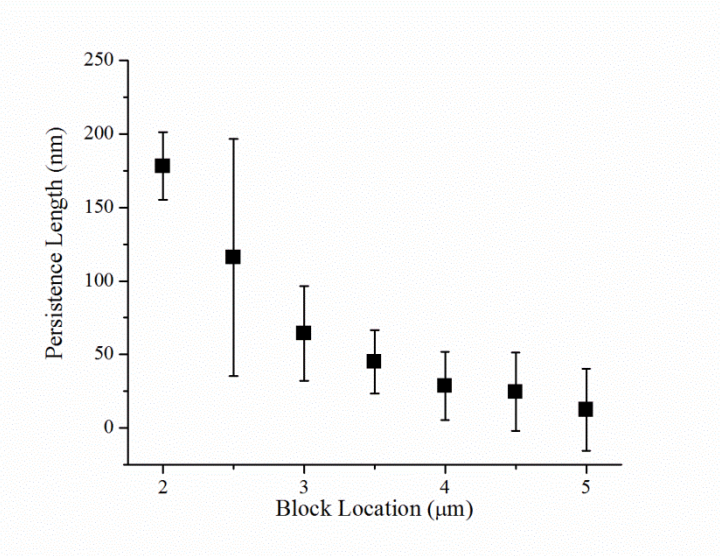

Figure 2.10 The apparent persistence length of the complex increases as the DNA:HK complex shortens in the presence of Zn^{2+}. Worm-like chain fitting revealed that as the complex is compacted, the apparent persistence length increases from 12.4 ± 28.0 nm up to 187.5 ± 23.0 nm as the HK-DNA complex is allowed to pull to a block location of 2 μm ($n = 3$).

The phenomenon of Zn^{2+} inducing the formation of a stiff DNA:HK complex is reversible upon injection of 1 mM EDTA in acetate buffer at pH 5. Within a few stretching/relaxation cycles, the initial contour length is recovered, with reappearance of force plateaus, showing that removal of Zn^{2+} allows the rigid complex to recover its original characteristics (Figure 2.9c). The dissociation constants of Zn^{2+}/EDTA and Zn^{2+}/Histidine are 1×10^{-16} M [72] and 8.8×10^{-13} M [73] respectively, so EDTA should readily chelate Zn^{2+} ions away from histidines in the rigid complex. Other cations such as Mg^{2+} and Ca^{2+} had no effect on force profiles and did not form a mechanically resistant complex (Figure 2.11).

The highly mechanically resistant complex induced by Zn^{2+} is proposed to originate from chelation by multiple imidazole groups in histidine residues [74].

Incorporation of a bi-histidine metal chelation site into a protein, GB1, has demonstrated an increase in mechanical stability in the presence of Ni^{2+} [75]. For DNA:HK, the fact that the relaxation by moving the block location is required to form the stiff complex suggests that participation of multiple histidines in HK polymers which are far apart from each other along the DNA is essential for polydentate coordinated complex formation.

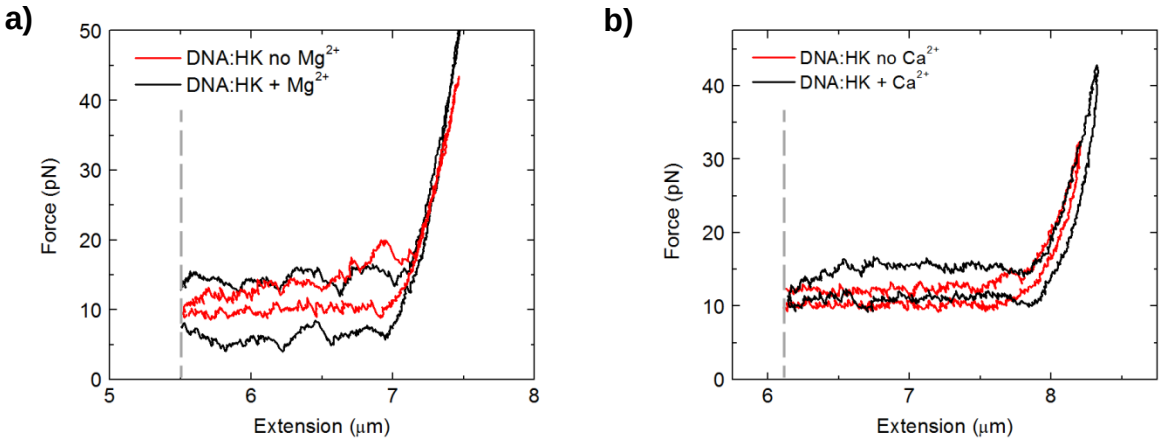

Figure 2.11 DNA:HK complexes maintain constant contour length in the presence of Mg^{2+} or Ca^{2+}. The addition of either (a) 1 mM Mg^{2+} or (b) 1 mM Ca^{2+} did not result in decreasing the contour length for a DNA:HK complex.

The rupture force of Ni^{2+}/histidine coordination is a few hundred pN based on force spectroscopy [74]. The dissociation constant of Zn^{2+}/histidine (8.8×10^{-13} M) is lower than that of Ni^{2+}/histidine (5×10^{-7} M) and the corresponding $\Delta G_{dissociation}$ is calculated to be 16.5 kcal/mol and 8.6 kcal/mol respectively [72, 76]. Although mechanical stability may not be directly correlated with thermodynamic stability [77], we expect that a similar or higher force would be needed to disrupt the DNA:HK in the presence of zinc ions, considering the nature of the interaction is the same.

Our mechanical measurements using a single DNA molecule complexed with peptides demonstrated that environmental changes can cause significant differences in the

mechanical properties of a DNA:peptide complex. Specifically, the DNA:HK complex showed dynamic changes in mechanical properties at multiple force levels which could be exploited during the gene delivery process. When a DNA:peptide complex is injected into the bloodstream, it may undergo shear or elongational forces which may disrupt the complex, increasing chances of degradation of DNA [78].

Previously, it was noted that supplementation of transfection medium with $ZnCl_2$ improved the transfection efficiency of a histidylated polylysine up to 40-fold [67]. It was believed that the fusogenic properties of Zn^{2+} with lipid membranes played a large role in endosomal escape. Based upon our data, addition of Zn^{2+} to histidine-containing peptides resulted in a highly mechanically stiff complex, which could be advantageous in maintaining the stability of the complex when it is in contact with bodily fluids. In addition, coordinated Zn^{2+} is expected to increase the zeta potential of the complex, which should enhance membrane interactions. Histidine protonation is likely to interact with endosomal membrane and destabilize it, enhancing endosomal escape. Both pathways will contribute to enhanced transfection efficiency. Zn^{2+} is considered relatively non-toxic and is maintained at micromolar concentrations in the blood plasma and millimolar concentrations in the cell; however, within the cytosol, concentrations of free Zn^{2+} are reduced to the femtomolar level by metalloregulatory proteins [79-81]. These Zn-binding proteins could compete for Zn^{2+} ions and facilitate release of the DNA:HK complex. Additionally, if protonation in the endosome occurs to the extent that the HK:DNA complex becomes overcharged, some HK molecules may be shed, accelerating the unpackaging process.

Recently, single molecule techniques have provided direct evidence about how mechanical force may influence gene regulation [59]. For instance, individual nucleosomes are disrupted at 20-40 pN [43]. The procession of RNA polymerase is halted at around 25 pN [60] and DNA helicase is known to exert 10-15 pN to separate DNA [62]. In our washing experiments, DNA:HK showed lower stretching and relaxation plateau forces than DNA:PLL, which suggests that HK is more easily removed from DNA than PLL. The fact that the stretching plateau force is ~5 pN suggests that HK is likely to be a more effective carrier in terms of allowing the unpackaging of DNA by endogenous nucleic acid processing systems. Previously, it was shown that multivalent cations such as spermine are completely washed away from DNA, as indicated by the disappearance of force plateaus [44]. In contrast, the DNA complex with PAMAM dendrimer does not show changes in force plateaus after washing, indicating that dendrimers are irreversibly bound [46]. One key parameter that may govern the mechanical response to washing is the number of charged groups per molecule. Spermine has a +4 charge and PAMAM (5^{th} generation) has +128 charges, whereas HK and PLL contain +17 (at pH >7) and +20 charges respectively. Despite small differences in total charge per molecule, the observed variation in washing effect for HK vs. PLL may be attributed to linear charge density along the peptide backbone; at pH 7.4, PLL has a charged group on every residue, while only ~25% of the residues along each HK branch are charged. Hence, both the total charge of the molecule and its charge density need to be considered to optimize interactions between DNA and condensing agents. It is also likely that secondary interactions such as hydrogen bonding between the HK peptide and nucleic acid may play a role in stabilizing the complex [82].

3.4 Conclusion

Transfection studies indicate the importance of the size and charge of cationic polymers in controlling transfection efficiency [83, 84]. However, there have been few studies probing how charge regulation affects mechanical properties of the complex directly under various environments. Poly-L-lysine, one of the first polymers studied for non-viral gene therapy, is a poor carrier unless coupled with endosomolytic agents [25, 27]. Polymers consisting of lysine and histidine or other imidazole-containing groups are able to efficiently transfect an array of cell lines, up to four orders of magnitude more effectively than PLL, without cytotoxic effects [34, 35].

Our observations at the single molecule level reveal that there are multiple levels of interaction forces between DNA and HK polymers depending on the environment. After washing, a minimal level of interaction forces (<5 pN) was observed for HK, but at pH 5, the stretching plateau increased to 14 pN. In the presence of Zn^{2+}, the complex became very strong and was not unraveled, indicating that a force greater than 100 pN is required. These forces and their responses to pH changes could be regulated judiciously by changing sequences and branching patterns, with the end goal being higher transfection efficiencies. Furthermore, the enhanced stability conferred by metal-ion chelation demonstrated here may be largely responsible for enhanced serum stability of the histidine containing peptide. The inclusion of histidine in the HK peptide allows for enhanced washing, force modulation based on pH, and stabilization by Zn^{2+}, all of which may contribute to enhanced transfection. Finally, we suggest that single molecule techniques may serve as a platform for screening condensing agents for desirable mechanical properties prior to *in vivo* experiments.

3 Observation of Multi-stage DNA Condensation by Dendronized Gold Nanoparticles and Polyethyleneimine Using Optical Tweezers

3.1 Introduction

For the past couple of decades, gene therapy has been researched for its potential applications to treat human diseases, such as muscular dystrophy, cystic fibrosis, neurological ailments, or cancer [85]. Identifying and transferring therapeutic genes into target cells can alter gene expression, implement posttranslational modifications to proteins, or produce cytotoxins and prodrug-activating enzymes, which can be powerful and effective therapies to cure fatal diseases [26].

There are two major modalities in gene delivery: recombinant viral vectors and synthetic non-viral vectors [26, 86]. Viral vectors are infectious agents that require hosts for replication and expression of its genome, parts of which can be replaced with a therapeutic gene. They have been successful in entering target cells and navigating to a nucleus for gene expression [85]. However, viral vectors have significant drawbacks such as the need for repeated administration, the possibility of dangerous immune reactions, the risk of reversion to a wild-type virus, and high manufacturing expenses, all of which make viruses less advantageous for clinical use. In contrast, synthetic vectors provide advantages in terms of safety, structural flexibility, and low cost of manufacturing [26]. These are typically positively charged materials which bind and condense negatively charged nucleic acids via electrostatic interactions. Current limitations of using synthetic vectors include poor gene transfer efficiency in physiological conditions, due to

extracellular barriers such as DNA complex bloodstream stability, as well as intracellular obstacles including endosomal escape, cytoplasmic transport, or unpackaging [26]. Microinjection experiments of plasmid DNA directly into the cytosol have demonstrated that nuclear localization is limited, emphasizing the importance of protection in the cytosol [4]. Furthermore, there is evidence that if DNA remains bound to the carrier within the nuclear envelope that transcription may be inhibited [87].

We hypothesize that mechanical regulation of interactions between DNA and a carrier based on environment are key to providing the appropriate protection and release necessary for successful transfection. In the realm of high-resolution force spectroscopy, optical tweezers are appropriate instruments for identifying and quantifying the forces involved with DNA condensation at the molecular level. A tightly focused laser beam is utilized to trap a dielectric particle in three dimensions, and the particle is manipulated by beam movement. Simultaneously, distance and force are detected with a resolution of 1 nm and 1 pN respectively [49, 52]. Optical tweezers have been utilized to demonstrate that cationic agents interact with DNA over a range of forces and kinetic steps for DNA:peptide or DNA:kahalalide complexes [58, 88]. They are able to distinguish transient and stepwise interactions that are otherwise difficult to observe in ensemble behaviors during condensation [58].

Our recent single molecule studies showed that there are histidine lysine branched peptide applies a force along the DNA upon binding and this force could be modulated by environmental conditions. Washing into peptide free buffer decreased interactions forces, whereas protonation at pH 5 and chelation of Zn^{2+} by the histidine residues were both able to increase the interaction forces, chelation leading to an order of magnitude increase

in force [88]. These interactions, measured at the single molecule level, provides insight as to how a DNA:cationic carrier will respond within the biological milieu.

The two cationic carriers investigated in this study are 25 kDa branched polyethylenimine (PEI) and a cationic dendronized gold nanoparticle (AuNP). PEI, whose transfection levels have been considered the gold standard in non-viral delivery, has been found to accumulate in cells and induce significant levels of apoptosis, with one PEI study reporting a cell death rate of 98% [28-30]. The overall ability of PEI to act as an effective delivery vehicle is often attributed to its buffering capacity. At physiological pH, approximately 15-20% of the amines are protonated [31].

In addition, the condensation and release process of G2-triethylenetetramine (TETA) nanoparticles will be examined. These nanoparticles have been previously developed with the aim to incorporate a PEI-like ligand, however with reduced toxicity due to the AuNP core.[40] G2-TETA has been demonstrated to be efficient for siRNA delivery with high knockdown efficiency and low toxicity [40]. This study aims to investigate the mechanical behaviors of DNA complexed with PEI or functionalized AuNP to compare them and correlate the mechanical profiles with their transfection efficiencies.

3.2 Materials and methods

3.2.1 Materials

25 kDa branched polyethyleneimine was purchased from Sigma Aldrich, St. Louis, MO. The synthesis of G2-TETA nanoparticles is described in detail in a previous paper, and they were generously supplied by the Rotello Research Group at the University of Massachusetts, Amherst [40]. Structures for both are shown in Chapter 1.

These dendronized nanoparticles are structured using a 2 nm diameter gold core decorated with polyethylenimine-like ligands. The ligands are based on a glutamic acid scaffold that is end terminated by cationic triethylenetetramine.

Streptavidin (SA)-coated beads (2.1-µm nominal size, Spherotech, Lake Forest, IL) and anti-digoxigenin (AD)-coated beads (4.26-µm nominal size, Spherotech, Lake Forest, IL) was used for the optical tweezer experiments. The double end-labeled ½ λ was prepared as described in Chapter 2.

3.2.2 Force measurements

The experimental setup used has been previously reported [88]. In summary, SA and AD beads are first blocked for 20 minutes with 5 mg/mL BSA and 0.1% Tween20. After incubation, beads are centrifuged, the supernatant (which contains excess BSA) is removed, and the beads are re-suspended in a buffer containing 10 mM Tris, 150 mM NaCl, and 0.05% sodium azide, pH 7.4. AD beads are then incubated with ½λ DNA for 10 minutes.

For the duration of the experiment, the SA beads are fixed on a micropipette tip and remain stationary. AD beads are held by the optical trap. A dsDNA tether is created by moving the SA bead into close proximity to the AD bead with DNA and allowing the biotin-labeled end to bind to the SA beads. The presence of a single DNA molecule between the beads was confirmed by detecting the overstretching region at ~65 pN as well as fitting with the Marko-Siggia WLC model. The rate of stretching and relaxation was 500 nm/sec and data was collected at a rate of 100 Hz without data smoothing. Stretching is performed by moving the trap relative to the micropipette, and force and extension are recorded.

.

3.2.3 General and pulse protocols for condensation

For the optical tweezer experiments, we stretched a single ½ λ-DNA and condensed the molecule using G2-TETA nanoparticles or PEI. The experimental setup used has been previously reported [88].

Injection of condensing agents in 10 mM Tris buffer (150 mM NaCl, 0.05% azide, pH 7.4) is injected into the chamber at a rate of 5 µL/min. During injection, a block location of 5.5 µm is maintained. After 100 µL has been injected, the block location is reduced by 500 nm increments and the complex is allowed adequate time to form a steady state at each location.

For the DNA:PEI salt and heparin stability experiments, in order to capture transient plateau profiles, a pulse method of condensation was utilized. For this protocol, cationic agent solution is injected 1 µL at a time, waiting 5 minutes between each injection. The injection is discontinued when the desired force profile has been achieved.

3.2.4 Changing the microfluidic environment

To change buffer conditions within the chamber, the complex is washed with 100 µL of a buffer, at a rate of 10 µL/min. With a channel volume of ~30 µL and the presence of laminar pressure driven flow, washing with ~3 times the channel volume is sufficient for complete solution exchange.

Stability in solutions containing either 5 mM glutathione (GSH), 5 mg/mL heparin (Sigma Aldrich, St. Louis, MO), 1 M NaCl, or 5% SDS in 10 mM Tris buffer (150 mM NaCl, 0.05% azide, pH 7.4) is also tested. To test pH response, 10 mM acetate buffer (150 mM NaCl, 0.05% azide, pH 5) is injected into the chamber.

3.2.5 Force profile analysis

The protocols for worm-like chain fitting, contour length analysis, and plateau force measurement reported in Chapter 2 were also utilized to analyze the single molecule data collected for the DNA:G2-TETA and DNA:PEI systems.

All statistics are reported as mean and standard deviation unless otherwise noted. Number of molecules averaged for a reported value is n=3 unless otherwise indicated.

3.3 Results

3.3.1 PEI Demonstrates Overcharging Behavior When Condensing DNA

When DNA is condensed with 10 nM PEI, a dynamic maximization and reduction of force plateaus was observed (Figure 3.1). Shortly after injection, there is a sudden appearance of stretching and relaxation plateau forces. These plateau forces have been seen to reach a maximum of up to 27.2 ± 11.5 pN (n=3) for the stretch, and 13.3 ± 11.2 pN (n=3) for the relaxation curve in 10 nM PEI experiments, requiring 2.93 ± 0.25 k_BT/bp to stretch the complex. After reaching that maximum plateau force, the curves begin to decrease in plateau value and hysteresis until the relaxation curve returns to WLC behavior with a little hysteresis. This dynamic process is illustrated in Figure 3.1, which shows curves at 100 s, 170s, and 1040s after beginning the injection of PEI. It is important to note that it takes 1200 seconds to complete the injection process and that all these curves are collected as PEI is continuously being added to the system.

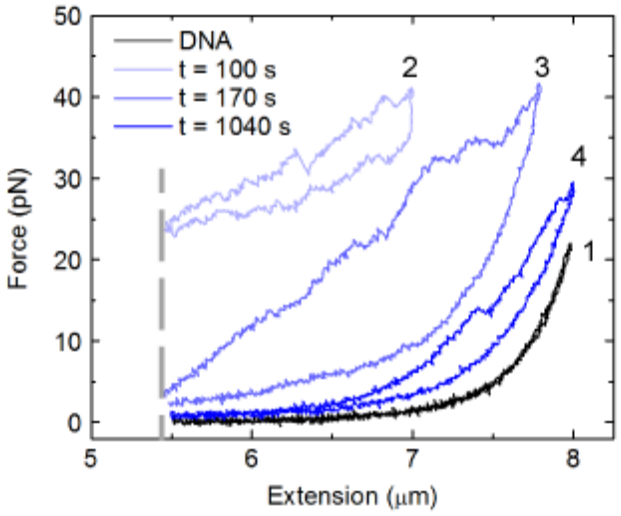

Figure 3.1 Dynamic plateau behavior is observed during condensation with 10 nM PEI. DNA pulling curves before (#1, black), and at various time points during injection of 10 nM PEI: 100 s (#2), 170 s (#3) and 1040 s (#4). Pulling cycles are taken between a minimum extension of 5.5 μm and a maximum pulling force of 40 pN or a maximum extension of 8 μm, whichever is reached first.

The same process is also observed for DNA fibers condensed with 5 nM PEI (data not shown). For the 5 nM condition, maximum plateaus observed are 30.7 ± 6.9 pN (n=7) and 20.8 ± 4.5 pN (n=7) for stretching and relaxation plateaus respectively. The appearance and disappearance of force plateaus during the injection process is evidence for overcharging of the DNA:PEI complex. The process of overcharging, or charge inversion, has been described for multivalent cations [45]. In this phenomena, the negatively charged DNA becomes less negative as multivalent cations bind and condense the fiber. As the concentration of the cations increases, the complex passes a net neutral point; at even higher concentrations, the complex is net positive and is considered overcharged. It has been shown that condensing force has a direct correlation to charge state, and that at near neutral conditions multivalent cations applied maximum condensing force on the DNA [45]. The dynamic appearance and then decrease in plateau

in the force profiles of PEI-condensed DNA suggest the ability to create an overcharged complex. The overcharged state (10 nM) involve minimal decrease in extension length (0.7 ± 0.5 µm shortening (n=3)), and its relaxation profile has mechanical properties similar to that of naked DNA ($\boldsymbol{L_p}$ = 47.4 ± 1.7 nm). The stretch curve however, shows a WLC fit with a persistence length of 19.0 ± 2.1 nm (n=3). We believe that the PEI bound DNA is able to exhibit naked like DNA mechanics in the overcharged state because the accumulation of positive charge creates the same repulsive columbic force that the high density of phosphates provided initially.

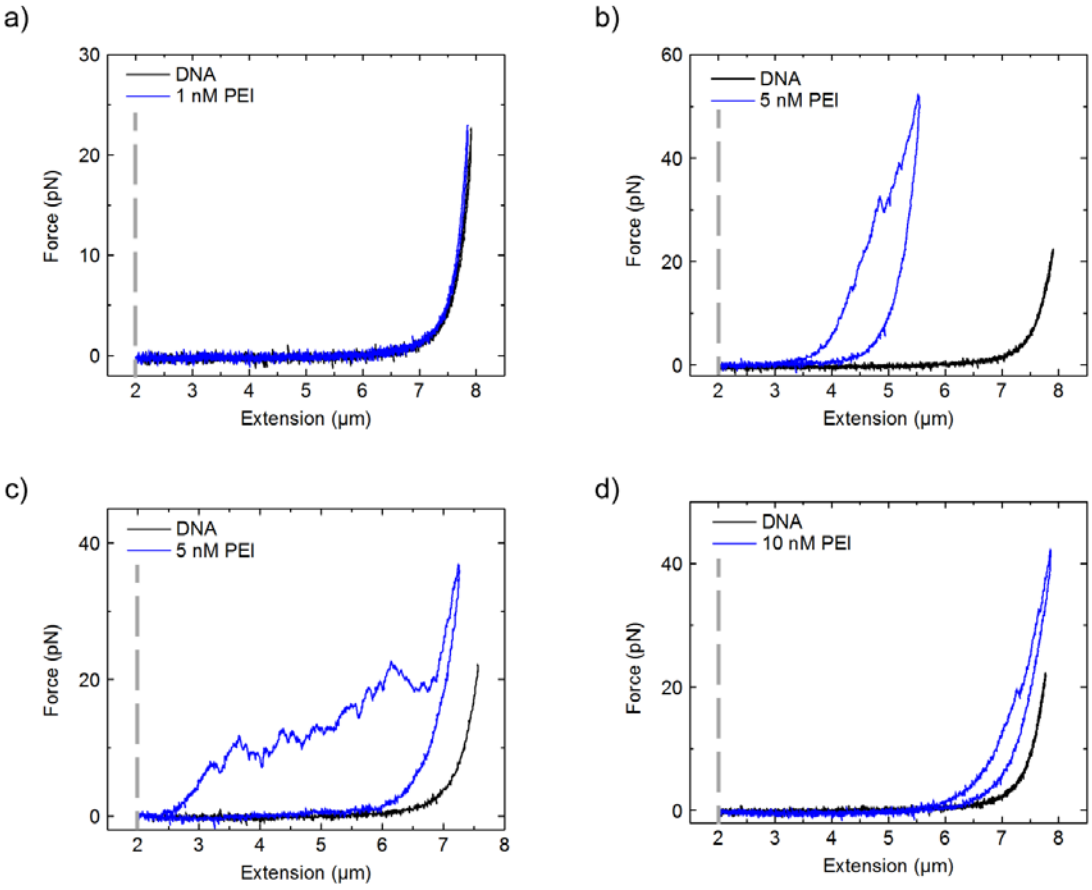

Figure 3.2 Representative force extension profiles of DNA condensed with varying concentrations of PEI. In all four profiles, the original DNA force profile is shown in light gray. Final profiles of DNA condensed with a) 1 nM, b,c) 5 nM, or d) 10 nM PEI are depicted in black.

The variation of force profiles for DNA:PEI complexes as a function of concentration further illustrate the likelihood of overcharging. Representative force profiles of DNA condensed with either 1 nM, 5 nM, or 10 nM PEI are shown (Figure 3.2). 1 nM PEI shows no hysteresis and has L_p of 40.6 ± 8.1 nm (Figure 3.2a) (n=3). There is no appreciable reduction in the contour length. At 5 nM concentration (Figure 3.2b-c), we see a decrease in persistence length down to 35.8 ± 13.5 nm, and an average shortening of 2.14 ± 1.76 μm (n=6). The decrease in persistence length can again be attributed to local bending due to the positive charges of a PEI molecule minimizing columbic repulsions between phosphates on the DNA backbone. At the 5 nM concentration, it is important to note that sawtooth unbinding events occurs over a broad range of force levels (10-40 pN). This is in contrast to other systems such as PAMAM dendrimer, poly-L-lysine, and histidine-lysine peptides which show narrow range of forces at which binding occurs [46, 88]. The discrepancy may be due to the high polydispersity of the branched PEI (polydispersity index = 2.5), thus effectively having a population of molecules with varying binding affinities. As the concentration is increased to 10 nM concentration (Figure 3d), observed persistence length increases back up to 47.4 ± 1.7 nm (n=3), and complexes exhibit an average shortening of 0.69 ± 0.56 μm (n=3). In this overcharged regime, long range bridging is unlikely to occur because of charge-charge repulsions between PEI molecules.

The concentration effect data demonstrates that DNA:PEI complexes can transition from undercharged, to neutral, to overcharged within an order of magnitude change in concentration. We believe that at 5 nM PEI the complex is already overcharged, as we are able to observe the dynamic appearance and decrease of plateaus.

However, the degree of overcharging can vary depending on actual number and size of PEI molecules bound, resulting in varying final contour lengths. It can be concluded that the mechanical response of a DNA molecule is sensitive to a narrow concentration range of PEI and that the net neutral condition leading to maximum condensation is between 1-5 nM. Furthermore, we observe a lack of condensation at the undercharged and overcharged regimes which is reminiscent of reentrant condensation observed in multivalent cation systems; exposure to multivalent cations induced compaction of DNA, however further increase in cation concentration allowed DNA to adopt an extended conformation [89].

3.3.2 Salt and Heparin Destabilize DNA:PEI Complexes

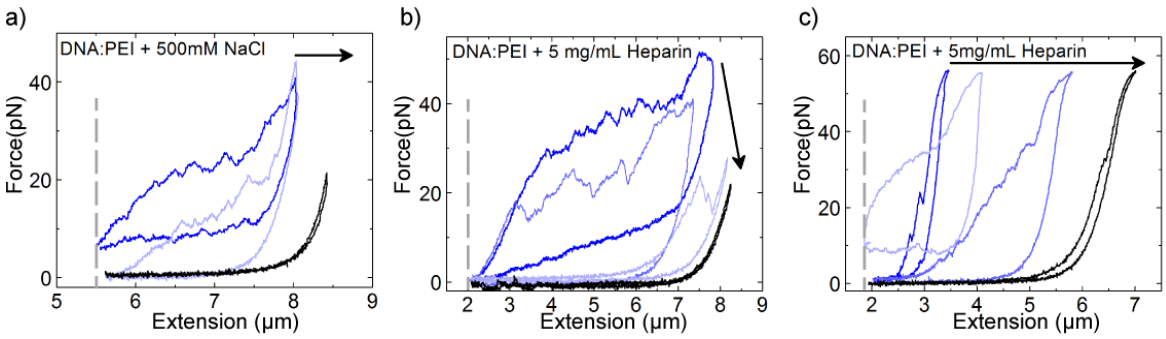

Figure 3.3 a) DNA condensed with 5 nM PEI exhibiting force plateaus was washed with 10 mM tris buffer (pH 7.4, 500 mM NaCl, 0.05% EDTA) and resulted in a decrease in plateau forces and then transition to original contour length and WLC mechanics. b) DNA condensed by injection of 5 µL of 10 nM PEI showed a similar effect when treated with 5 mg/mL heparin in 10 mM tris buffer (pH 7.4, 150 mM NaCl, 0.05% EDTA). c) DNA condensed by injection of 8 µL of 10 nM PEI showed formation of a strongly condensed complex with a decreased contour length. Washing with heparin resulted in the appearance of plateaus which then continued to decrease in force and hysteresis while recovering ~ 3µm contour length.

A major assumption of the overcharging model is that electrostatics are the major contributing force in determination of the mechanical properties of condensed DNA. To verify this hypothesis, complexes were prepared using the pulse method to produce a

force profile with stable plateau forces; washing with high salt (500 mM NaCl) demonstrates return to naked-DNA properties (Figure 3.3a). A complex formed with 1 nM PEI exhibiting plateaus but did not show the full dynamic increase and decrease in plateau values, was treated with 500 nM NaCl. This salt concentration was sufficient to remove both the stretching and relaxation plateaus, as well as return the molecule to the original complex length (Figure 3.3a, black curve). A similar effect was able to be accomplished by exposing a complex condensed with 10 nM PEI (limited to 5 µL injection rather than the full 100 µL to capture the complex in a mechanical state where the force plateaus are preserved) to the tris buffer supplemented with 5 mg/mL heparin (Figure 3.3b). In both of these cases the dynamic response first show a decrease in plateau forces, which directly translates to a decrease in interaction forces between the PEI and DNA, leading to recovery of worm like chain mechanics.

Another complex was formed by injecting 8 µL of 10 nM PEI and collapsed to a 3.9 ± 0.1 µm contour length. The full injection volume of 100 µL is not used so as to capture the transient plateau behavior of the DNA:PEI complex. As heparin is introduced into the chamber, there is an appearance of stretching and relaxation plateaus, followed by decrease in plateaus, and all accompanied by a recovery of contour length (Figure 3.3c). The initial appearance of plateaus follows the hypothesis that PEI is able to exert strong electrostatic interactions at forces >50 pN. The addition of heparin into the system can compete with DNA to interact with PEI thus decreasing the concentration of bound PEI available to condense DNA, until the DNA is released. In experiments b-c perturbation of the condensate with either high salt or heparin recovered 93.68 ± 10.94%

of the contour length. In fact, both high salt conditions as well as heparin have been shown to disrupt condensates in bulk [90].

Additionally, complexes condensed with 10 nM PEI were washed with 10 mM Tris buffer containing 1 M NaCl (not shown). Addition of 1 M NaCl to the buffer showed destabilization of the complex, a disappearance of hysteresis, and 0.5 µm recovery of contour length (not shown). The high salt treatment screened electrostatic interactions and allowed for release of PEI, thus providing evidence that electrostatic interactions play an essential role in stabilization of the condensed DNA.

Washing back in to the low salt (150 mM) condition, showed a collapse of the molecule and significant shortening, with 4.2 µm (n=1) of shortening (not shown). This force profile is reminiscent of DNA condensed with 5 nM PEI. This confirms that 1 M NaCl removes some PEI from the complex, thus decreasing the net charge and leading to the formation of a more stable compact complex. This salt effect showed that electrostatic interactions are important both in regulating the condensation of the complex as well as direct binding of PEI to DNA.

3.3.3 DNA:PEI Complex Mechanics are pH Sensitive

Exposure to a decrease in pH was used to simulate the low pH environment that the DNA complex would experience inside the endosome. Using a slow pulse method of injection we could ensure that limited PEI was bound. 5 µL of 1 nM PEI was injected 1 µL at a time, waiting 5 minutes between each injection. The resulting force profile (Figure 3.4a, black) exhibited limited hysteresis, no and no observed binding or unbinding events when brought to 2 µm block, and no observations of plateaus. Fitting with the worm like chain model resulted in a persistence length of 45.5 ± 0.1 nm (n=1)

and contour length of 8.4 µm. Any unbound or free PEI was washed using 1 mM Tris (150 mM NaCl and 0.05% azide) buffer injected at a rate of 10 µL/min.

The drop to pH 5 was achieved by injection of 100 µL of 10 mM acetate buffer (150 mM NaCl and 0.05% azide), introduced into the chamber at a rate of 10 µL/min. Injection of acetate caused the appearance of hysteresis along with a decrease in the extensible length of the complex (Figure 3.4a). As the block location is reduced the complex continues to form a mechanically non-decondensible region with a final contour length of 3.7 ± 0.6 µm (n=1). The appearance of hysteresis, plateaus, and rigid structures at pH 5 is likely due to the protonation of the PEI molecules that remains bound during washing. The increased positive charge density of PEI at low pH allows the molecules to initiate condensation via increased electrostatic interactions between PEI and DNA. This transition also resembles a mechanical transition of a complex from 1 nM PEI to 5 nM PEI as described earlier.

Reversibility of pH behavior was tested by two methods: washing with a high ionic strength condition (1 M NaCl) as well as cycling back to pH 7 (10 mM Tris, 150 mM NaCl, and 0.05% azide. Washing with 1 M NaCl (Figure 3.4b) allows the complex to recover extension within 240 seconds (at an average rate of 975 nm/min), as electrostatic interactions are screened. The complex returns to full contour length (8.4 µm (n=1)) WLC force profile with no hysteresis or shortening and a persistence length is 46.6 ± 0.1 nm.

Additionally, cycling back from pH 5 to Tris at pH 7.4 was able to recover some contour (to 5.2 µm, or 40% of the contour that was incorporated into the mechanically rigid region) and the portion recovered exhibited a persistence length of 46.1 ± 0.1 nm,

however, a different progression of force profiles was observed (Figure 3.4c). Instead of seeing the rapid opening and decrease in stretching curve values, there is a slow (~103 nm/min) extension of WLC shaped curves. This slow progression over a time scale of 1205 seconds demonstrated that bound PEI may be difficult to deprotonate, either due to pKa shift or inaccessibility of the solvent to the ionizable group. The reversibility of the pH effect, either by high salt or increase of pH, confirms that electrostatic interactions are the major driving force for condensation at low pH.

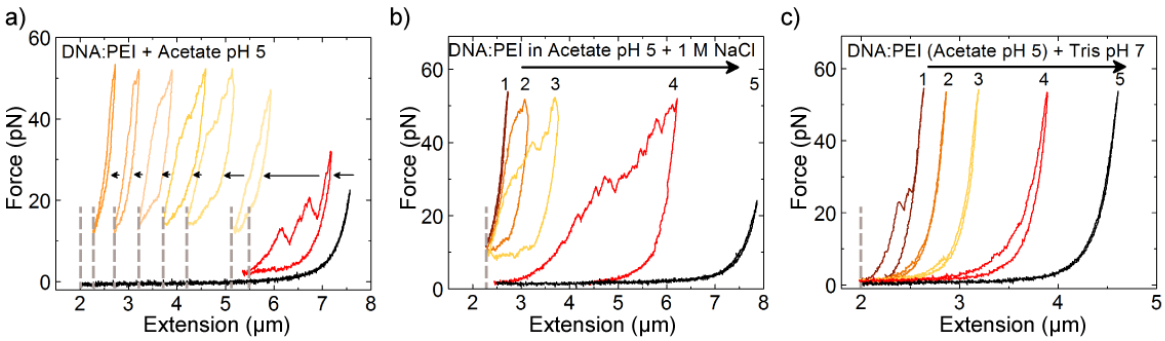

Figure 3.4 The effect of pH on force vs extension profile of DNA:PEI complex. a) Force curves at pH 7.4 after washing (black) and at pH 5 are shown in black and red respectively. Decrease of the block location by 500 nm (yellow to brown) resulted in a further decrease of extension forming a mechanically rigid complex as indicated by arrows. b) Recovery of extension upon washing with 1 M NaCl. Numbers indicate sequence of stretching and relaxation cycles. c) Recovery of extension upon washing with 10 mM Tris (150 mM NaCl and 0.05% azide). Numbers indicate sequence of stretching and relaxation cycles.

Force response as a function of pH has been previously observed for histidine-lysine (HK) peptide, but with a few notable differences; HK peptide showed a recovery of well-defined stretch and relaxation plateaus whereas PEI demonstrated formation of a mechanically rigid complex [88]. The increased strength of interaction leading to the reduction in extensible length may be due to total charge of the molecule.

3.3.4 G2-TETA Gold Nanoparticles Bind and Condense DNA

To observe the effect of G2-TETA concentration on the condensation behavior of DNA we performed a titration, where a single DNA molecule was exposed to progressively increasing concentrations of G2-TETA: 1 nM, 5 nM, 10 nM, and 50 nM (Figure 3.5). At 1 nM and 5 nM concentrations (Figure 3.5a-b), we observed no change from a worm like chain profile. The 1 nM condition maintained a persistence length of 42.7 nm (n=1), but for the 5 nM condition the persistence length was reduced to 11.8 nm (n=1). This reduction signifies binding and local bending, however the concentration bound is not sufficient to induce condensation. The 10 nM condition (Figure 3.5c) exhibits evidence of binding based upon the appearance of hysteresis and a small reduction in contour length which indicates the formation of interactions that cannot be disrupted by the force applied with the optical tweezers. However formation of this mechanically resistant region is limited as compared to 50 nM G2-TETA (Figure 3.5d). This suggests that the source of mechanical rigidity is concentration related and is sourced from the AuNP themselves; thus decreasing the concentration limits the amount of non-mechanically reversible collapse the molecule may experience.

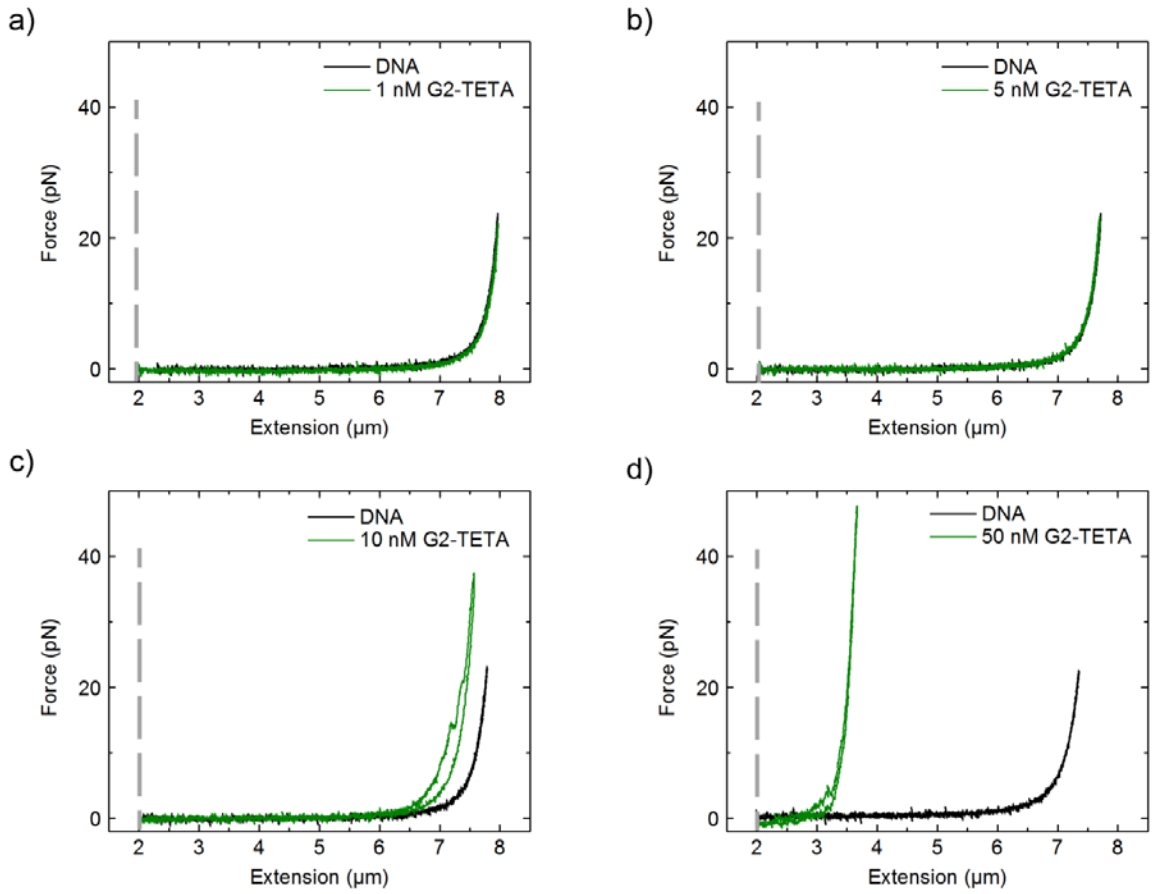

Figure 3.5 Representative force profiles of DNA condensed with a) 1 nM, b) 5 nM, c) 10 nM, and d) 50 nM G2-TETA nanoparticles are shown. Initial naked DNA profiles for each experiment are indicated by light gray curves.

Exposure to 50 nM G2-TETA (Figure 3.6a) reproducibly showed distinct deviation from naked DNA mechanics with dynamic nature of the interactions in two stages. In the first stage, as G2-TETA binds to DNA, the force profile of naked DNA (black trace in Figure 3.6a) begins to show plateaus in the stretching and relaxation cycles (Figure 3.6a). The presence of these plateaus indicates that upon binding, G2-TETA nanoparticles exert a tension along the DNA fiber to actively condense the complex. The plateaus increases to a maximum relaxation force of 4.6 ± 1.7 pN and a stretching force of 9.1 ± 3.9 pN $(n = 8)$ (Figure 3.6a, initial binding). At maximal

plateau force, the complex requires 1.25 ± 0.31 k_BT/bp to extend. However, as G2-TETA continues to be injected and after this maximum plateau force is reached, the complex enters the second phase of condensation where the plateaus then begin to decrease with an associated decrease in the extensible length of the complex.

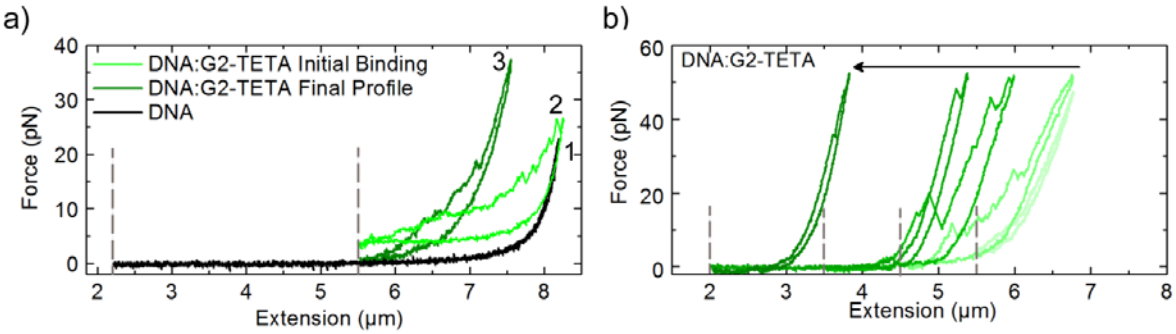

Figure 3.6 Force extension profiles of a) naked DNA (#1, black), DNA as it initially interacts with 50 nM G2-TETA (#2, gray), and DNA:G2-TETA complex after 100 µL of injection (#3, black). Block location is maintained at 5.5 µm until injection is completed. B) Post injection, force profiles for DNA:G2-TETA at decreasing separation distance between the beads (indicated by gray dotted lines) are shown.

By the end of the 100 µL injection (Figure 3.6a, final profile), the relaxation curve returned to worm-like chain behavior without a force plateau; by fitting using the WLC model, we observe that the persistence length is decreased approximately in half from 42.0 ± 3.3 nm (n=9) in the naked DNA condition to 28.3 ± 8.8 nm (n=4)after binding with the gold nanoparticles. This is likely due to local bending of the DNA due to charge neutralization of the phosphate backbone [69]. This persistence length decrease has been observed in other systems including multivalent cations, anti-cancer drug Kahalalide F (KF), and peptide condensation [58, 70, 88]. The sequential decrease of extensible length as the block location decreases suggests that a mechanically rigid complex forms after the molecule is relaxed, although we see indications of disruption of some interactions in the stretching as indicated by hysteresis in stretch-relax cycling.

Initially, the beads are maintained at a 5.5 µm separation from one another. In addition to the disappearance of plateau forces, the molecule also undergoes 1.1 ± 0.5 µm (n=7) loss of extensibility when the block was located at ~5.5 µm . As this separation distance is decreased, we observe an associated decrease in the contour length of the complex (Figure 3.6b). The average final contour length was 4.2 ± 0.8 µm (n=5) at a block location of 2 µm. Physically, this represents that as the ends of the bound DNA are brought into closer proximity to each other, that segments along the strand have increased probability of interaction. These interactions lead to strong bonds which are unable to be reversed by mechanical forces up to 50 pN. Throughout the reduction in extensible length, the force profile retains a WLC shape, with minimal to no hysteresis. When fitting, we see an increase of L_p up to a final value of 135.18 ± 14.8 nm at the 2 µm block (n=3). The shape of the force profile along with the increased persistence length indicates that a very stiff complex is formed; a similar behavior is observed when DNA is collapsed by hydrophobic peptide, KF [58].

3.3.5 SDS Destabilizes DNA:G2-TETA Complexes

To gain better understanding of the nature of the intermolecular interactions stabilizing the complex, buffer conditions were changed to the following conditions: 1 M NaCl, 5 mg/mL heparin, pH 5 Acetate buffer, 2% Tween 20, 5 mM glutathione (GSH, and 5% sodium dodecyl sulfate (SDS) (Figure 3.7b-d). The only condition that was able to dissociate the complex is 5% SDS in buffer. When exposed to SDS, we observe significant recovery of contour length to a final length of 6.7 ± 0.4 µm (n=3), which is equivalent to the recovery of 61.5 ± 11.8% of the contour length lost (Figure 3.7a). Destabilization by a surfactant indicates the importance of hydrophobic interactions in

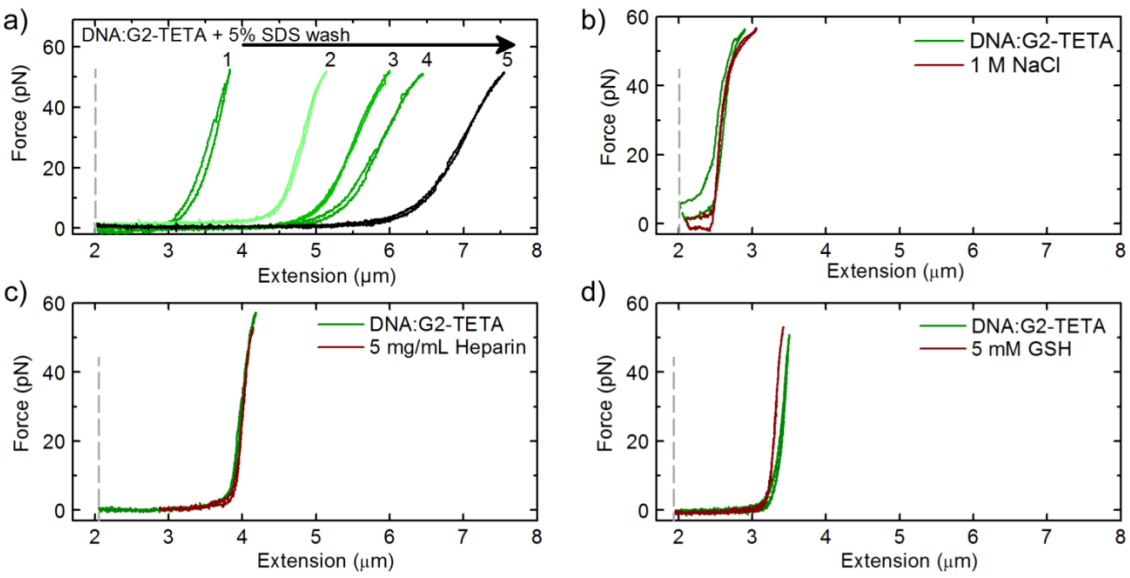

Figure 3.7 The effect of SDS on force vs. extension profile of DNA:G2-TETA complex. Force curves in Tris buffer (#1, light gray) and after injection of 5% SDS (#5, black) are shown. The dynamic transition of force profiles during injection of SDS is demonstrated by curves 2-4. The effect of 1 M NaCl or 5 mg/mL heparin on force vs. extension profile of DNA:G2-TETA complex. The light gray profiles in b-d) were obtained after condensing DNA with 50 nM G2-TETA and reducing the block location to 2 μm separation between the beads. Black force profiles result from injection of either b) 1 M NaCl, c) 5 mg/mL heparin, and d) 5 mM GSH and show limited change and no recovery of contour length.

the formation of the stiff, compact state of the DNA:G2-TETA condensate. In fact, the force required to expand a collapsed hydrophobic polymer in aqueous solution (>50 pN, for polystyrene (PS), poly(4-tert-butylstyrene) (PtBS), and poly(4-vinylbiphenyl) (PVBP) in aqueous solution) in is good agreement with observed inability to reach full extension with a range of 50 pN of force [71]. Additionally, hydrophobic interactions likely require sufficient time, after backbone charge neutralization, to organize and rearrange into stable hydrophobic contacts along the DNA which is observed in DNA condensation by Kahalalide [58]. This behavior of hydrophobic remodeling and growth can explain the second phase of condensation. The source of the hydrophobic collapse is likely due to the charge neutralization by DNA decreasing the solubility of the G2-TETA nanoparticles.

In fact, for lower generation (G0 and G1) TETA nanoparticles, complexation with siRNA led to precipitation of the nanoplexes [40].

1 M NaCl, 5 mg/mL heparin, and 5 mM GSH were all unsuccessful in disrupting these strongly aggregated interactions and we observed negligible changes in contour length (<100nm). If condensation is electrostatically driven, we would expect that 1M NaCl to screen these columbic attractions. Similarly, heparin would act as a competing agent for the cationic agents [91]. Based on results from the high salt and heparin conditions, we can conclude that the strong interaction is not primarily due to electrostatic forces. Decreasing the pH from 7.4 to 5.0 also did not elicit a mechanical change, suggesting that the ionizable groups on the nanoparticle surface are inaccessible when bound to condensed DNA or that upon binding the TETA moiety experiences a pKa shift. Exposure to GSH to simulate the intracellular environment was expected to release DNA via ligand exchange at the gold surface. However, after the complex is condensed into this rigid state, GSH also seems to be unlikely to penetrate to the nanoparticle surface where it could potentially undergo ligand exchange. We suspect that the condensation is driven by hydrophobic interactions, yet Tween 20 was unable to show decondensation of the rigid structures either (data not shown). However, when the nanoparticles are incubated with Tween 20 prior to binding DNA (and Tween 20 remains present in the buffer), the formation of the shortened complex is inhibited (data not shown). Because of the hydrophobic nature of the complex, it is unlikely that the salt, heparin, or GSH containing buffers are able to access the interface of the columbic attraction or the AuNP surface. As a result, the complex remained robust against these possible destabilizing conditions.

These results are in good agreement with those previously published which suggest that DNA wraps around the AuNP core [92, 93] and demonstrates release and recovery of DNA after exposure to SDS. At this point, the only discrepancy between bulk experiments and single-molecule is release due to GSH exposure [63], however, this deviation may be due to the bulk experiment using 37-mer DNA as compared to the 24kbp ½ λ –DNA used in this study. The larger DNA molecule may lead to a more highly aggregated complex with the G2-TETA particles buried within the bulk, thus preventing ligand exchange upon binding. Thus far our work suggests that G2-TETA nanoparticles stably bind DNA and may be efficient in protecting it in various biologically relevant environments.

3.4 Discussion

Our single molecule studies have elucidated two dynamic condensation mechanisms: G2-TETA undergoes electrostatic association, followed by hydrophobic collapse and PEI condenses DNA into a complex that varies from undercharged to overcharged state. Mechanically, in both pathways, dynamic initial binding profiles are characterized by the appearance of force plateaus followed by a return of the relaxation curve to WLC mechanics. In addition, both systems have demonstrated the ability to form mechanically non-extensible regions. This mechanically non-decondensible region has important implications in the ability to provide protection to the nucleic acid and lend to the stability of complex, which are essential to circumvent biological barriers for efficient transfection [26].

In both systems, experiments were carried out to identify the major molecular level interactions that were the source of the loss of extensible length. It was found that 1 M NaCl can restore significant a portion (93%) of the DNA:PEI contour length, and result in the disappearance of plateaus and hysteresis. This indicates that electrostatic shielding is sufficient to disrupt many of the interactions within the complex. In contrast the only treatment which restores a significant portion (82%) of contour length in DNA:G2-TETA complexes is 5% SDS ; there is no recovery under a high salt condition, suggesting a large contribution of hydrophobic interactions in the collapse and stabilization of condensates.

Based on these results, we have proposed a mechanism for the condensation of DNA by G2-TETA gold nanoparticles. First there is association of the positive ligands to the phosphate backbone of the DNA fiber which is responsible for the appearance of the force plateau. As the DNA binds and neutralizes the surface charges, it may bend around the particles similar to DNA organization around histone octamers. This step is reflected in the force profile as the decrease of plateaus coupled with shortening of the molecule at the high block location. Electrostatically driven binding is also supported by the reduction in persistence length upon interaction, suggesting decreased backbone repulsions. Upon reduction of the molecular extension, the neutralized segments of the complex form hydrophobically stabilized contacts. This continues and the complex forms a collapsed structure that is mechanically rigid. After cationic groups are neutralized by binding to DNA, the hydrophobic contributions are likely due to the ethylene groups as well as the 8-carbon chain used as a linker from the TETA molecule to the AuNP surface.

Out of the systems explored here by single molecule force spectroscopy, G2-TETA is the only gene delivery system where hydrophobic forces are the primary force leading to mechanical stability. These stable complexes may be disrupted as the polyplex comes into contact with lipid membranes, and especially phosphotidylserine, because it is an anionic amphiphile like SDS. Phosphatidylserine is located specifically on the cytosolic-side of the cell membrane. Therefore, if destabilization is specific to anionic amphiphiles (as suggested by the response to SDS vs. Tween 20) then destabilization of the molecule would only occur after internalization, release into the cytosol, and interaction with the inner leaflet of the cellular membrane. In this sense, release of nucleic acid may be targeted to occur only after internalization within in the cell.

In order to reduce the hydrophobic character of the complexes, and take advantage of intracellular concentrations of gluthatione's ability to release ligands from the gold core, it may be necessary to limit the length of the nucleic acid. It has been shown that in bulk studies, that GSH can release 37-mer DNA from cationic gold nanoparticles systems [92]. In light of this information, it is possible that G2-TETA may be much more applicable for siRNA delivery [40]. Additionally, hydrophobicity of a gene delivery vehicle has been demonstrated to play a role in the protection and release of the DNA from the endosomal vesicle, although its precise mechanism is unclear [94].

In contrast, PEI follows a primarily electrostatically driven condensation pathway. As in the case of G2-TETA, initially at low concentrations (1 nM), PEI binds DNA via columbic attraction and induces local bending. Accumulation of bending, looping and bridging results in tension along the DNA backbone which manifests itself as force plateaus. As the complex nears net neutrality, force plateaus increase to a maximum

value due to the minimization of columbic repulsion (concentrations between 1nM and 5 nM) and maximal van der Waal's interactions. At concentrations beyond this net neutral point, further accumulation of PEI along the backbone results in an overcharged complex, where the columbic repulsion minimizes (5 nM) or even eliminates (10 nM) the plateau force. Shortened contour length is likely a combination of electrostatic attraction, stabilized by hydrophobic interactions between neutralized ethylene portions of the PEI polymer which are allowed to form due to the absence of electrostatic repulsion from either DNA-DNA or PEI-PEI; resulting in a rigid complex which is able to be partially decondensed by high salt condition.

Comparison of these two systems to DNA condensed with poly-L-lysine (PLL) or branched histidine-lysine (HK) peptide show some key mechanical differences [88]. Firstly, HK and PLL condensed DNA do not show the rapid increase, maximization and decrease of plateau forces: condensation by either peptide shows the appearance of stretching and relaxation plateaus that are stable at the maximum value in the presence of free peptide. For HK, the relaxation plateau occurs 6.6 ± 0.4 pN, and similarly PLL is at 8.1 ± 1.4 pN. Additionally, we note that in the PLL and HK systems, that loss of extensible length is not formed with peptide alone. DNA:PLL complexes did not undergo this phenomena at all; however, for HK system, Zn^{2+} chelation by the histidine residues was able to provide mechanically rigid interactions.

The data reported has several implications for gene delivery especially in the role of balancing protection and release, which are essential functions of a successful gene delivery vehicle [95]. Among PEI, G2-TETA, PLL, HK, multivalent cations, and the PAMAM dendrimer, PEI has been shown to exert the most force on DNA during the

process of condensation based on the observed plateau forces and the amount of work required to extend the condensed complex (Table 1) [44-46, 88]. Additionally, bound PEI resists washing, similar to what is observed for the PAMAM dendrimer [46]. In contrast, PLL and HK demonstrate a decrease of plateau forces when washed, and multivalent cations showed an immediate transition back to WLC mechanics when washed [44, 88]. The increased interaction forces and the resistance to washing suggest that PEI in interacting with DNA in a stronger manner than the other systems. This may be partly due to the high charge density and branched structure of PEI. A 25 kDa PEI molecule contains ~580 monomer subunits, therefore having a maximum potential of a +580 charge. In comparison, at full protonated form PLL may only reach a maximum charge of +19, and HK can achieve up to a +117. Competition with RNA can partially destabilize complex as well, however, complexes formed using branched PEIs showed increased resistance to dissociation as compared to linear PEI, demonstrating the role of total charge and geometry on the complex stability [90]. Additionally, the change in PEI:DNA mechanics upon protonation suggest that PEI may facilitate escape via the proton sponge theory; furthermore, the ability to induce a mechanically rigid complex at low pH may allow for increased protection of the DNA in the endosome.

	Geometry	# of Amines/Molecule	Maximum Stretch Plateau Force (pN)	kBT/bp Required for Stretching
PLL	Linear	19	12.6 ± 1.6	1.05 ± 0.14
HK	Branched	117	11.2 ± 0.7	1.11 ± 0.07
G2-TETA	Branched	960	9.1 ± 3.9	1.25 ± 0.31
PEI	Branched	580	27.2 ± 11.5	2.93 ± 0.25

Table 1. Summary of Carrier Properties and Mechanical Features.

In terms of nucleic acid release, we have demonstrated that PLL/HK/PEI complexes can be destabilized via electrostatic competition. In the bloodstream and cellular milieu, many molecules may act as efficient competitors. In bulk, PEI complexes have been disrupted using salt, heparin, and BSA.[90] Also, cellular components such as glycosaminoglycans and serum albumin compete with DNA to bind to polycations [11]. However, due to its stronger interaction, PEI may be more resistant to washing off during still provide adequate protection in extracellular and cytosolic environments. Thus, the single molecule mechanics suggest that release of the DNA may be a rate limiting step for transfection. Previous studies on the localization and state of DNA do show that DNA localized in the nucleus remains bound to PEI, which may limit the DNA's ability to be biologically active [21, 22, 96]. In this sense, the interactions between PEI and DNA may still need optimization. Indeed studies have shown improvement in transfection efficiency when PEI has been partially acetylated, thus reducing the maximum charge achievable [32]. Careful modulation of binding affinity to facilitate release may be a key component to achieving maximum transfection efficiency of DNA:PEI complexes.

3.5 Conclusion

This work highlights the necessity of a gene delivery vector to be dynamic in nature, both providing stability, yet the ability to release nucleic acid in the appropriate location. However, at this point, the mechanism for release of long DNA (in the process of intracellular trafficking) from the nanoparticles is unclear, and the surface properties of G2-TETA may need to be modulated prior to condensation in order for it to perform as an efficient gene delivery vector for DNA.

Modulation of DNA:PEI mechanics is achieved via ionic strength, protonation state, and competition by heparin. Using single molecule force spectroscopy, we are able to identify two independent methods for providing DNA condensates with stability, as well as identify the processes required to trigger release of nucleic acid. This body of work also demonstrates how single molecule methods may be utilized for pre-screening of gene delivery agents to identify potential roadblocks and rate limiting behavior prior to *in vivo* studies.

4 Guanidinylated Triblock Copolymer Shows Sensitivity to Ionic Environments Compared to Base Copolymer

4.1 Introduction

Gene therapy has great potential for preventing and treating hereditary diseases such as cystic fibrosis or cancer [26]. A therapeutic gene must be packaged and protected as it travels from the bloodstream to the cell, and be released inside the cell to reach the nucleus. This pathway has many extracellular and intracellular obstacles requiring protection of the nucleic acid from degradation, cumulating in the ultimate challenge of DNA release to allow for transcription and further processes once the DNA is within the nucleus.

The progress of gene therapy research has been limited by development of a safe and effective delivery vehicle. Vectors carry DNA through physiological mediums and are classified as either viral or non-viral. Viral vectors, such a retroviruses and adenoviruses, integrate their payload into the cell genome for gene expression but have unpredictable immune responses, which has limited studies primarily to the animal testing stage and preventing advances in human clinical trials [86, 97]. Fortunately, non-viral vectors may be tailored to minimize specific immune responses while also offering larger-scale synthesis and easier manipulation for different chemical functionality [97]. Cationic polymers, such as gold nanoparticles and polyethylenimine (PEI), have proven to be successful for DNA condensation but have yet to overcome low transfection efficiency or high cytotoxicity, respectively [30]. Peptides have also been explored as potential gene delivery agents because of their biocompatibility and well-controlled

synthesis process [98]. More specifically, lysine and arginine containing peptides have been of interest because they are basic amino acids, capable of assuming positive charge at neutral pH, and they are very hydrophilic. Cationic nature carriers have been shown to effectively condense DNA [46, 88], and ionizability is thought to be an important aspect in endosomal escape, a major barrier to entering the nucleus of a cell [98, 99].

In this study, we investigated two copolymer vectors. The base copolymer used is a block copolymer are composed of a hydrophobic poly(ε-caprolactone) (PCL) block which is attached via a disulfide bond, a tetraethylenepentamine (TEPA) decorated poly (glycidyl methacrylate) (PGMA) which is combined with oligo(ethylene glycol) monomethyl ether methacrylate (OEGMA) developed by the Pun group at the University of Washington[41]. We also used a guanidinylated copolymer which maintains the same composition of the base copolymer, but where 89% of the primary amines in TEPA have been converted to guanidine groups [42]. Both polymers showed comparable transfection efficiency to a 25 kDa branched polyethylenimine, with the guanidinylated copolymer outperforming the other two *in vitro* in both Hela and PC-12 cell lines [42].

Our method utilizes optical tweezers, which can simulate assorted physiological conditions via a microfluidic chamber where DNA condensation occurs. DNA is tethered between two beads, one trapped by tightly focused laser beams and the other held stationary by a pipette tip [49]. As the laser beams oscillate to stretch or relax DNA, changes in distance and force as small as 1 nm and 1 pN, respectively, are detected and recorded in force-extension curves [100]. With exquisite control of the system and sensitive measurements, we can quantify the forces and define the intermolecular

interactions involved in DNA condensation, and just as importantly, the process of DNA decondensation.

4.2 Materials and methods

4.2.1 Materials

Streptavidin (SA)-coated beads (2.1-µm nominal size, Spherotech, Lake Forest, IL) and anti-digoxigenin (AD)-coated beads (4.26-µm nominal size, Spherotech, Lake Forest, IL) are tethered to a double end-labeled ½ λ DNA construct was synthesized by the methods described in Chapter 2.

4.2.2 Polymer synthesis and preparation

Synthesis of the base copolymer and the guanidinylation process have both been previously described [41, 101], and the structures are shown in figure 1.3. Both base and guanidinylated copolymer were developed, synthesized and generously donated by the Pun Laboratory at the University of Washington. To make 1 mM stock solutions, the lyophilized copolymer is dissolved completely in water. Then, using 1M HCl, the pH is adjusted to ~6.4. The stock solution is stored at 4° C.

4.2.3 TCEP pretreatment of copolymer

To explore the role of the hydrophobic group, the triblock copolymers were pre-incubated with 50 molar equivalents of tris(2-carboxyethyl)phosphine (TCEP, Sigma Aldrich, St. Louis, MO) for 24 hours. Before use, the treated solution is centrifuged for 10 minutes at 16,000 × g. The supernatant is removed and diluted for use in the experiments. Further testing of the complex condensation and response is tested as described above.

4.2.4 Complex preparation in the microfluidic chamber

For this study, custom built optical tweezers were employed to directly record real time changes in the interaction forces between DNA and carrier [66]. Before the pulling experiment, the beads are first blocked for 20 minutes with 5 mg/mL BSA and 0.1% Tween20. After incubation, beads are centrifuged, the supernatant containing excess BSA is removed, and the beads are resuspended in a buffer containing 10 mM Tris, 150 mM NaCl, and 0.05% sodium azide, pH 7.4. AD beads are then incubated with ½λ DNA for 10 minutes. The SA beads are trapped on a micropipette tip and remain stationary during the course of the experiments. AD beads are held and manipulated by the optical trap. A dsDNA tether is created by moving the AD bead into close proximity to the SA bead and allowing the biotin-labeled end to bind to the SA beads. The presence of a single DNA molecule between the beads was confirmed by overstretching region at ~65 pN or by fitting with the Marko-Siggia worm-like chain model [52]. The beads are separated by a ~5.5 µm block distance imposed by the optical trap which prevents loop formation or the beads from touching or allowing nonspecific adsorption of DNA onto the bead surfaces. The pulling experiments were conducted with a pulling rate of 500 nm/sec. The data collection rate was 100 Hz and no data smoothing was performed.

100 nM copolymer solution in 10 mM Tris buffer (150 mM NaCl, 0.05% azide, pH 7.4) is injected into the chamber at a rate of 5 µL/min. During injection, a block location of 5.5 µm is maintained. After 100 µL has been injected, the block location is reduced by 500 nm increments and the complex is allowed adequate time to form a steady state at each location.

4.2.6 Destabilizing conditions to disrupt condensed DNA complexes

To change buffer conditions within the chamber, the complex is washed with 100 µL of a buffer, at a rate of 10 µL/min. With a channel volume of ~30 µL and the presence of laminar pressure driven flow, washing with ~3 times the channel volume is sufficient for complete solution exchange.

5 mM glutathione (GSH) (Sigma Aldrich, St. Louis, MO), 5 mg/mL heparin (Sigma Aldrich, St. Louis, MO), 1 M NaCl, or a combination of the aforementioned in 10 mM Tris buffer (150 mM NaCl, 0.05% azide, pH 7.4) are used to test complex stability. To test pH response, 10 mM acetate buffer (150 mM NaCl, 0.05% azide, pH 5) is injected into the chamber.

4.3 Results

4.3.1 Base copolymer exhibits dynamic condensation of DNA

Similar to what has been previously seen for DNA condensation by G2-TETA nanoparticles, the base copolymer shows a dynamic two-step condensation process accompanied by the formation of a mechanically non-extensible region. First, indicators of binding are the appearance of plateaus (Figure 4.1a). The stretching plateau was observed at 26.1 ± 9.8 pN (n=11) and the relaxation plateau was calculated to be 14.3 ± 12.0 pN (n=11); these force profiles show a large standard deviation due to transient and non-steady state nature of plateaus. At these plateau values, the energy required to extend the complex is 2.04 ± 0.47 kBT per base pair (bp). Within a few stretch-relax cycles, continued injection leads to the disappearance of plateaus associated with a limited extension of the complex. During this process, the observed hysteresis disappears and the relaxation curve returns to worm-like chain behavior with a measured persistence length

of 46.1 ± 0.3 nm (n=2). On average, at the 5.5 µm block location, the contour length decreases 1.1 ± 0.6 µm (n=11).

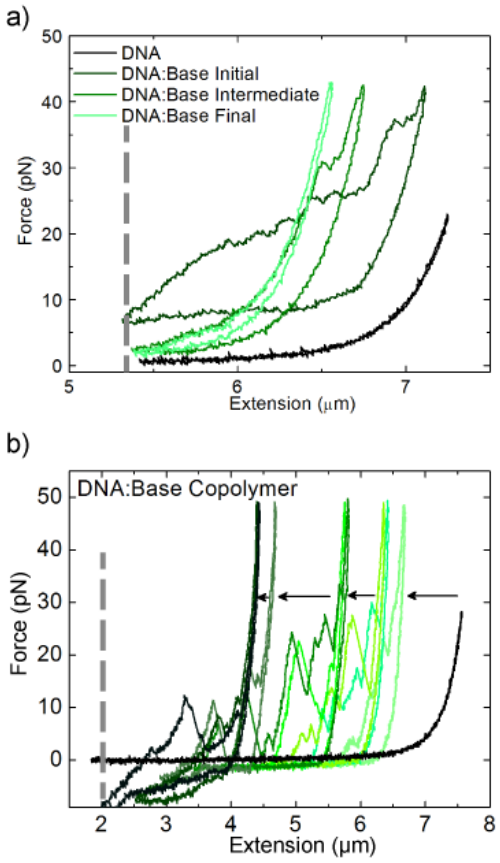

Figure 4.1 (a) Force vs. extension profiles during injection and (b) after completed injection of 100 µL of 100 nM base copolymer. In both, the force vs extension curve of naked DNA is shown in black. (a) Injection of base copolymer first induces a force plateau which then decreases as the complex reduces its extensible length and hysteresis is minimized (d) Sequential movements of the block location (from 5.5 µm to 2.0 µm) by 500 nm increments resulted in continued decrease in extension, as well as the appearance of a rigid region in the complex at extensions less than 4 µm.

These force profiles allows us to observe initial binding exerting tension manifested as appearance of force plateaus, rapid increase of the plateau force and then a gradual decrease of these forces with a decrease of extension. This behavior of reaching maximal plateau force and then its decrease is analogous to overcharging behavior as described for DNA:PEI complexes in Chapter 3.

As the block location is reduced in 500 nm increments from 5.5 μm to 2.0 μm, the complex's extensible length decreases as the block is reduced (Figure 4.1b). At the final 2 μm block location, the contour length had been reduced to 5.2 ± 1.1 μm (n=8), and the relaxation curve maintains WLC shape and a persistence length of 46.8 ± 1.3 nm (n=7). Sawtooth patterns at lower block locations in the stretching curve may indicate unfolding events of either kinks or loops along the DNA introduced by the bound copolymer. The fact that the relaxation curve retains a worm-like chain shape indicates that these binding events take place after the DNA is relaxed. Apparent shortening after the block is shifted indicates that the multiple bridging interactions formed could not be disrupted by forces up to 50 pN.

Additionally, in many cases (30%) a negative repulsive force was observed at the lower block locations, indicating the formation of a rigid aggregate between the beads (Figure 4.1b). This phenomena was also observed for DNA condensed with the hydrophobic cancer drug kahalalide F [58].

4.3.2 Simultaneous perturbation of hydrophobic and electrostatic interactions are required for destabilization of DNA:base copolymer

Next, stability and response of the condensed DNA:base copolymer complex to external changes of environment was probed. The base copolymer complex is resistant to perturbation by the exposure of condensed complex to acetate buffer (10 mM, 150 mM NaCl, 0.05% azide, pH 5), 1 M NaCl, 5 mg/mL heparin, or 5 mM glutathione (GSH). (not shown). GSH was expected to show a loss of the hydrophobic block leading to ease of destabilization so it was surprising not to see any noticeable changes. However, the complexes are disrupted by the combination of either 5 mM GSH and 1 M NaCl solution

or 5 mM GSH and 5 mg/mL heparin solution. The combination of 1M NaCl and 5 mM GSH was able to restore the contour length to 7.3 ± 1.2 μm (Figure 4.2a) (n=3). This accounts for 60.1 ± 39.1% restoration of the contour length lost. The final profiles maintained WLC characteristics and in two cases the final value of the persistence length was decreased as compared to naked-DNA mechanics (16.3 & 17.0 nm), and in the third case the persistence length returned to DNA-like mechanics (46.9 nm). This result indicates that the simultaneous disruption of electrostatic bonds and reduction and removal of the hydrophobic region was necessary to destabilize the complex and allow unpackaging of the DNA. Additionally, the two instances of depressed persistence length suggests that some of the bound copolymer may be resistant to washing in high salt conditions. Remaining cationic polymer still bound to DNA would induce local bending thus decreasing the measured persistence length [69]. Depending on the actual number of molecules bound to the DNA fiber, we can expect some variation in the final persistence length achieved.

Similarly, the combination of 5 mg/mL heparin and 5 mM GSH was also able to restore the contour length to 7.1 ± 1.4 μm, or restoration of 62.0 ± 23.0% of total contour lost (Figure 4.2b) (n=3). In contrast to the GSH and salt combination, in all three experimental runs, destabilization with GSH and heparin allowed for the persistence length to return to 46.6 ± 0.2 nm (n=3). Comparison of this data to the GSH and salt data indicates that heparin may be more effective at removing bound copolymer as compared to salt. This is likely due to the multivalency of heparin, which will compete with DNA efficiently due to its high negative charge density.

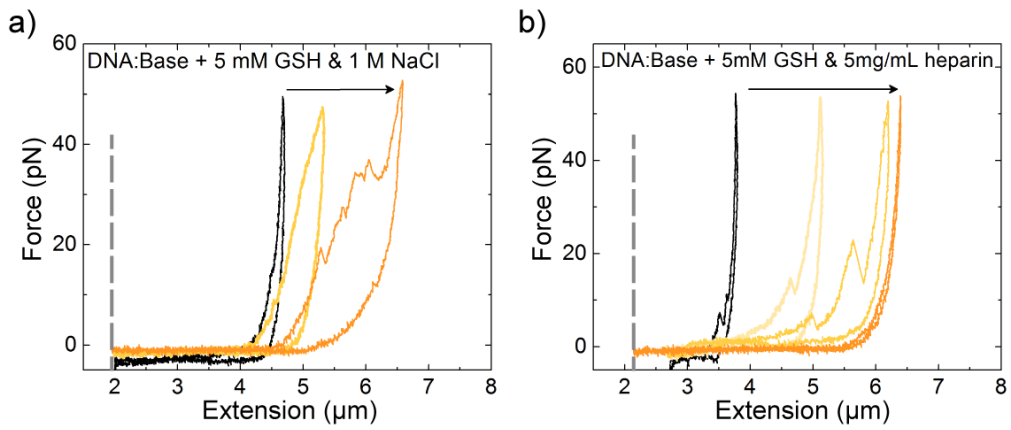

Figure 4.2 Mechanical destabilization of the DNA:base copolymer complex. Recovery of extension for the DNA:base copolymer complex (black) was achieved upon washing with 10 mM tris buffer containing (a) 1 M NaCl and 5 mM GSH or (b) 5 mg/mL heparin and 5 mM GSH.

4.3.3 TCEP pretreatment of base copolymer allows for electrostatic modulation of mechanical properties

Pre-incubation of the base copolymer with TCEP has been shown to be effective for the reduction of the disulfide bond and removal of the hydrophobic PCL block [41]. Condensation of the DNA with 100 nM TCEP-treated base copolymer also displays dynamic plateau behavior. Again continued injection leads to maximization of the plateau forces, and then a decrease back to worm-like chain behavior. Additionally, some loss of extensibility is observed, with an average of 0.7 ± 0.3 μm shortening at the 5.5 μm block location (n=3). Reduction of the block to the 2 μm location did not result in reduction of extensible length and maintained contour length of 5.7 ± 1.2 μm (n=6), similar to the value when compared to the complex formed without TCEP pretreatment (Figure 4.3a, blue). It is of note that the hydrophobic region is not required to form the mechanically non-extensible region of the complex; the TEPA-OEGMA statistical block can form interactions with the DNA that require > 50 pN force to disrupt.

When the condensate is washed with 1 M NaCl, expansion of the complex to 6.9 ± 1.0 µm (65.4 ± 30.4% of lost contour restored) (n=5) is observed, and any hysteresis is removed (Figure 4.3a, cyan). The final persistence length of the salt destabilized complex is 46.2 ± 1.1 nm (n=5). Further cycling of salt concentration to 150 mM shows return of hysteresis and shortening to a very short rigid complex; again cycling back to 1 M salt recovers full length of the complex (Figure 4.3b). These data indicate that base copolymer or the TCEP-treated copolymer can overcharge complex and that electrostatic interactions are sufficient for MND formation. Additionally, we observe that TCEP pretreated base copolymer is resistant to high salt washing which is in direct contrast to what is observed for multivalent cations and cationic peptides [44, 88].

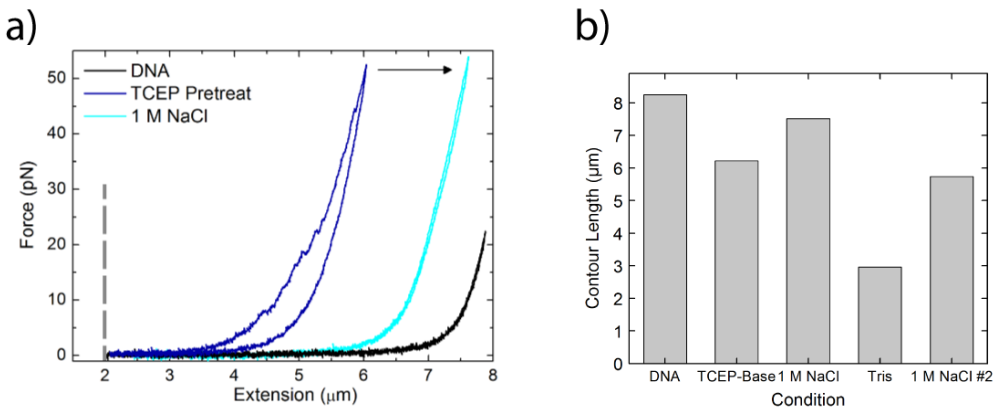

Figure 4.3 a) Representative force profile of DNA condensed with TCEP-pretreated base copolymer is shown (blue). Washing with 1 M NaCl restores contour length and worm-like chain mechanics (cyan). b) Contour length of a single molecule of DNA as is it condensed with TCEP-treated base copolymer, washed with 1 M NaCl, returned to tris buffer, and cycled back to 1 M NaCl wash.

Unlike its triblock counterpart, TCEP-treated base copolymer, which had been high salt washed, does show a mechanical response when the pH is decreased from pH

7.4 to pH 5 (Figure 4.4a). The response to the pH drop included an appearance of plateaus, hysteresis, and sawtooth accompanied by decrease in extension. These changes are attributed to protonation of the secondary amines in the copolymer leading to increased charge density (and likely binding affinity). Enhanced condensation forces due to protonation has been previously observed in the case of the histidine-lysine based polymer [88]. Cycling the buffer back to the original 10 mM tris buffer (pH 7.4, 150 mM NaCl, 0.05% azide) deprotonates the copolymer, removes hysteresis, and returns the DNA strand back to WLC mechanics (Figure 4.4b). The ability to reversibly modulate the extensible length via the copolymer's protonation state demonstrates that electrostatic interactions are a key contributor to mechanical stability of the complex.

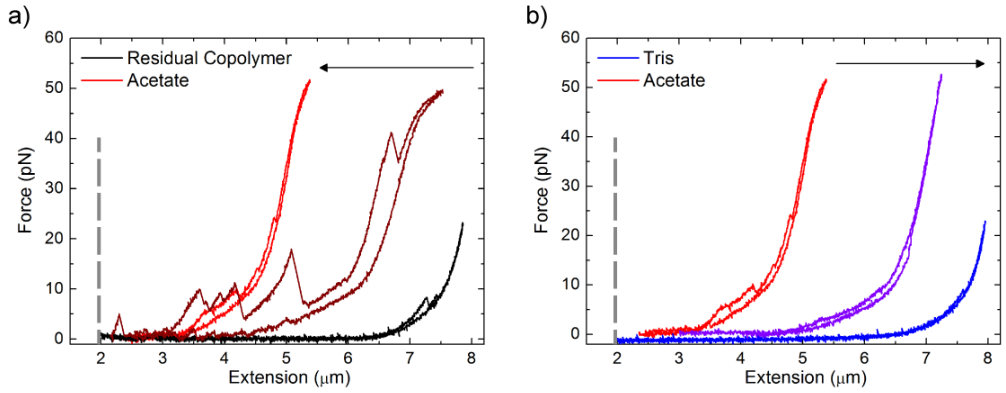

Figure 4.4 a) A force profile of DNA condensed with TCEP-pretreated base copolymer the washed with high salt condition is shown (black). Hysteresis indicate that some copolymer is bound. Using 10 mM acetate (150 mM NaCl, 0.05% azide) to change the environment to pH 5 led to increased hysteresis and shortening of the complex (red). Intermediate curve is indicated in dark red. b) This behavior was reversible by washing with 10 mM tris buffer pH 7.4 (150 mM NaCl, 0.05% azide) (blue). Intermediate curve is indicated in purple.

4.3.4 Guanidinylated copolymer exhibits maximal plateaus during condensation

Condensation of DNA with 100 nM of the guanidinylated copolymer also exhibited dynamic condensation behavior (Figure 4.5a). Shortly after injection of the

condensing agent, both stretching and relaxation plateaus reach their maximum values of 23.4 ± 5.1 pN and 9.2 ± 3.4 pN respectively (n=6); the energy required for extension at this point is 1.90 ± 0.32 kBT per bp. The plateaus then decreased and worm-like chain behavior is re-established in the relaxation curve. As the block location is decreased, the complex does lose some extensible length, arriving to a final contour length of 5.6 ± 1.5 µm (n=6) which is similar to that achieved by base copolymer complexes (Figure 4.5b). None of the DNA:guanidinylated copolymer complexes displayed the repulsive interactions observed for the DNA:base copolymer complexes.

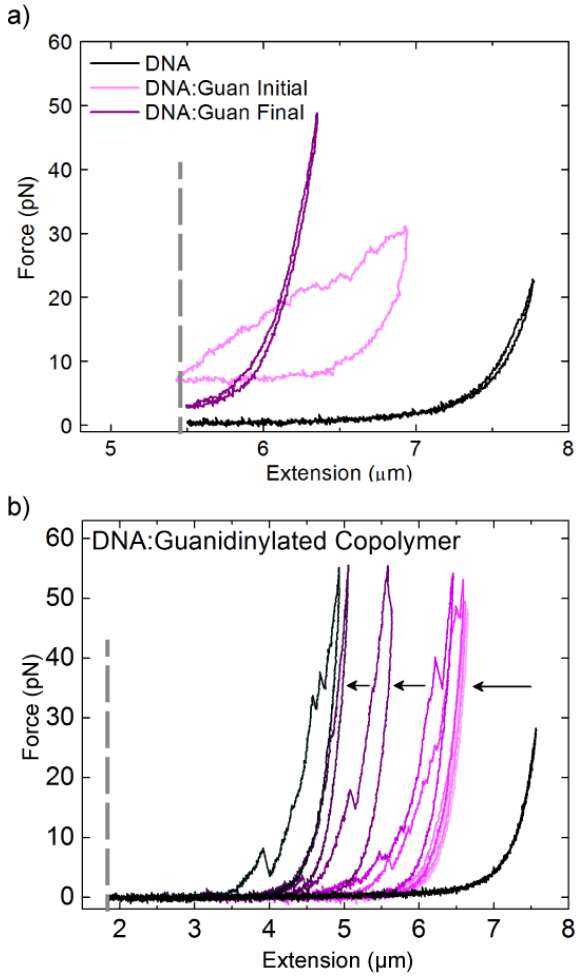

Figure 4.5 (a) Force vs. extension profiles during injection and (b) after completed injection of 100 µL of 100 nM guanidinylated copolymer. In both, the force vs extension curve of naked DNA is shown in black. (a) Injection of guanidinylated

copolymer first induces a force plateau which then decreases as the complex reduces its extensible length and hysteresis is minimized. (b) Sequential movements of the block location by 500 nM resulted in continued decrease in extension.

5.3.5 1 M NaCl destabilizes DNA:guanidinylated copolymer complexes

When the complex is exposed to tris buffer containing 5 mM GSH, no changes in force profiles is observed (data not shown). However whereas DNA:base copolymer complexes did not respond to high salt conditions, the loss in contour length of DNA:guanidinylated copolymer complexes during copolymer injection is restored with 1 M NaCl alone, resulting in an extensible length of 6.9 ± 1.0 µm (Figure 5.6) (n=5). This contour corresponds to restoration of 77.2 ± 19.6% of total length lost. In the guanidinylated system, the concurrent presence of GSH is not necessary to see destabilization of the condensed DNA complexes.

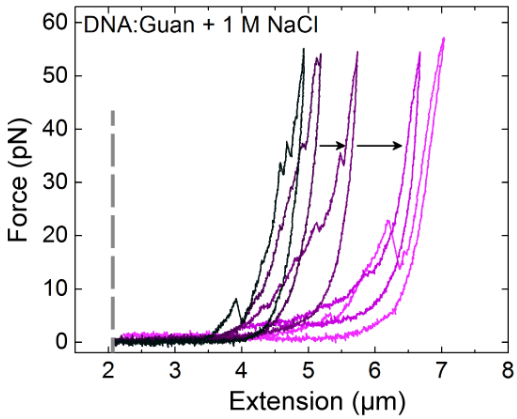

Figure 4.6 Electrostatic destabilization of the DNA:guanidinylated copolymer complex. Recovery of extension for the DNA:guanidinylated copolymer complex (black) was achieved upon washing with 10 mM tris buffer containing 1 M NaCl.

After the high salt wash, returning the complex to tris buffer environment (150 mM NaCl), retains the WLC force profile, indicating that the concentration of bound

polymer has been reduced. However, it is demonstrated that not all the polymer is removed because exchanging the buffer to acetate buffer, pH 5, gives new binding events and induces significant reduction in extensible length, forming very rigid complex (contour = 3.8 ± 1.1 µm, n=1) (Figure 4.7a). To test whether this process was reversible and the interactions were still dominantly electrostatic, the complex was washed back into tris buffer, pH 7.4. The reduction in extensible length was completely reversible and contour length prior to acetate exposure was fully regained (Figure 4.7b). These data suggest limited role of the hydrophobic block in stabilization of the condensate.

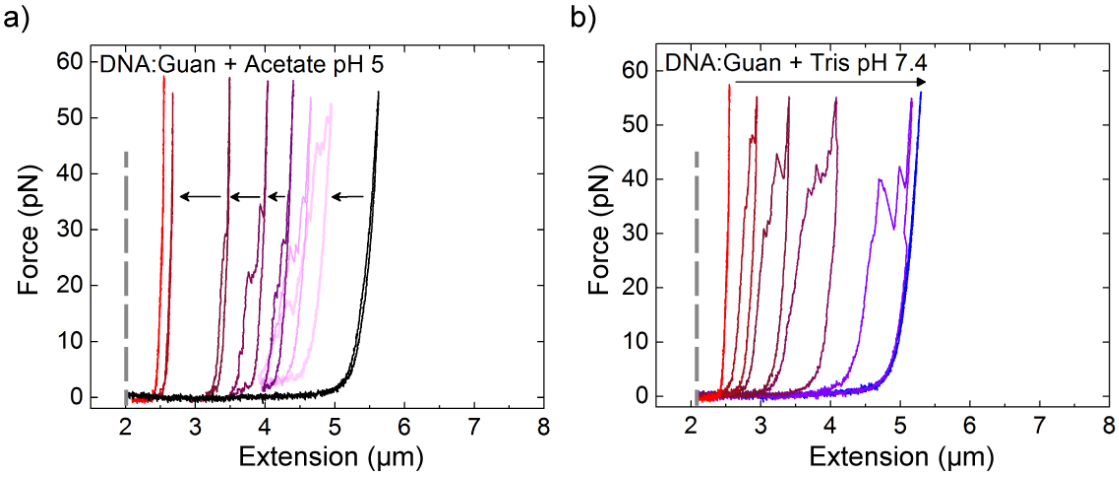

Figure 4.7 Guanidinylated copolymer complex exhibits a pH response. a) After condensation with guanidinylated copolymer the complex was washed with high salt condition and the resulting force profile is shown (black). Using 10 mM acetate (150 mM NaCl, 0.05% azide) to change the environment to pH 5 led to increased hysteresis and shortening of the complex (red). Intermediate curves are shown with arrows showing progression of condensation. b) This behavior was reversible by washing with 10 mM tris buffer pH 7.4 (150 mM NaCl, 0.05% azide) (blue). Intermediate curve are shown in purple showing expansion and return to WLC mechanics.

4.3.6 TCEP-treated guanidinylated copolymer shows resistance to washing in ionic environments

To further probe the role of the hydrophobic PCL block on the guanidinylated copolymer, TCEP pretreatment was performed prior to condensation. Again, the

appearance and disappearance of plateaus after reaching maximal plateau force of 20.9 ± 0.2 pN (n=2) in the stretch and the relaxation plateau was 9.1 ± 4.9 µm (n=2) was observed. However, it is important to note that this number is skewed downwards because we also observed the case where the plateaus were high enough to demonstrate considerable shortening which made calculation of the plateau value was not possible. Additionally, the complex showed reduction in extensible length to 6.1 ± 0.7 µm (n=3) at the high block location. Similar to the guanidinylated triblock copolymer, the diblock remained mostly extensible, retaining contour lengths of 4.9 ± 1.8 µm (n=2) at the 2 µm block location (Figure 4.8a, blue). Significant contour length that was lost as the block was moved from 5.5 µm to 2 µm block was recoverable by 1 M salt (Figure 4.8a, cyan). However, while 1 M NaCl was sufficient to recover full extensible length, some hysteresis remained. When the salt concentration is further increased to 2 M the hysteresis is completely removed, indicating that higher salt is required to show WLC behaviors (Figure 4.8a, green).

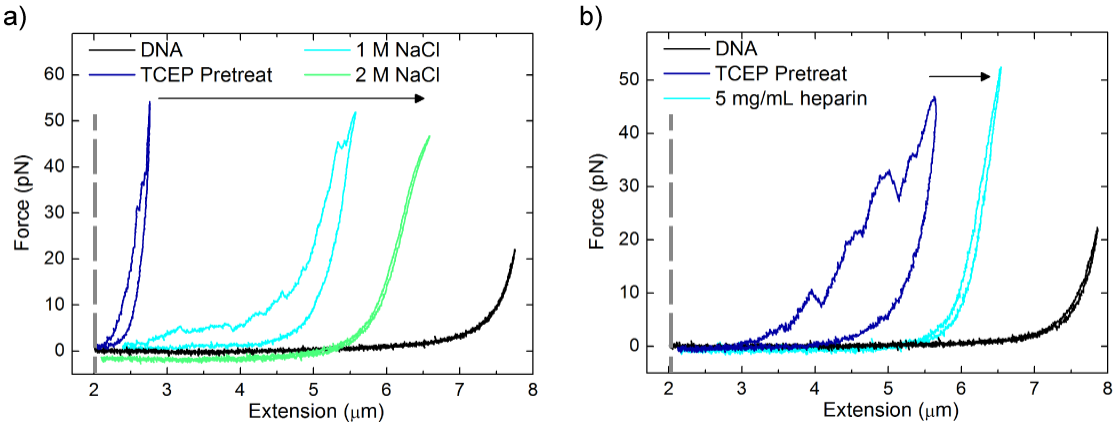

Figure 4.8 a) Representative force profile of DNA condensed with TCEP-pretreated guanidinylated copolymer is shown (blue). Washing with 1 M NaCl restores contour length, however, hysteresis remains (cyan). 2 M NaCl further restores contour length and returns the fiber to WLC mechanics with no hysteresis (green). b) Representative force profile of DNA condensed with TCEP-pretreated guanidinylated copolymer is shown

(blue). Washing with 5 mg/mL heparin restores contour length and is able to remove hysteresis (cyan).

Analogously, instead of using high salt conditions, 5 mg/ml heparin can also reverse shortening and return the DNA to a WLC shaped profile (Figure 4.8b, cyan). As compared to the TCEP-treated base copolymer, more stringent conditions are required by TCEP-treated guanidinylated copolymer suggesting enhanced high force interactions and resistance to washing.

4.4 Discussion

Stimuli-responsive gene delivery vehicles have been designed to tackle the bottlenecks of stability, endosomal escape, and payload release [102]. Additionally, the incorporation of guanidine groups has been demonstrated to be efficient at delivering drugs and nucleic acids intracellularly due to enhanced DNA binding affinity, and the charged group's propensity to interact with cell surface phosphates and sulfates enables improved uptake and internalization of complexes [103-106]. In this work, we compared the mechanical properties of DNA condensed with either a triblock copolymer previously developed for *in vivo* gene delivery [41] or its guanidinylated counterpart. Both copolymers exhibited similar condensation dynamics and formation of complexes with mechanically rigid regions. Key features of the condensation process include plateau appearance, maximization, and reduction, which is likely to be correlated with charged state of the DNA complex. Formation of a mechanically non-extensible region is proposed to be due to long range intramolecular interactions of the complex that forms as different parts of the complex approach each other during stretch-relaxation cycles.

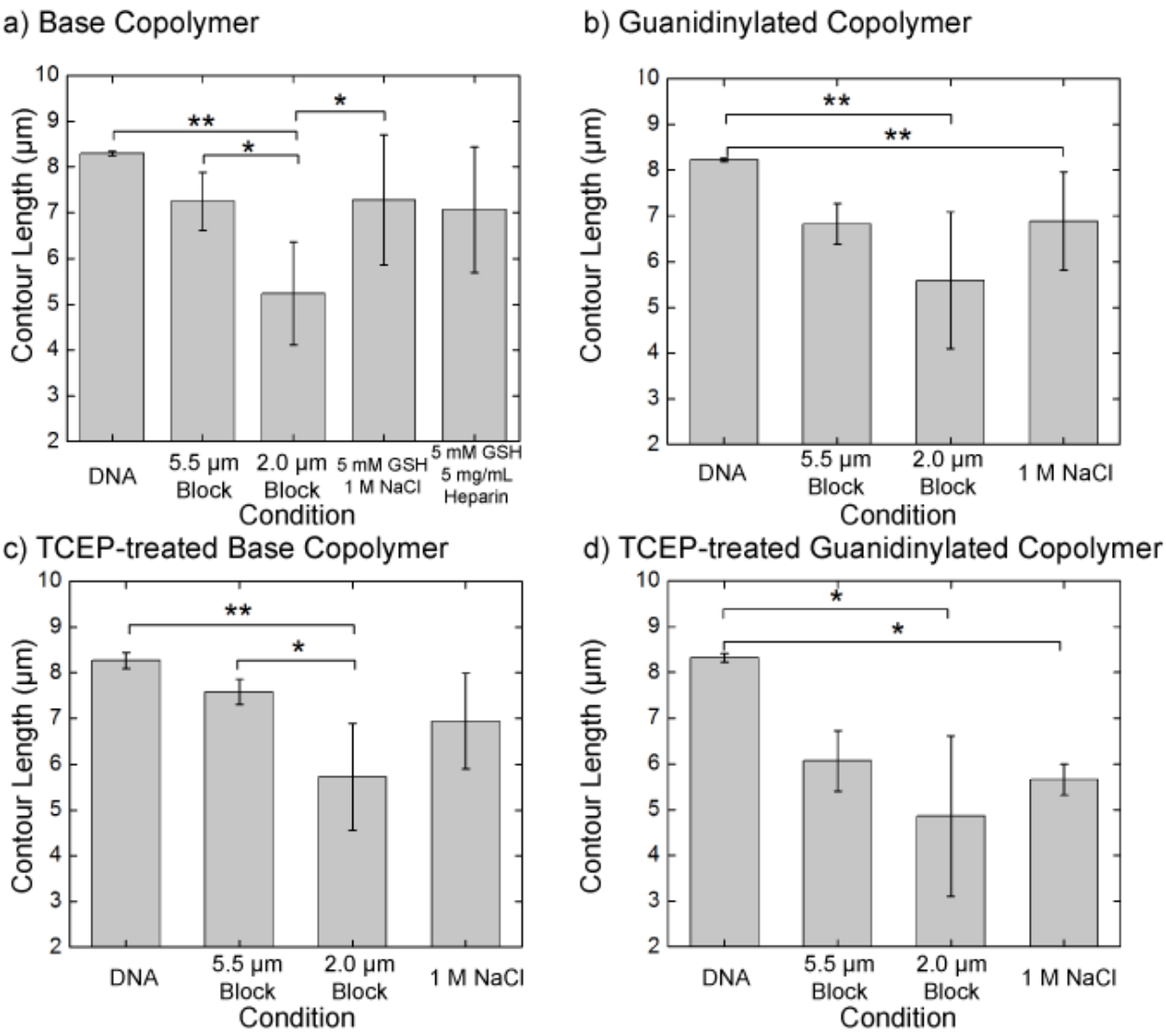

Figure 4.9 Contour length as a function of condensing agent and condition. (Tukey honest significance difference test, *p < 0.05, **p < 0.01)

The differences between the two structures become apparent when probing stability with respect to changes in environment, summarized in Figure 4.9. Base copolymer shows a combination of both hydrophobic and electrostatic stabilization of condensed complex, since it responded only when combination of salt and GSH was used. In contrast, guanidinylated copolymer displayed limited hydrophobic contributions and was largely destabilized by high salt conditions. This behavior is surprising, as the hydrophobic block content is approximately the same (15-16% by molecular mass) for

each variation of the polymer. At this moment we hypothesize that this phenomenon may be due to differences in condensate structure due to different binding processes between base copolymer and guanidinylated copolymer. It has been shown that DNA condensed with base copolymer forms spherical polyplexes, however more studies need to be performed to determine whether or not they are forming micelles [41, 42]. Recent studies reported that lysine allows for cooperative assembly that is dependent on peptide length while arginine undergoes non-cooperative assembly for more uniform and densely packed DNA [107, 108].

We hypothesized that pretreatment of the copolymers with TCEP would allow for mechanical properties to be manipulated via electrostatics (ionic strength and protonation state of the copolymer) due to the loss of the hydrophobic block. We found that this was indeed the case; the base copolymer's reduced contour length could now be recovered without the assistance of GSH. The guanidinylated copolymer exhibited similar behavior to the TCEP treated base copolymer as well as the untreated copolymer. However, it is notable that TCEP-treated guanidine based copolymer showed resistance to washing with salt, and 2 M NaCl concentration was required to remove all hysteresis from the force profile. This may be due to enhanced interaction between the polymer and the DNA after removal of the hydrophobic block, which could be sterically preventing optimal binding. Additionally, it has been shown that poly arginine binds DNA with a higher affinity than poly-lysines [109-111] in part due to the protonation being resonance-stabilized.

Recently the transfection efficiencies of these two copolymers have been reported [42]. *In vitro*, guanidine based copolymer displayed enhanced transfection, despite slightly increased toxicity. However, it was also demonstrated that *in vivo* the base

copolymer outperformed the guanidinylated one. This was attributed to better extracellular stability of the base copolymer. Based on our findings, we can conclude that this is likely to be the case, as complexes formed by condensation with base copolymer needed both GSH and salt to initiate cargo release; these conditions would be limited to intracellular compartments and would allow for targeted nucleic acid release in these specific areas, as glutathione levels are in the µm concentration in the bloodstream [112] but maintain millimolar levels in the cytoplasm [113]. On the other hand, DNA:guanidinylated complexes would be susceptible to destabilization in a blood stream and early unpackaging by biomolecules such as albumins and sulfated extracellular matrix components (heparin) would lower its efficiency *in vivo*.

4.5 Conclusion

In this study, we compared the mechanical signatures of DNA condensed by a primary amine or guanidine based analogs of a triblock copolymer. While the representative force profiles of the complexes are similar, we identify a limited role of the hydrophobic block in stabilization of the DNA:guanidinylated copolymer complex. These differences in stability are likely responsible for the differences observed in the transfection efficiencies for the two polymers *in vivo* vs. *in vitro*. Single molecule data is able to demonstrate that the inclusion of guanidine groups in the copolymer, while enhancing binding to DNA, reduces the role of the PCL block in providing stability to the complex. This work highlights the ability of the optical tweezers to observe dynamic mechanical responses of condensed DNA and the potential for single molecule studies to be used as a method for *in situ* differentiation of non-viral gene delivery vectors.

5 Identification of Key Mechanical Criteria for Maximum Transfection Efficiencies

Characterization of polyplex stability is necessary for optimization of controlled protection of and release of DNA for gene delivery [95]. While they are exposed to the extracellular milieu, nucleic acids must be protected from early release or degradation; within the intracellular spaces, an appropriate delivery vehicle should release the cargo in the cytosol or within the nucleus. An important step in the process of engineering a gene delivery vehicle is to correlate the mechanical properties with bulk transfection results.

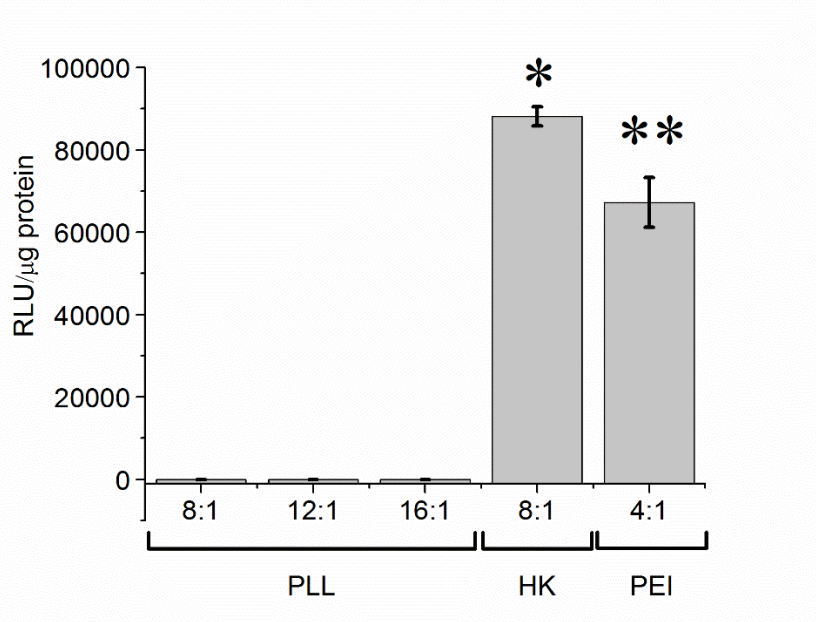

Figure 5.1 Efficacy of PLL vs. HK vs. PEI for transfection of a luciferase-expressing plasmid. For PLL several w/w ratios were tried and the optimal ratio for HK and PEI were used. HK displayed much greater transfection efficiency expressing 88138.4 ± 2362.7 and 67233.8 ± 5992.8 RLU/µg respectively as compared to 1.442 ± 1.2 RLU/µg for PLL at a ratio of 16:01. (n=8, ANOVA test, $P < 0.01$). *Data collected by Dr. Qixin Leng

In comparing the transfections of PEI, HK peptide, and 19-mer PLL, we observe a large range of transfection efficiencies (Figure 5.1). At weight ratios of 8:1-16:1 PLL showed minimal transfection, while PEI and HK peptide were able to reach transfection efficiencies three orders of magnitude higher.

At present, DNA transfection data has not been published for the G2-TETA nanoparticles; however, it has been shown as an efficient delivery vehicle for siRNA showing up to ~40% knockdown of β-gal *in vitro* [40]. The utility of the gold nanoparticles for DNA complexation however may be questionable, as the binding of siRNA to lower generation nanoparticles resulted in precipitation, demonstrating that complexation can lead to significant van der Walls interactions and aggregation. Due to its increased total charge, as compared to lower generation TETA nanoparticles, G2-TETA may be resistant to precipitation via complexation of siRNA however long DNA may be able to neutralize and bind a sufficient amount of nanoparticles to demonstrate aggregation.

Transfection results for the base copolymer as compared to the guanidinylated copolymer demonstrate varying trends for transfection. *In vitro* assays in Hela, Z310, and primary neuroprogenitor cells indicated that guanidinylated copolymer enhanced gene transfer over polyplexes prepared using base copolymer [42]. In contrast, *in vivo* delivery to murine brains showed an order of magnitude lower level of luciferase activity compared to base copolymer. It was hypothesized that the presence of proteoglycans, and specifically, heparan sulfate which is prevalent in the extracellular matrix surrounding proliferating neural progenitor cells [114], may cause early dissociation of the complex.

Key mechanical features of condensed DNA have been identified in earlier chapters. A large range of condensation forces have been demonstrated. All of the condensing agents in this body of work have been cationic in nature. Electrostatic interactions can range in magnitude, as we observe varying levels of condensing force (plateau forces) as well as force required to extend the complexes after condensation. While HK and PLL required the application of ~30 pN to return the complex to an extended conformation (Figure 2.3), maximum forces of >50 pN were unable to fully extend DNA:PEI (Figure 3.4) or DNA:guanidinylated complexes (Figure 4.5) despite their primarily electrostatically driven collapse.

Many biological molecules are ionized, and interaction of these charged molecules with condensed DNA complex have been shown to lead to early disintegration of complexes. Extracellular species include serum albumin and polyglycans. Intracellular competitors include proteins and RNA in the cytoplasm, and DNA in the nuclear fraction. However, other intermolecular interactions may complement the electrostatic interactions to improve stability. Isothermal calorimetry and nuclear magnetic resonance data show evidence of hydrogen bonding between HK peptide and siRNA [82]. G2-TETA and the triblock copolymers also employ hydrophobic interactions to increase stability.

In our single molecule studies we identified interactions that were resistant to >50 pN of applied force. Sources of this stability were from electrostatics, hydrophobic aggregation, chelation of divalent metal ions, or a combination. These interaction forces are above what biological machinery is capable of producing, therefore active dissociation is unlikely. Thus this mechanically non-decondensible response should be a

requirement for stability in the extracellular spaces and during uptake, and through incorporation into the endosome.

Upon internalization of polyplex, continued acidification of the endosome will lead to dynamic mechanical responses for DNA condensed by HK, PEI, or guanidinylated copolymer. This has been visualized as an increase in plateau forces, or formation of interactions which are unable to be disrupted via mechanical pulling. This response is desirable due to the fact that it signifies that the cationic agents retain functional groups that can still be protonated and suggest that the proton sponge effect may play a role in endosomal escape. Simultaneously, it is observed that protonation can increase the binding force level observed, which in turn results in greater protection of the nucleic acid.

During successful transfection, the DNA must be released from the carrier molecules at some point. Mechanically this is represented as a disappearance of hysteresis, sawtooth patterns in the stretch curve, force plateaus, and return to worm-like chain profile. Thus, complexes such as DNA:G2-TETA or DNA:base copolymer may demonstrate inefficient release of the cargo as they require stringent conditions for disassociation. However, naked DNA-like mechanics are not sufficient criteria with which to determine complete release. For instance, DNA:guanidinylated copolymer that has been treated with 1 M NaCl exhibits return of hysteresis and loss of extensible length when pH is dropped to 5, clearly demonstrating that some bound copolymer remains and is sufficient to produce dynamic mechanical responses. In this case, the optical tweezers may be an ideal instrument to measure true release of the DNA. Classical methods such

as fluorescence or gel electrophoresis may not be sensitive enough to detect residual molecules bound.

Based on the correlation of the presented single molecule findings and bulk transfection results, three key mechanical criteria have been identified for carriers. Firstly, upon condensation, the complex should stably collapse into a structure which is resistant to opening against 50 pN of force. Additionally, the carrier should show a change in mechanics associated with a drop in pH from 7.4 to 5.0, demonstrating an ability to buffer the endosome and provide increased level of interactions. Finally, intracellular conditions should return mechanics to original naked-DNA parameters; full release can be probed by again exposing the fiber to a pH 5.0 environment.

6 Future Work and Outlook

The work in this dissertation will motivate additional projects that will contribute to a more comprehensive understanding of the biophysical aspect of DNA condensation, leading to more informed design of gene delivery vectors. The utility of single molecular tweezers is realized in its real time observation of dynamic mechanical behavior of DNA complexes, which has not been previously reported, and the ability to probe complex biological systems in a simplified manner. As such, more destabilizing conditions such as the effects of molecular crowding on the mechanical properties of condensed DNA complexes can be explored. Furthermore, the optical tweezers could be used to test a library of agents to correlate structure and function of condensing agents.

6.1 Role of molecular crowding

Biomolecules such as proteins may also play a role in the biomechanical response of the DNA-peptide complexes. Macromolecules may occupy as much as 20-30% of the total volume of a cell [115]. This corresponds to ~200-300 g l^{-1} concentration; and even in blood plasma there is an approximate concentration of 80 g l^{-1}. Locally, charged proteins may act as salts, or compete to interact with the nanoplex components. Alternately, the crowded biological environment could deplete water molecules around the nanoplex and therefore further the condensation via osmotic effect. There is a need to examine the response to crowding to see how a carrier can overcome cytosolic conditions and successfully delivery nucleic acids to the nucleus.

Our strategy is to isolate and de-convolute the complex interactions that may occur within the biological milieu.

6.1.1 Experimental approach

The crowding effect has previously been probed by using up to 20% (w/v) BSA (Sigma-Aldrich) and polyethylene glycol (PEG)[116, 117]. In an analogous fashion the condensed DNA complexes will be exposed to 5%, 10%, 15%, and 20% BSA or PEG (MW 8000) at both pH 7.4 and pH 5.0. Additionally, lower molecular weight PEG may be used to determine the effect of co-solute size on complex stability.

6.1.2 Expected results, interpretation, possible pitfalls

The crowding effect may have interesting implications to the unpackaging of the DNA. Firstly, negatively charged proteins such as albumin, or other physiologically relevant molecules such as glycosaminoglycans that the polyplex may encounter, could potentially compete with the DNA to bind to the cations. Additionally, these charged complexes in the vicinity may deplete the water around the DNA molecule causing condensation. Finally, presence of a high concentration of negative charges may also cause columbic repulsion and also lead to DNA compaction. DNA compaction due to crowding by BSA has been previously reported [116]. However, it important to note that doubling the salt concentration from 100 mM to 200 mM was enough to reverse the compaction and unfold the DNA. It is unclear if crowding will cause disintegration of the complex due to competition binding to cations, or whether the high concentration and close proximity to these charged macroions will lead to DNA collapse. It is even possible that both could occur leading to compacted DNA in the absence of cationic condensing agent. A control experiment to obtain a force profile of DNA condensed due to depletion forces would need to be conducted with naked DNA in a 20% BSA solution.

To compare an anionic vs. a neutral crowded environment, polyethylene glycol will also be tested as crowding agent. Crowding with PEG has shown to be able to stabilize or destabilize naked DNA depending on duplex length as well as PEG size [117].

6.2 Mechanical response to biological environments

While microfluidic setup allows for precise control of environmental conditions, it is also important to explore the mechanical responses of the condensed DNA complexes to physiologically relevant conditions. Three compartments which are important to test are the bloodstream, cytosol, and nuclear environments. The ideal gene delivery candidate should demonstrate release in the nuclear environment, yet protection in the other two scenarios.

Serum, such as fetal bovine serum, can be introduced into the chamber to demonstrate the mechanical response of the DNA:cationic carrier complex within the bloodstream. Analogously, cell lysate may be used to test cytosolic stability, and *Xenopus laevis* egg extract can emulate the nuclear environment.

Using such conditions allows for visualization of the complex mechanics and further screening of a carrier's ability to protect and release the nucleic acid in the various biological compartments.

6.3 Design of a new optimal transfection agent based on a library and screening of agents with the OT as in situ testing of novel agents

Key mechanical criteria for a good transfection agent have been identified in Chapter 5. However, at this moment, the effect that varying design parameters such as: total charge, size, geometry, species and distribution of amines, buffering capacity, interaction with other molecules, and flexibility, and optimal range will have on the mechanical response has not been quantified or well characterized. Our strategy is to directly measure **condensation** and **disassociation** forces and determine the associated mechanical contribution due to specific residues. Rational design of novel gene delivery carriers will be facilitated by systematically developing a library of peptides to address these design parameters and quantifying the associated change in mechanical response.

6.3.1 Experimental approach

Based on preliminary data collected, along with previously published single-molecule studies, the aim is to design an appropriate peptide carrier using side groups to add functionality in a modular fashion. Synthesis of the novel peptide will start out by comparing the behaviors of 3, 5, 10, 15, 20-mer PLL. Based on the desired washing behavior, the peptide with the appropriate length can be chosen. Arginine content may also be increased to optimize DNA binding. Additionally, incorporation of specific amino acids between lysine residues can add functionality. For instance, incorporation of histidine will make the peptide pH responsive as well as add stability through chelation of divalent metals. As discussed in Chapter 2, histidine may also promote extracellular stability through chelation.

Increasing peptide hydrophobicity is another strategy which we can employ to promote polyplex stability. The nine amino acids that have hydrophobic side chains are glycine, alanine, valine, leucine, isoleucine, proline, phenylalanine, methionine, and

tryptophan. Inclusion of cysteine can incorporate reducible disulfide bonds into the peptide structure to allow for targeted separation of peptide in reducing intracellular conditions.

Following characterization of representative force profiles of the DNA:peptide complex, the dynamic mechanical responses will also be tested to determine forces necessary to disrupt the interactions and what environmental conditions can modulate stability. Development of a library which can correlate structural changes to specific mechanical features may enable modular design of future transfections agents.

6.4 Concluding remarks

It has been suggested that the appropriate modulation of mechanics may be the key to successful gene delivery [95]. This includes providing adequate protection in biological compartments where DNA is subject to degradation, providing a mechanism for cellular uptake and endosomal escape, nuclear localization, and finally release for transcription. The optical tweezers are an ideal system for studying the dynamic mechanical behavior of these complexes. The deviation between a historically poor transfection agent (PLL) and a good one (PEI) have been identified. Key mechanical criteria have been identified for efficient transfection and development of a structure vs function map will facilitate the design of future transfection agents. Design parameters such as: total charge, size, geometry, species and distribution of amines, buffering capacity, interaction with other molecules, and flexibility, and optimal range can be identified based on the mechanical properties and response of the DNA complexes tested. The hypothesis is that by designing a novel peptide which emphasizes the mechanical

responses demonstrated as key criteria by other delivery systems, a superior transfection agent will be produced.

7 Appendix A – Efficacy of Bovine Serum Albumin (BSA) Blocking

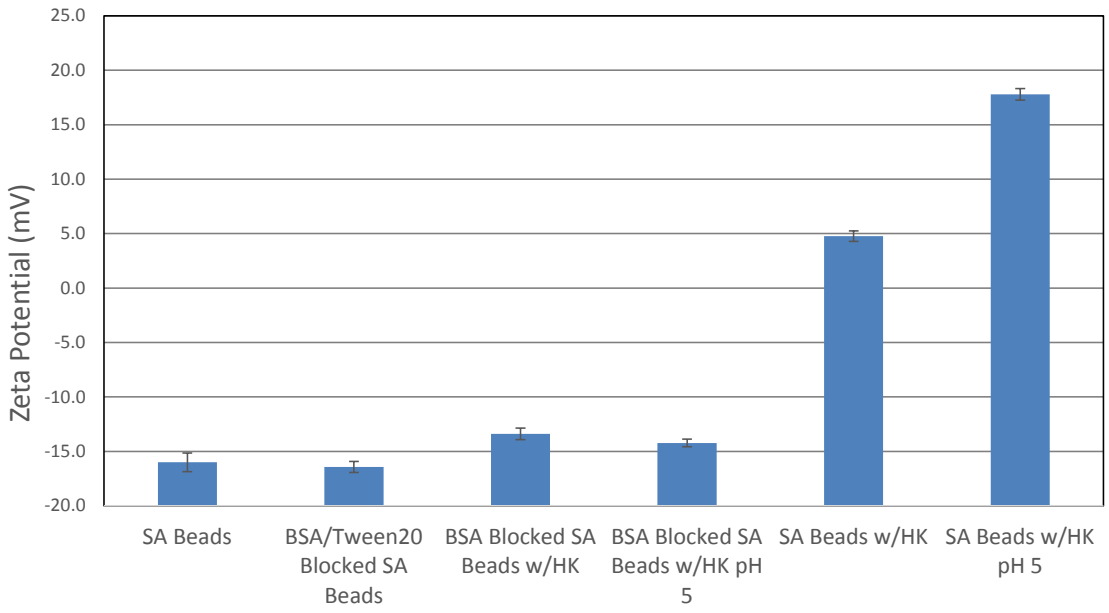

Figure 7.1 Zeta potential measurements of SA beads with and without BSA blocking.

Zeta potential measurements were taken to quantify the BSA's ability to prevent coating of the negatively charged streptavidin or anti-digoxigenin bead surfaces with cationic agent. To block the beads, SA beads were incubated for 20 minutes in a 5 mg/mL BSA and 0.1% Tween20 solution, then centrifuged for 5 minutes in a mini tabletop centrifuge and supernatant is aspirated to remove excess BSA. The incubation process is repeated with 1 µM HK peptide, and again excess is removed by centrifugation and aspiration. Finally the beads are resuspended in either 10 mM tris buffer, pH 7.4, or 10 mM acetate buffer, pH 5.

Zeta potential measurements were taken with a Zetasizer Nano (Malvern) and triplicate measurements were taken, reported as mean and standard deviation (Figure 7.1). Using a one-way Anova, and the Tukey Honest Significance Difference tests, our results indicate that BSA blocked SA beads (-16.4 ± 0.5 mV) demonstrated no significant change in zeta potential as compared to the untreated SA beads (-16.0 ± 0.9 mV) ($p = 0.05$). In both samples that were BSA blocked and then incubated with HK, the zeta potential remained negative, though increased as compared to the control SA beads ($p < 0.05$). However, we do see a much larger increase in zeta potential when the HK is incubated on unblocked beads, up to 4.8 ± 0.5 mV for the HK coated beads in tris, and 17.8 ± 0.5 mV for the HK coated beads in acetate. This suggests that BSA blocking is indeed preventing cationic peptide from binding to the bead surfaces.

In another control experiment, we wanted to see what force profile features would appear if condensation were initiated at the surface of the bead. SA beads are BSA blocked, and ½ λ DNA is "deposited" on SA bead by forming a tether between the AD and SA beads, then breaking the tether. A second set of AD beads, which have been incubated with 1 μM HK peptide, are used to recapture and pull the DNA fiber. The resulting force profiles are recorded (Figure 7.2). The force profiles remain worm-like chain in the relaxation, but show hysteresis in the stretch curve and a few large stick slip unbinding events.

The same experimental procedure is then repeated with AD beads that have been incubated with 5 mg/mL BSA and 0.1% Tween20 solution, washed and then incubated with 1 μM HK. During interaction with 5 different coated beads, no hysteresis was observed and the fiber maintained naked DNA mechanics (Figure 7.3).

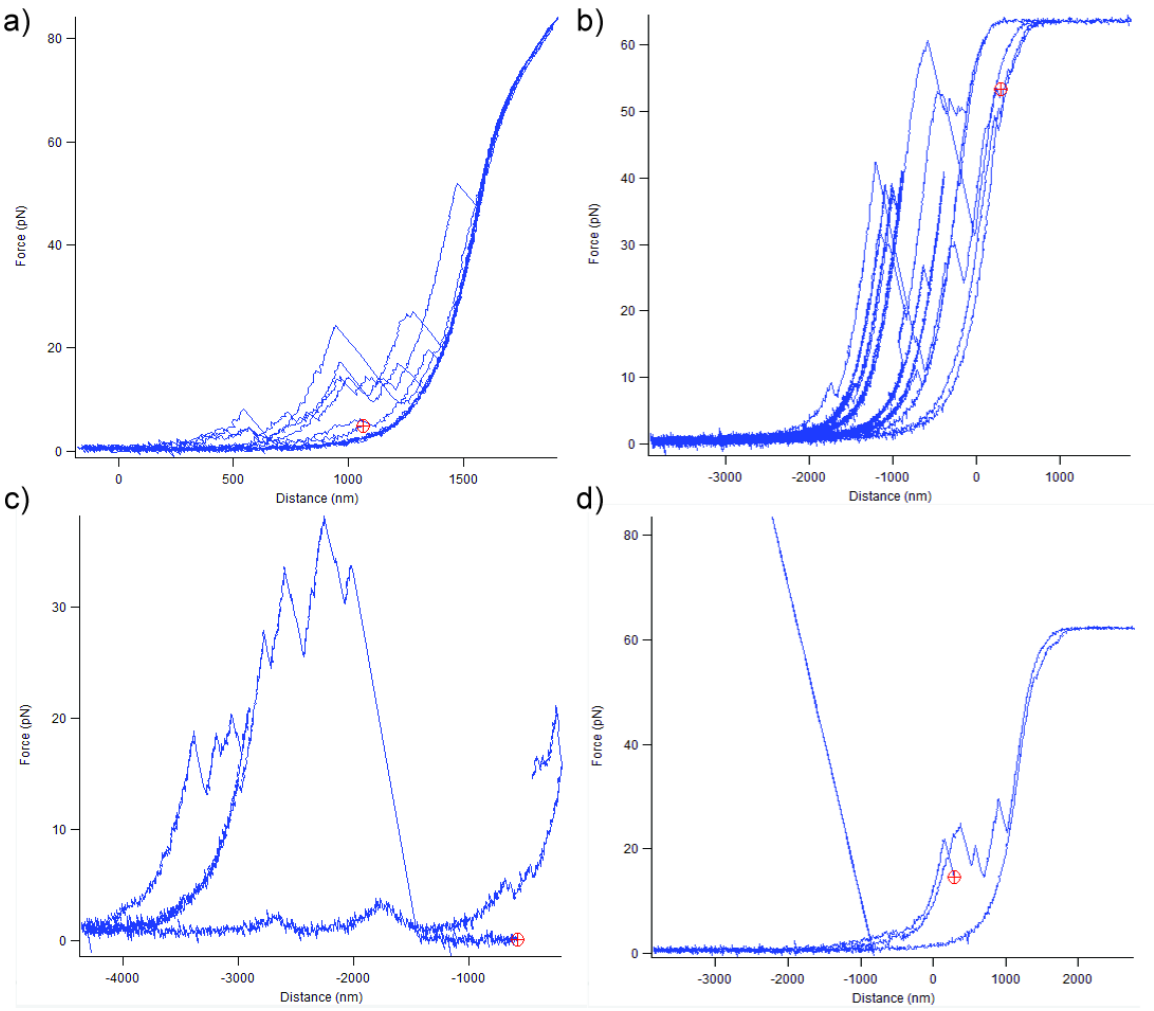

Figure 7.2 Force vs. extension curves of DNA pulled with HK coated AD beads.

These experiments demonstrate again that BSA inhibits binding of HK to bead surface. Additionally, we did not see the formation of plateaus when DNA interacted with HK coated beads; thus suggesting that experimental data showing plateau behavior is not likely nucleating on the bead surface.

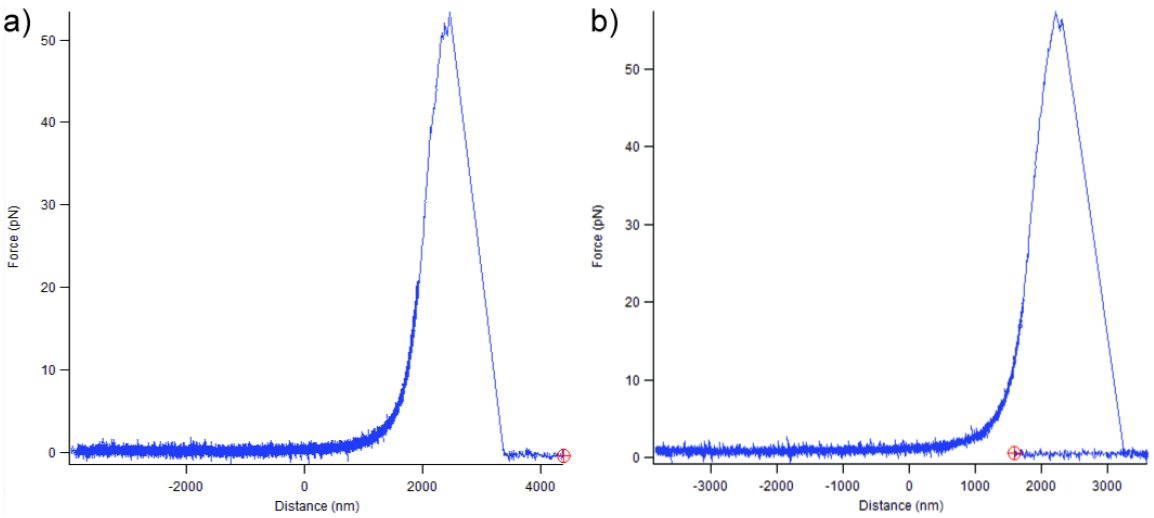

Figure 7.3 Force vs. extension curves of DNA pulled with HK incubated AD beads that were pre-blocked with BSA.

Bibliography

1. Vile, R.G., S.J. Russell, and N.R. Lemoine, *Cancer gene therapy: hard lessons and new courses.* Gene Therapy, 2000. **7**(1): p. 2-8.
2. Kerr, D., *Clinical development of gene therapy for colorectal cancer.* Nature Reviews Cancer, 2003. **3**(8): p. 615-622.
3. McNeish, I.A., S.J. Bell, and N.R. Lemoine, *Gene therapy progress and prospects: cancer gene therapy using tumour suppressor genes.* Gene Therapy, 2004. **11**(6): p. 497-503.
4. Yin, H., R.L. Kanasty, A.A. Eltoukhy, A.J. Vegas, J.R. Dorkin, and D.G. Anderson, *Non-viral vectors for gene-based therapy.* Nature Reviews Genetics, 2014. **15**(8): p. 541-555.
5. Nguyen, J. and F.C. Szoka, *Nucleic Acid Delivery: The Missing Pieces of the Puzzle?* Accounts of Chemical Research, 2012. **45**(7): p. 1153-1162.
6. Tachibana, R., H. Harashima, N. Ide, S. Ukitsu, Y. Ohta, N. Suzuki, H. Kikuchi, Y. Shinohara, and H. Kiwada, *Quantitative analysis of correlation between number of nuclear plasmids and gene expression activity after transfection with cationic liposomes.* Pharmaceutical Research, 2002. **19**(4): p. 377-381.
7. James, M.B. and T.D. Giorgio, *Nuclear-associated plasmid, but not cell-associated plasmid, is correlated with transgene expression in cultured mammalian cells.* Molecular Therapy, 2000. **1**(4): p. 339-346.
8. Zuidam, N.J. and Y. Barenholz, *Electrostatic parameters of cationic liposomes commonly used for gene delivery as determined by 4-heptadecyl-7-hydroxycoumarin.* Biochimica Et Biophysica Acta-Biomembranes, 1997. **1329**(2): p. 211-222.
9. Kawabata, K., Y. Takakura, and M. Hashida, *The Fate of Plasmid DNA after Intravenous-Injection in Mice - Involvement of Scavenger Receptors in Its Hepatic-Uptake.* Pharmaceutical Research, 1995. **12**(6): p. 825-830.
10. Mumper, R.J. and A.P. Rolland, *Plasmid delivery to muscle: Recent advances in polymer delivery systems.* Advanced Drug Delivery Reviews, 1998. **30**(1-3): p. 151-172.
11. Ruponen, M., S. Yla-Herttuala, and A. Urtti, *Interactions of polymeric and liposomal gene delivery systems with extracellular glycosaminoglycans: physicochemical and transfection studies.* Biochimica Et Biophysica Acta-Biomembranes, 1999. **1415**(2): p. 331-341.
12. Mislick, K.A. and J.D. Baldeschwieler, *Evidence for the role of proteoglycans in cation-mediated gene transfer.* Proceedings of the National Academy of Sciences, 1996. **93**(22): p. 12349-12354.
13. Ghinea, N. and M. Hasu, *Charge Effect on Binding, Uptake and Transport of Ferritin through Fenestrated Endothelium.* Journal of Submicroscopic Cytology and Pathology, 1986. **18**(4): p. 647-659.

14. Wiethoff, C.M. and C.R. Middaugh, *Barriers to nonviral gene delivery.* Journal of Pharmaceutical Sciences, 2003. **92**(2): p. 203-217.

15. Rehman, Z.u., D. Hoekstra, and I.S. Zuhorn, *Mechanism of polyplex-and lipoplex-mediated delivery of nucleic acids: real-time visualization of transient membrane destabilization without endosomal lysis.* ACS Nano, 2013. **7**(5): p. 3767-3777.

16. Zhang, Z.Y. and B.D. Smith, *High-generation polycationic dendrimers are unusually effective at disrupting anionic vesicles: Membrane bending model.* Bioconjugate Chemistry, 2000. **11**(6): p. 805-814.

17. Klemm, A.R., D. Young, and J.B. Lloyd, *Effects of polyethyleneimine on endocytosis and lysosome stability.* Biochemical Pharmacology, 1998. **56**(1): p. 41-46.

18. Sonawane, N.D., F.C. Szoka, and A. Verkman, *Chloride accumulation and swelling in endosomes enhances DNA transfer by polyamine-DNA polyplexes.* Journal of Biological Chemistry, 2003. **278**(45): p. 44826-44831.

19. Pollard, H., G. Toumaniantz, J.L. Amos, H. Avet-Loiseau, G. Guihard, J.P. Behr, and D. Escande, *Ca2+-sensitive cytosolic nucleases prevent efficient delivery to the nucleus of injected plasmids.* Journal of Gene Medicine, 2001. **3**(2): p. 153-164.

20. Pollard, H., J.S. Remy, G. Loussouarn, S. Demolombe, J.P. Behr, and D. Escande, *Polyethylenimine but not cationic lipids promotes transgene delivery to the nucleus in mammalian cells.* Journal of Biological Chemistry, 1998. **273**(13): p. 7507-11.

21. Breuzard, G., M. Tertil, C. Goncalves, H. Cheradame, P. Geguan, C. Pichon, and P. Midoux, *Nuclear delivery of NFκB-assisted DNA/polymer complexes: plasmid DNA quantitation by confocal laser scanning microscopy and evidence of nuclear polyplexes by FRET imaging.* Nucleic Acids Research, 2008. **36**(12): p. e71-e71.

22. Cohen, R.N., M.A. van der Aa, N. Macaraeg, A.P. Lee, and F.C. Szoka, *Quantification of plasmid DNA copies in the nucleus after lipoplex and polyplex transfection.* Journal of Controlled Release, 2009. **135**(2): p. 166-174.

23. Chan, C., T. Senden, and D. Jans, *Supramolecular structure and nuclear targeting efficiency determine the enhancement of transfection by modified polylysines.* Gene Therapy, 2000. **7**(19): p. 1690-1697.

24. Subramanian, A., P. Ranganathan, and S.L. Diamond, *Nuclear targeting peptide scaffolds for lipofection of nondividing mammalian cells.* Nature Biotechnology, 1999. **17**(9): p. 873-877.

25. Saccardo, P., A. Villaverde, and N. Gonzalez-Montalban, *Peptide-mediated DNA condensation for non-viral gene therapy.* Biotechnology Advances, 2009. **27**(4): p. 432-438.

26. Pack, D.W., A.S. Hoffman, S. Pun, and P.S. Stayton, *Design and development of polymers for gene delivery.* Nature Reviews Drug Discovery, 2005. **4**(7): p. 581-593.

27. Plank, C., B. Oberhauser, K. Mechtler, C. Koch, and E. Wagner, *The Influence of Endosome-Disruptive Peptides on Gene-Transfer Using Synthetic Virus-Like Gene-Transfer Systems.* Journal of Biological Chemistry, 1994. **269**(17): p. 12918-12924.

28. Godbey, W.T. and A.G. Mikos, *Recent progress in gene delivery using non-viral transfer complexes.* Journal of Controlled Release, 2001. **72**(1-3): p. 115-125.

29. Putnam, D. and R. Langer, *Poly(4-hydroxy-L-proline ester): Low-temperature polycondensation and plasmid DNA complexation.* Macromolecules, 1999. **32**(11): p. 3658-3662.

30. Lv, H., S. Zhang, B. Wang, S. Cui, and J. Yan, *Toxicity of cationic lipids and cationic polymers in gene delivery.* Journal of Controlled Release, 2006. **114**(1): p. 100-109.

31. Suh, J., H.J. Paik, and B.K. Hwang, *Ionization of Poly(Ethylenimine) and Poly(Allylamine) at Various Phs.* Bioorganic Chemistry, 1994. **22**(3): p. 318-327.

32. Forrest, M.L., G.E. Meister, J.T. Koerber, and D.W. Pack, *Partial acetylation of polyethylenimine enhances in vitro gene delivery.* Pharmaceutical Research, 2004. **21**(2): p. 365-371.

33. Midoux, P., C. Pichon, J.J. Yaouanc, and P.A. Jaffres, *Chemical vectors for gene delivery: a current review on polymers, peptides and lipids containing histidine or imidazole as nucleic acids carriers.* British Jornal of Pharmacology, 2009. **157**(2): p. 166-78.

34. Midoux, P. and M. Monsigny, *Efficient gene transfer by histidylated polylysine pDNA complexes.* Bioconjugate Chemistry, 1999. **10**(3): p. 406-411.

35. Putnam, D., C.A. Gentry, D.W. Pack, and R. Langer, *Polymer-based gene delivery with low cytotoxicity by a unique balance of side-chain termini.* Proceedings of the National Academy of Sciences of the United States of America, 2001. **98**(3): p. 1200-1205.

36. Ghosh, P., G. Han, M. De, C.K. Kim, and V.M. Rotello, *Gold nanoparticles in delivery applications.* Advanced Drug Delivery Reviews, 2008. **60**(11): p. 1307-1315.

37. Pissuwan, D., T. Niidome, and M.B. Cortie, *The forthcoming applications of gold nanoparticles in drug and gene delivery systems.* Journal of Controlled Release, 2011. **149**(1): p. 65-71.

38. Ghosh, P.S., C.K. Kim, G. Han, N.S. Forbes, and V.M. Rotello, *Efficient Gene Delivery Vectors by Tuning the Surface Charge Density of Amino Acid-Functionalized Gold Nanoparticles.* ACS Nano, 2008. **2**(11): p. 2213-2218.

39. Arents, G., R.W. Burlingame, B.C. Wang, W.E. Love, and E.N. Moudrianakis, *The Nucleosomal Core Histone Octamer at 3.1-a Resolution - a Tripartite Protein Assembly and a Left-Handed Superhelix.* Proceedings of the National Academy of Sciences of the United States of America, 1991. **88**(22): p. 10148-10152.

40. Kim, S.T., A. Chompoosor, Y.C. Yeh, S.S. Agasti, D.J. Solfiell, and V.M. Rotello, *Dendronized Gold Nanoparticles for siRNA Delivery.* Small, 2012. **8**(21): p. 3253-3256.

41. Wei, H., L.R. Volpatti, D.L. Sellers, D.O. Maris, I.W. Andrews, A.S. Hemphill, L.W. Chan, D.S.H. Chu, P.J. Horner, and S.H. Pun, *Dual Responsive, Stabilized Nanoparticles for Efficient In Vivo Plasmid Delivery.* Angewandte Chemie-International Edition, 2013. **52**(20): p. 5377-5381.

42. Choi, J.L., J.-K.Y. Tan, D.L. Sellers, H. Wei, P.J. Horner, and S.H. Pun, *Guanidinylated block copolymers for gene transfer: A comparison with amine-based materials for in vitro and in vivo gene transfer efficiency.* Biomaterials, 2015. **54**: p. 87-96.

43. Bennink, M.L., S.H. Leuba, G.H. Leno, J. Zlatanova, B.G. de Grooth, and J. Greve, *Unfolding individual nucleosomes by stretching single chromatin fibers with optical tweezers.* Nature Structural Biology, 2001. **8**(7): p. 606-610.

44. van den Broek, B., M.C. Noom, J. van Mameren, C. Battle, F.C. Mackintosh, and G.J. Wuite, *Visualizing the formation and collapse of DNA toroids.* Biophysical Journal, 2010. **98**(9): p. 1902-10.

45. Besteman, K., K. Van Eijk, and S.G. Lemay, *Charge inversion accompanies DNA condensation by multivalent ions.* Nature Physics, 2007. **3**(9): p. 641-644.

46. Ritort, F., S. Mihardja, S.B. Smith, and C. Bustamante, *Condensation transition in DNA-polyaminoamide dendrimer fibers studied using optical tweezers.* Physical Review Letters, 2006. **96**(11): p. 118301.

47. Bustamante, C., Z. Bryant, and S.B. Smith, *Ten years of tension: single-molecule DNA mechanics.* Nature, 2003. **421**(6921): p. 423-7.

48. Lang, M.J., P.M. Fordyce, A.M. Engh, K.C. Neuman, and S.M. Block, *Simultaneous, coincident optical trapping and single-molecule fluorescence.* Nature Methods, 2004. **1**(2): p. 133-9.

49. Ashkin, A., J.M. Dziedzic, J.E. Bjorkholm, and S. Chu, *Observation of a Single-Beam Gradient Force Optical Trap for Dielectric Particles.* Optics Letters, 1986. **11**(5): p. 288-290.

50. Smith, S.B., Y. Cui, and C. Bustamante, *Optical-trap force transducer that operates by direct measurement of light momentum.* Methods in Enzymology, 2003. **361**: p. 134-62.

51. Moffitt, J.R., Y.R. Chemla, S.B. Smith, and C. Bustamante, *Recent Advances in Optical Tweezers.* Annual Review of Biochemistry, 2008. **77**: p. 205-228.

52. Wang, M.D., H. Yin, R. Landick, J. Gelles, and S.M. Block, *Stretching DNA with optical tweezers.* Biophysical Journal, 1997. **72**(3): p. 1335-46.

53. Sischka, A., K. Toensing, R. Eckel, S.D. Wilking, N. Sewald, R. Ros, and D. Anselmetti, *Molecular mechanisms and kinetics between DNA and DNA binding ligands.* Biophysical Journal, 2005. **88**(1): p. 404-11.

54. Mihailovic, A., I. Vladescu, M. McCauley, E. Ly, M.C. Williams, E.M. Spain, and M.E. Nunez, *Exploring the interaction of ruthenium(II) polypyridyl complexes with DNA using single-molecule techniques.* Langmuir, 2006. **22**(10): p. 4699-709.

55. Vladescu, I.D., M.J. McCauley, I. Rouzina, and M.C. Williams, *Mapping the phase diagram of single DNA molecule force-induced melting in the presence of ethidium.* Physical Review Letters, 2005. **95**(15): p. 158102.

56. Brower-Toland, B.D., C.L. Smith, R.C. Yeh, J.T. Lis, C.L. Peterson, and M.D. Wang, *Mechanical disruption of individual nucleosomes reveals a reversible multistage release of DNA.* Proceedings of the National Academy of Sciences of the United States of America, 2002. **99**(4): p. 1960-1965.

57. Brower-Toland, B., D.A. Wacker, R.M. Fulbright, J.T. Lis, W.L. Kraus, and M.D. Wang, *Specific contributions of histone tails and their acetylation to the mechanical stability of nucleosomes.* Journal of Molecular Biology, 2005. **346**(1): p. 135-146.

58. Camunas-Soler, J., S. Frutos, C.V. Bizarro, S. de Lorenzo, M.E. Fuentes-Perez, R. Ramsch, S. Vilchez, C. Solans, F. Moreno-Herrero, F. Albericio, R. Eritja, E. Giralt, S.B. Dev, and F. Ritort, *Electrostatic binding and hydrophobic collapse of Peptide-nucleic Acid aggregates quantified using force spectroscopy.* ACS Nano, 2013. **7**(6): p. 5102-13.

59. Milstein, J.N. and J.C. Meiners, *On the role of DNA biomechanics in the regulation of gene expression.* Journal of The Royal Society Interface, 2011. **8**(65): p. 1673-81.

60. Wang, M.D., M.J. Schnitzer, H. Yin, R. Landick, J. Gelles, and S.M. Block, *Force and velocity measured for single molecules of RNA polymerase.* Science, 1998. **282**(5390): p. 902-907.

61. Yu, J., J. Moffitt, C.L. Hetherington, C. Bustamante, and G. Oster, *Mechanochemistry of a Viral DNA Packaging Motor.* Journal of Molecular Biology, 2010. **400**(2): p. 186-203.

62. EssevazRoulet, B., U. Bockelmann, and F. Heslot, *Mechanical separation of the complementary strands of DNA.* Proceedings of the National Academy of Sciences of the United States of America, 1997. **94**(22): p. 11935-11940.

63. Han, G., N.S. Chari, A. Verma, R. Hong, C.T. Martin, and V.M. Rotello, *Controlled recovery of the transcription of nanoparticle-bound DNA by intracellular concentrations of glutathione.* Bioconjugate Chemistry, 2005. **16**(6): p. 1356-1359.

64. Maier, B., D. Bensimon, and V. Croquette, *Replication by a single DNA polymerase of a stretched single-stranded DNA.* Proceedings of the National Academy of Sciences of the United States of America, 2000. **97**(22): p. 12002-12007.

65. Smith, D.E., S.J. Tans, S.B. Smith, S. Grimes, D.L. Anderson, and C. Bustamante, *The bacteriophage phi 29 portal motor can package DNA against a large internal force.* Nature, 2001. **413**(6857): p. 748-752.

66. Smith, S.B., Y.J. Cui, and C. Bustamante, *Optical-trap force transducer that operates by direct measurement of light momentum.* Biophotonics, Pt B, 2003. **361**: p. 134-162.

67. Pichon, C., B. Guerin, M. Refregiers, C. Goncalves, P. Vigny, and P. Midoux, *Zinc improves gene transfer mediated by DNA/cationic polymer complexes.* Journal of Gene Medicine, 2002. **4**(5): p. 548-559.

68. Stone, M.D., Z. Bryant, N.J. Crisona, S.B. Smith, A. Vologodskii, C. Bustamante, and N.R. Cozzarelli, *Chirality sensing by Escherichia coli topoisomerase IV and the mechanism of type II topoisomerases.* Proceedings of the National Academy of Sciences of the United States of America, 2003. **100**(15): p. 8654-8659.

69. Rouzina, I. and V.A. Bloomfield, *DNA bending by small, mobile multivalent cations.* Biophysical Journal, 1998. **74**(6): p. 3152-3164.

70. Baumann, C.G., V.A. Bloomfield, S.B. Smith, C. Bustamante, M.D. Wang, and S.M. Block, *Stretching of single collapsed DNA molecules.* Biophysical Journal, 2000. **78**(4): p. 1965-78.

71. Li, I.T. and G.C. Walker, *Signature of hydrophobic hydration in a single polymer.* Proceedings of the National Academy of Sciences of the United States of America, 2011. **108**(40): p. 16527-32.

72. Trzaskowski, B., L. Adamowicz, and P.A. Deymier, *A theoretical study of zinc(II) interactions with amino acid models and peptide fragments.* Journal of Biological Inorganic Chemistry, 2008. **13**(1): p. 133-137.

73. Nyborg, J.K. and O.B. Peersen, *That zincing feeling: the effects of EDTA on the behaviour of zinc-binding transcriptional regulators.* Biochemical Journal, 2004. **381**(Pt 3): p. e3-4.

74. Conti, M., G. Falini, and B. Samori, *How strong is the coordination bond between a histidine tag and Ni-nitrilotriacetate? An experiment of mechanochemistry on single molecules.* Angewandte Chemie-International Edition, 2000. **39**(1): p. 215-218.

75. Cao, Y., T. Yoo, and H.B. Li, *Single molecule force spectroscopy reveals engineered metal chelation is a general approach to enhance mechanical stability of proteins.* Proceedings of the National Academy of Sciences of the United States of America, 2008. **105**(32): p. 11152-11157.

76. Zhao, C., L.M. Hellman, X. Zhan, W.S. Bowman, S.W. Whiteheart, and M.G. Fried, *Hexahistidine-tag-specific optical probes for analyses of proteins and their interactions.* Analytical Biochemistry, 2010. **399**(2): p. 237-45.

77. Li, H.B., A.F. Oberhauser, S.B. Fowler, J. Clarke, and J.M. Fernandez, *Atomic force microscopy reveals the mechanical design of a modular protein.*

Proceedings of the National Academy of Sciences of the United States of America, 2000. **97**(12): p. 6527-6531.

78. Zhang, X.H., K. Halvorsen, C.Z. Zhang, W.P. Wong, and T.A. Springer, *Mechanoenzymatic Cleavage of the Ultralarge Vascular Protein von Willebrand Factor.* Science, 2009. **324**(5932): p. 1330-1334.

79. Fosmire, G.J., *Zinc toxicity.* American Journal of Clinical Nutrition, 1990. **51**(2): p. 225-7.

80. Goulle, J.P., L. Mahieu, J. Castermant, N. Neveu, L. Bonneau, G. Laine, D. Bouige, and C. Lacroix, *Metal and metalloid multi-elementary ICP-MS validation in whole blood, plasma, urine and hair. Reference values.* Forensic Science International, 2005. **153**(1): p. 39-44.

81. Outten, C.E. and T.V. O'Halloran, *Femtomolar sensitivity of metalloregulatory proteins controlling zinc homeostasis.* Science, 2001. **292**(5526): p. 2488-2492.

82. Chou, S.T., K. Hom, D. Zhang, Q. Leng, L.J. Tricoli, J.M. Hustedt, A. Lee, M.J. Shapiro, J. Seog, J.D. Kahn, and A.J. Mixson, *Enhanced silencing and stabilization of siRNA polyplexes by histidine-mediated hydrogen bonds.* Biomaterials, 2014. **35**(2): p. 846-55.

83. Rungsardthong, U., T. Ehtezazi, L. Bailey, S.P. Armes, M.C. Garnett, and S. Stolnik, *Effect of polymer ionization on the interaction with DNA in nonviral gene delivery systems.* Biomacromolecules, 2003. **4**(3): p. 683-90.

84. Strand, S.P., S. Danielsen, B.E. Christensen, and K.M. Varum, *Influence of chitosan structure on the formation and stability of DNA-chitosan polyelectrolyte complexes.* Biomacromolecules, 2005. **6**(6): p. 3357-3366.

85. Verma, I.M. and N. Somia, *Gene therapy -- promises, problems and prospects.* Nature, 1997. **389**(6648): p. 239-42.

86. Niidome, T. and L. Huang, *Gene therapy progress and prospects: nonviral vectors.* Gene Therapy, 2002. **9**(24): p. 1647-52.

87. Schaffer, D.V., N.A. Fidelman, N. Dan, and D.A. Lauffenburger, *Vector unpacking as a potential barrier for receptor-mediated polyplex gene delivery.* Biotechnology and Bioengineering, 2000. **67**(5): p. 598-606.

88. Lee, A., A. Karcz, R. Akman, T. Zheng, S. Kwon, S.T. Chou, S. Sucayan, L.J. Tricoli, J.M. Hustedt, Q. Leng, J.D. Kahn, A.J. Mixson, and J. Seog, *Direct observation of dynamic mechanical regulation of DNA condensation by environmental stimuli.* Angewandte Chemie, International Edition in English, 2014. **53**(40): p. 10631-5.

89. Nguyen, T.T.R., I.; Shklovskii, B.I. , *Reentrant Condensation of DNA Induced by Multivalent Counterions.* Journal of Chemical Physics, 2000. **112**(5).

90. Bertschinger, M., G. Backliwal, A. Schertenleib, M. Jordan, D.L. Hacker, and F.M. Wurm, *Disassembly of polyethylenimine-DNA particles in vitro: implications for polyethylenimine-mediated DNA delivery.* Journal of Controlled Release, 2006. **116**(1): p. 96-104.

91. Moret, I., J. Esteban Peris, V.M. Guillem, M. Benet, F. Revert, F. Dasi, A. Crespo, and S.F. Alino, *Stability of PEI-DNA and DOTAP-DNA complexes: effect of alkaline pH, heparin and serum.* Journal of Controlled Release, 2001. **76**(1-2): p. 169-81.

92. Han, G., C.T. Martin, and V.M. Rotello, *Stability of gold nanoparticle-bound DNA toward biological, physical, and chemical agents.* Chemical Biology & Drug Design, 2006. **67**(1): p. 78-82.

93. Goodman, C.M., N.S. Chari, G. Han, R. Hong, P. Ghosh, and V.M. Rotello, *DNA-binding by functionalized gold nanoparticles: Mechanism and structural requirements.* Chemical Biology & Drug Design, 2006. **67**(4): p. 297-304.

94. Sandhu, K.K., C.M. McIntosh, J.M. Simard, S.W. Smith, and V.M. Rotello, *Gold nanoparticle-mediated Transfection of mammalian cells.* Bioconjugate Chemistry, 2002. **13**(1): p. 3-6.

95. Grigsby, C.L. and K.W. Leong, *Balancing protection and release of DNA: tools to address a bottleneck of non-viral gene delivery.* Journal of The Royal Society Interface, 2010. **7 Suppl 1**: p. S67-82.

96. Godbey, W.T., K.K. Wu, and A.G. Mikos, *Tracking the intracellular path of poly(ethylenimine)/DNA complexes for gene delivery.* Proceedings of the National Academy of Sciences of the United States of America, 1999. **96**(9): p. 5177-5181.

97. Li, S. and L. Huang, *Nonviral gene therapy: promises and challenges.* Gene Therapy, 2000. **7**(1): p. 31-4.

98. De Laporte, L., J. Cruz Rea, and L.D. Shea, *Design of modular non-viral gene therapy vectors.* Biomaterials, 2006. **27**(7): p. 947-54.

99. Varkouhi, A.K., M. Scholte, G. Storm, and H.J. Haisma, *Endosomal escape pathways for delivery of biologicals.* Journal of Controlled Release, 2011. **151**(3): p. 220-8.

100. Neuman, K.C. and A. Nagy, *Single-molecule force spectroscopy: optical tweezers, magnetic tweezers and atomic force microscopy.* Nature Methods, 2008. **5**(6): p. 491-505.

101. Carlson, P.M., J.G. Schellinger, J.A. Pahang, R.N. Johnson, and S.H. Pun, *Comparative study of guanidine-based and lysine-based brush copolymers for plasmid delivery.* Biomaterials Science, 2013. **1**(7): p. 736-744.

102. Ganta, S., H. Devalapally, A. Shahiwala, and M. Amiji, *A review of stimuli-responsive nanocarriers for drug and gene delivery.* Journal of Controlled Release, 2008. **126**(3): p. 187-204.

103. Brancia, F.L., S.G. Oliver, and S.J. Gaskell, *Improved matrix-assisted laser desorption/ionization mass spectrometric analysis of tryptic hydrolysates of proteins following guanidination of lysine-containing peptides.* Rapid Communications in Mass Spectrometry, 2000. **14**(21): p. 2070-2073.

104. Futaki, S., *Membrane-permeable arginine-rich peptides and the translocation mechanisms.* Advanced Drug Delivery Reviews, 2005. **57**(4): p. 547-558.

105. Wender, P.A., W.C. Galliher, E.A. Goun, L.R. Jones, and T.H. Pillow, *The design of guanidinium-rich transporters and their internalization mechanisms.* Advanced Drug Delivery Reviews, 2008. **60**(4-5): p. 452-472.

106. Kim, I.D., C.M. Lim, J.B. Kim, H.Y. Nam, K. Nam, S.W. Kim, J.S. Park, and J.K. Lee, *Neuroprotection by biodegradable PAMAM ester (e-PAM-R)-mediated HMGB1 siRNA delivery in primary cortical cultures and in the postischemic brain.* Journal of Controlled Release, 2010. **142**(3): p. 422-430.

107. Mann, A., G. Thakur, V. Shukla, A.K. Singh, R. Khanduri, R. Naik, Y. Jiang, N. Kalra, B.S. Dwarakanath, U. Langel, and M. Ganguli, *Differences in DNA Condensation and Release by Lysine and Arginine Homopeptides Govern Their DNA Delivery Efficiencies.* Molecular Pharmaceutics, 2011. **8**(5): p. 1729-1741.

108. DeRouchey, J., B. Hoover, and D.C. Rau, *A Comparison of DNA Compaction by Arginine and Lysine Peptides: A Physical Basis for Arginine Rich Protarnines.* Biochemistry, 2013. **52**(17): p. 3000-3009.

109. Mascotti, D.P. and T.M. Lohman, *Thermodynamics of oligoarginines binding to RNA and DNA.* Biochemistry, 1997. **36**(23): p. 7272-7279.

110. Standke, K.H. and H. Brunnert, *Estimation of Affinity Constants for Binding of Model Peptides to DNA by Equilibrium Dialysis.* Nucleic Acids Research, 1975. **2**(10): p. 1839-1849.

111. Wehling, K., H.A. Arfmann, K.H.C. Standke, and K.G. Wagner, *Specifity of DNA Basic Polypeptide Interactions - Influence of Neutral Residues Incorporated into Polylysine and Polyarginine.* Nucleic Acids Research, 1975. **2**(6): p. 799-807.

112. Jones, D.P., J.L. Carlson, P.S. Samiec, P. Sternberg, V.C. Mody, R.L. Reed, and L.A.S. Brown, *Glutathione measurement in human plasma Evaluation of sample collection, storage and derivatization conditions for analysis of dansyl derivatives by HPLC.* Clinica Chimica Acta, 1998. **275**(2): p. 175-184.

113. Anderson, M.E., F. Powrie, R.N. Puri, and A. Meister, *Glutathione monoethyl ester: preparation, uptake by tissues, and conversion to glutathione.* Archives of Biochemistry and Biophysics, 1985. **239**(2): p. 538-548.

114. Mercier, F. and E. Arikawa-Hirasawa, *Heparan sulfate niche for cell proliferation in the adult brain.* Neuroscience Letters, 2012. **510**(2): p. 67-72.

115. Ellis, R.J., *Macromolecular crowding: obvious but underappreciated.* Trends in Biochemical Sciences, 2001. **26**(10): p. 597-604.

116. Krotova, M.K., V.V. Vasilevskaya, N. Makita, K. Yoshikawa, and A.R. Khokhlov, *DNA compaction in a crowded environment with negatively charged proteins.* Physical Review Letters, 2010. **105**(12): p. 128302.

117. Nakano, S., H. Karimata, T. Ohmichi, J. Kawakami, and N. Sugimoto, *The effect of molecular crowding with nucleotide length and cosolute structure on DNA duplex stability.* Journal of the American Chemical Society, 2004. **126**(44): p. 14330-14331.